Tampere University

FARZIN JAVANSHOUR

Interfacial Toughening Strategies for Impact and Fatigue Tolerant Structural Biocomposites

Tampere University Dissertations 800

Tampere University Dissertations 800

FARZIN JAVANSHOUR

Interfacial Toughening Strategies for Impact and Fatigue Tolerant Structural Biocomposites

ACADEMIC DISSERTATION
To be presented, with the permission of
the Faculty of Engineering and Natural Sciences
of Tampere University,
for public discussion in the auditorium S2
of the Sähkötalo building, Korkeakoulunkatu 3, Tampere,
on the 9th of June 2023, at 12 o'clock.

ACADEMIC DISSERTATION
Tampere University, Faculty of Engineering and Natural Sciences
Finland

Responsible supervisor and Custos	Associate Professor Essi Sarlin Tampere University Finland	
Supervisor	Professor Pasi Kallio Tampere University Finland	
Pre-examiners	Doktoringenieur Vincent Placet University of Franche-Comté France	Associate Professor Julie Teuwen Delft University of Technology The Netherlands
Opponents	Associate Professor Julie Teuwen Delft University of Technology The Netherlands	Doctor of Science (Technology) Olli Väntsi MM Kotkamills Boards Oy Finland

Cover design: Roihu Inc.

ISBN 978-952-03-2894-8 (print)
ISBN 978-952-03-2895-5 (pdf)
ISSN 2489-9860 (print)
ISSN 2490-0028 (pdf)
http://urn.fi/URN:ISBN:978-952-03-2895-5

HILIINEUTRAALI PAINOTUOTE
ClimateCalc CC-000025/FI
PunaMusta Printing

Carbon dioxide emissions from printing Tampere University dissertations have been compensated.

PunaMusta Oy – Yliopistopaino
Joensuu 2023

ABSTRACT

Biocomposites reinforced with continuous natural plant fibres such as flax can replace conventional composites in various fields. For instance, flax fibres have higher density-normalised stiffness than glass fibres, higher damping than synthetic fibres, environmental merits, and good end-of-life options. Although the industry regulations on energy consumption and circularity have continuously accelerated the production volume of flax fibre reinforced structural composites, their share in the plastics and composites market is not yet optimum. One of the main issues is their long-term durability under dynamic loading conditions, which is critical for their main application fields, such as boats, sports and automotive. Regardless of the type of polymer matrices and their toughness, flax fibre composites subjected to impact and fatigue loading present brittle behaviour.

In this thesis, various interfacial toughening strategies and their effects on low-velocity impact resistance and fatigue performance of flax fibre composites are elucidated. The aim was to promote energy dissipation through interfacial sliding between fibre-matrix while providing sufficient interfacial adhesion for effective load transfer between fibre and matrix. The three main strategies were: (i) to deposit functionalised multi-layer graphene oxide crystals on the fibre to enable synergy between interfacial adhesion and sliding under dynamic loads, (ii) to coat fibres with a biobased thermoplastic coating to create a ductile phase between flax-epoxy, and (iii) to benefit from ductility of non-dried fibres through moisture insensitive in-situ polymerisation of the poly (methyl methacrylate) (PMMA) thermoplastic resin.

The interfacial toughening results showed the possibility of creating synergy between properties such as stiffness and toughness for flax-PMMA and flax-epoxy composites with 40−100% better impact perforation energy, suppressed fibre failure, and 17−20% better fatigue performance. The scientific impact of this thesis was to elaborate on dynamic failure modes and means to tailor natural plant fibre composites as durable structural materials for sports and automotive applications.

CONTENTS

LIST OF FIGURES

LIST OF TABLES

SYMBOLS

A	Cross-sectional area (mm^2)
A_{emb}	Embedded area (mm^2)
E	Elastic modulus (GPa)
E^{P}	Perforation impact energy (J)
E^{Th}	Perforation threshold impact energy (J)
F^{max}	The maximum force (N)
F^{wet}	Wetting force (N)
G_{12}^{offset}	Shear chord modulus of elasticity (GPa)
m_f	Mass of fibre reinforcement (kg)
p	Fibre perimeter (mm)
R	Fatigue load (stress) ratio
S	Mechanical stress (MPa)
S_0	Ultimate quasi-static tensile strength (MPa)
$T^{radiometric}$	Radiometric temperature (°C)
T^{true}	True temperature (°C)
V_C	The volume of composite (mm^3)
V_f	Fibre volume fraction (%)
γ_{LV}	Surface tension (mN/m)
γ_{12}	Engineering shear strain
$\gamma_{12}^{failure}$	Engineering shear strain at failure
ε	Emissivity
$\varepsilon^{failure}$	Strain at failure
ε_{Li}	Longitudinal normal strain
ε_{Ti}	Lateral normal strain
ε_{ij}	Strain tensor component
ε_{eq}	von Mises strain
ρ_f	The density of fibre (g/cm^3)
$\sigma^{failure}$	Tensile failure strength (MPa)
τ_{12}^{offset}	In-plane offset shear stress (MPa)

$\boldsymbol{\tau}_{12}^{max}$	In-plane maximum shear stress (MPa)
$\boldsymbol{\tau}^{app}$	Apparent interfacial shear strength (MPa)

ABBREVIATIONS

ASTM	American Society for Testing and Materials
CA	Cellulose acetate
CFRP	Carbon fibre reinforced plastic
DIC	Digital image correlation
DMA	Dynamic mechanical analysis
FTIR	Fourier transform infrared spectroscopy
GO	Graphene oxide
GFRP	Glass fibre reinforced plastic
IFBT	Impregnated fibre bundle testing
IFSS	Interfacial shear strength (MPa)
ILSS	Interlaminar shear strength (MPa)
IR	Infrared
MMA	Methyl methacrylate
PMMA	Poly (methyl methacrylate)
SEM	Scanning electron microscopy
SE	Symmetric and even composite lay-up
TGA	Thermogravimetric analysis
UD	Unidirectional fabric or composite
X-CT	X-ray computed tomography
XPS	X-ray photoelectron spectroscopy
XRD	X-ray diffraction

LIST OF APPENDED JOURNAL ARTICLES

Paper I: Effect of graphene oxide surface treatment on the interfacial adhesion and the tensile performance of flax epoxy composites.
Composites Part A, 2021, 106270 – Published by Elsevier

Farzin Javanshour, Karthik Ram Ramakrishnan, Rama Kanta Layek, Pekka Laurikainen, Alexandros Prapavesis, Pasi Kallio, Mikko Kanerva, Aart Willem Van Vuure, Essi Sarlin.

Paper II: Effect of graphene oxide fibre surface modification on low-velocity impact and fatigue performance of flax fibre reinforced composites.
Unpublished manuscript

Farzin Javanshour, Alexandros Prapavesis, Kimmo Lahtonen, Nazanin Pournoori, Mikko Kanerva, Aart Willem Van Vuure, Essi Sarlin.

Paper III: Modulating impact resistance of flax epoxy composites with thermoplastic interfacial toughening.
Composites Part A, 2021, 106628 – Published by Elsevier

Farzin Javanshour, Alexandros Prapavesis, Tuomas Pärnänen, Olli Orell, Maria Clara Lessa Belone, Rama Kanta Layek, Mikko Kanerva, Pasi Kallio, Aart Willem Van Vuure, Essi Sarlin.

Paper IV: Impact and fatigue tolerant natural fibre reinforced thermoplastic composites by using non-dry fibres.
Composites Part A, 2022, 107110 – Published by Elsevier

Farzin Javanshour, Alexandros Prapavesis, Nazanin Pournoori, Guilherme Corrêa Soares, Olli Orell, Tuomas Pärnänen, Mikko Kanerva, Aart Willem Van Vuure, Essi Sarlin.

CONTRIBUTION OF AUTHORS

Farzin Javanshour was responsible for the literature survey and conceptualisation of the research questions. The author performed fibre surface modifications, manufacturing of composites, specimen preparation for various characterisation methods according to the testing standards, and mechanical characterisations. The author carried out the optical profilometry and spectroscopy characterisations. The data analysis of all results, visualisation and writing of the original drafts for journal articles were done by the author.

Alexandros Prapavesis performed the X-ray computed tomography of composites and tensiometry experiments. Essi Sarlin conducted the scanning electron microscopy. Kimmo Lahtonen performed the X-ray photoelectron spectroscopy and the data analysis. Olli Orell provided training and supervision on digital image correlation for strain monitoring in quasi-static mechanical testing of composites. The setup and software for drop-weight impact testing were developed by Tuomas Pärnänen. Nazanin Pournoori and Guilherme Corrêa Soares performed the in-situ synchronised optical and infrared imaging during drop-weight impact testing. Computer code to analyse microbond testing data was developed by Pekka Laurikainen. All co-authors participated in the review and editing of the manuscripts.

The supervisory team were composed of Essi Sarlin, Mikko Kanerva, Pasi Kallio, and Aart Willem Van Vuure, who acquired the FibreNet MSCA-ITN funding for the doctoral studies and actively participated in research planning and validation of the scientific findings and reviewing the manuscripts. Julien Rion acted as industry mentor for doctoral studies. Rama Kanta Layek mentored fibre surface modifications, especially graphene oxide synthesis. Karthik Ram Ramakrishnan provided mentorship for Paper I.

ACKNOWLEDGEMENTS

I would like to express my gratitude to the supervisory team, including Essi Sarlin, Mikko Kanerva, Pasi Kallio, and Aart Willem Van Vuure, who offered the opportunity and scientific support to freely explore and work on the ancient natural fibres and adapt them for the modern engineering applications. The doctoral study (Aug. 2018—Aug. 2022) was funded by European Union's Horizon 2020 research and innovation programme under the Marie Skłodowska-Curie grant agreement No 764713-FibreNet and Tampere University. Being part of the FibreNet MSCA-ITN network, I had the opportunity to network, attend various international research and training events, share the findings, and receive feedback from academic and industrial experts in the field.

I had the pleasure of collaborating with an ambitious and competent group of peer researchers such as Alexandros Prapavesis, Olli Orell, Markus Kakkonen, Tuomas Pärnänen, Rama Layek, Royson Donate Dsouza, Nazanin Pournoori, Guilherme Corrêa Soares, Pekka Laurikainen, Sarianna Palola, Jarno Jokinen, Lauri Jutila, Lijo George, Pauli Hakala, and Karthik Ram Ramakrishnan. Also, it was rewarding to have the support of the research assistant and interns such as Apolline Féré, Trishna Kharkongor Chengappa, and Quynh Nguyen. I appreciate the technical support and training the laboratory coordinator and specialists provided, including Jarmo Laakso, Leo Hyvärinen, Merja Ritola, and Kati Mökkönen. I also cherish coffee time brainstorming discussions with Yentl Swolfs, Olivier De Almeida, and Kaan Bilge.

I acknowledge the support of industrial mentors, especially Fibrobotics Oy (Tampere, Finland), which provided the foundation for micromechanical testing of fibre-matrix adhesion and Bcomp (Fribourg, Switzerland) for providing natural fibre fabrics.

Finally, I would like to thank my dear family and better half Zeynep, for always being there.

1 INTRODUCTION

Biocomposites reinforced with continuous natural plant fibres can replace conventional materials and composites in structural applications such as sporting products, boats, and automobiles. Natural fibres such as flax and hemp offer low density, competitive mechanical properties with glass fibres, many times better damping than carbon fibres, and radio-transparency, besides environmental merits, which can further promote the sustainability aspect of composites. Specifically, flax fibres have the highest tensile elastic modulus and strength among other natural fibres and are mainly produced in Europe. Naturally, the application of natural fibres is dependent on their geographic harvest location. The harvest and production of natural fibres can have a positive socio-economic impact, especially in less developed regions. There is a growing interest in biocomposites due to the environmental issues and regulations on CO_2 emissions (e.g., Euro 6 regulation of EU) and recycling (e.g., 2000/53/EC EU end-of-life vehicle directive). For instance, the biocomposites' market value estimated at USD 4.46 billion in 2016 is expected to reach USD 10.89 billion by 2024. Regardless of their merits and ever-growing interest in developing commercialised structural biocomposites, the share of natural fibre composites in the industrial market is not yet optimum. The main limitation for further exploitation of flax fibre composites is their long-term durability. Specifically, the fatigue and impact resistance of flax fibre composites is limited due to the brittle nature of fibres.

Surface modification of flax fibres can alter their composites' brittle nature by adjusting the interfacial strength and especially interfacial toughness between fibre and matrix. The interfacial toughness is a critical factor for fatigue and impact performance. Various fibre surface modification strategies have been proposed in the literature to improve the compatibility and interfacial shear strength of flax fibres with polymer matrix systems. However, the understanding and number of studies focusing on the interfacial toughness between fibre and matrix and the relevant fibre modification methods are very limited. Particularly, the contribution of various flax fibre modification methods on the low-velocity impact and fatigue performance of their composites is not yet investigated. Addressing the mentioned scientific gaps

can positively impact the market share and competitiveness of flax fibre composites in structural applications.

This thesis work elucidated various interfacial toughening mechanisms and their effects on drop-weight impact and tension-tension fatigue tolerance of flax fibre composites. The upcoming chapters include aims and scope which provides hypothesis and research questions of this thesis, literature review and background in connection with the research questions, materials and methods, integrated results and discussions section based on appended journal articles which address all research questions concisely and coherently, conclusions and research impact, references, and appended journal articles.

2 AIMS AND SCOPE

The main objective of this thesis work was to elucidate interfacial toughening strategies to address the brittle nature of flax fibre composites. The primary goal was to enhance the low-velocity impact resistance and fatigue performance of biocomposites for their long-term in-service durability and sustainability.

Based on the state-of-the-art findings, the impact failure mode of natural fibre composites is dominated by fibre failure with limited interfacial debonding and delamination, which restricts the extent of energy dissipation. As the weakest point in impact resistance of biocomposites is fibre failure, the effect of conventional impact toughening methods such as interlaminar toughening and matrix toughening might be limited. Also, the selection of tough and stiff thermoplastic polymers as a matrix system is bounded to those with processing temperatures below 200 °C, which is the degradation temperature of natural fibres. Therefore, it was envisioned that interfacial toughening could be one of the most effective methods to tackle the impact and fatigue tolerance of natural fibre composites. Particularly, by promoting energy dissipation through fibre pull-outs and delamination while providing sufficient bonding strength for effective load transfer between fibre and matrix. The hypotheses, research questions and relevant journal articles are described in the next page of this section.

Hypothesis I. Graphene oxide (GO) crystals are rich in oxygen-containing functional groups, which can potentially form hydrogen bonds with flax fibres' surface and enhance the compatibility and interfacial adhesion with epoxy resin. Also, GO is composed of layers of oxidised graphene sheets stacked with van der Waals forces. Under dynamic loading conditions, such as impact and fatigue, the multi-layer nature of GO might promote interfacial sliding and energy dissipation between flax fibre and epoxy resin.

Research question I. What is the role of multi-layer graphene oxide surface modification of flax fibres on the interfacial properties between flax-epoxy, and how does it affect the impact and fatigue performance of composites? (Addressed in the appended article I and II)

Hypothesis II. A ductile thermoplastic coating of flax fibres might modestly decrease the interfacial adhesion, promote energy dissipation through fibre pull-outs, and potentially deflect the crack path towards the matrix. It was hypothesised that thermoplastic interfacial toughening of flax-epoxy composites could alter the fibre failure dominant impact mode of composites.

Research question II. How can interfacial toughness be enabled in brittle natural fibre composites, and how is it relevant to the impact resistance of flax-epoxy composites? (Addressed in the appended articles III)

Hypothesis III. The inherent moisture bound to natural fibres acts as a natural plasticiser. It was hypothesised that the in-situ polymerisation of poly (methyl methacrylate) (PMMA) might not be sensitive to moisture, as MMA monomers are emulsion polymerised in an aqueous medium. The radical in-situ polymerisation of non-dry-flax-PMMA composite with preconditioned fibres (e.g., at 50% RH) can potentially enhance the ductility of composites and offer good interfacial adhesion between fibre and matrix.

Research question III. How can the moisture affinity of natural fibres be harnessed as an interfacial toughening method to achieve impact-resistant structural biocomposites without compromising their fatigue performance? (Addressed in the appended articles IV)

3 BACKGROUND AND STATE OF THE ART

3.1 An introduction to flax fibres as green reinforcements for structural composite applications

Flax (*Linum usitatissimum L.*) is a nonwood type of biofibre extracted from the plant stem and therefore is categorised as bast fibre. Flax fibre bundles are located within the peripheral section of the plant stem. During the harvest, flax plants are usually cut into meter-long strips and laid on the soil for retting. During the retting process, fungi degrade the pectin, which binds fibre bundles within the bast fibre [1]. This retting process is aided by the air humidity (dew) and is therefore known as dew-retting. The straw and woody stem are removed from the dew-retted flax by combing the flax bundles during the scutching step. The scutched bundles are further aligned and individualised by combing in hackling step and then spun into yarns. Currently, continuous spun flax yarns and fabrics are the only structural natural fibre reinforcement industrially available in the market (Figure 1). However, the processing and production lines for other competitive bast fibres, such as hemp, are being developed [1–3].

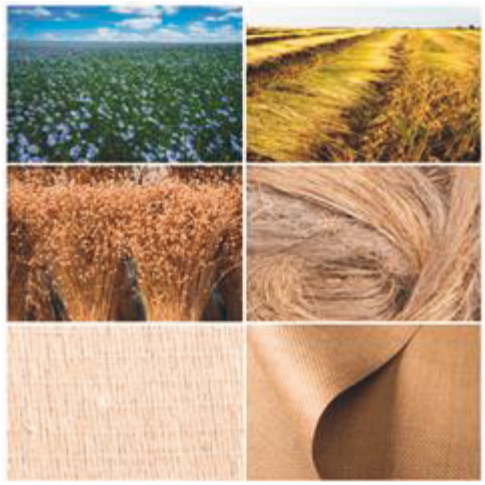

Fig 1. Flax fibres from farm to fabric.

Industrially spun continuous flax yarns are often made of twisted technical flax fibres which are extracted during the hackling process (Figure 2). The approximate range for length and diameter of technical flax fibres are 300−1000 mm and 50−100 μm, respectively. Each technical fibre is composed of many single elementary flax fibres. The approximate range for length and diameter of elementary flax fibres are 10−60 mm and 6−30 μm, respectively.

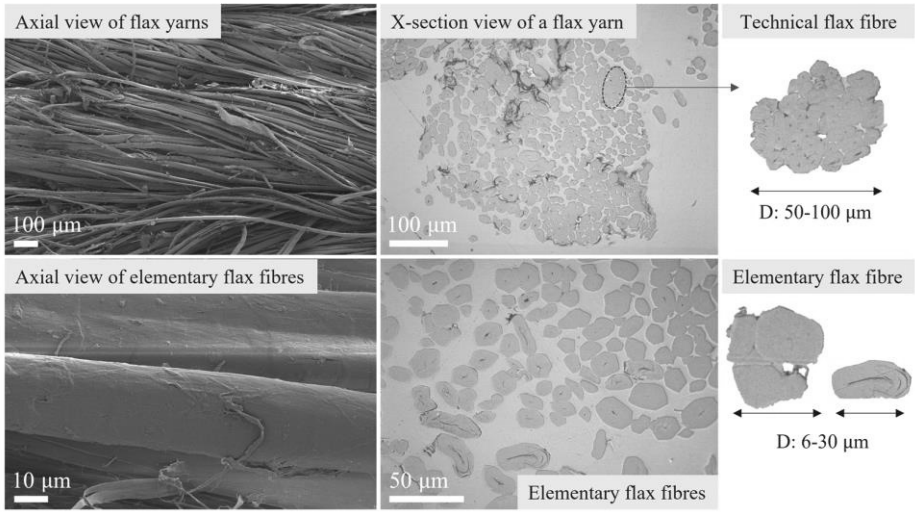

Fig 2. Morphological overview of flax yarns, technical and elementary fibres.

The single elementary flax fibres are composed of four layers of cell walls, namely primary cell wall and secondary cell walls S1−S3 [4]. The thickness of S1, S2, and S3 cell walls are respectively 0.2−5 μm [5], 5−10 μm [5], and 0.5−1 μm [6]. Each cell wall is reinforced with crystalline cellulose nanofibrils in an amorphous matrix of hemicellulose and lignin [7]. 80−90% of the fibre volume is located within the S2 cell wall (also named as G layer), which contains about 80% crystalline cellulose and 20% hemicellulose and pectin [8]. The nanofibrils within the S2 cell wall are packed together in a spiral way along the fibre axis [9,10]. Due to the large volume of the S2 layer, the microfibril angle (MFA) of crystalline cellulose along the fibre axis is a critical factor for the mechanical properties of natural fibres. The MFA of flax fibres based on second-harmonic microscopy with controlled polarisation (P-SHG) method is found to be 2°−7° [11]. Other MFA assessment methods, such as X-ray diffraction, have also confirmed that the MFA of flax fibre is less than 10° [6], the lowest value, compared to other natural fibres [5,11]. The MFA is inversely

correlated with elastic Young's modulus, and the high in-plane elastic modulus value of flax fibres is related to their low microfibril angle [5].

Besides the MFA, the biochemical composition of fibres is an important factor that governs natural fibres' physical and mechanical performance [5,12]. Flax is composed of cellulose (60−85%), hemicellulose (14−20%), lignin (1−3%), pectin (1.8−15%), and lipophilic compounds on the fibre surface (1−6%) [13]. The percentage of cellulose in flax (60−85%) is similar to hemp (55−90%) but notably higher compared to other natural fibres such as abaca (60−68%), bamboo (36−54%), jute (58−71%), sisal (52−65%), and different species of wood (38−45%) [13]. The low microfibril angle in the most prominent cell wall (S2) and high cellulose content have endowed flax fibres with the highest stiffness and strength among all natural fibres [13]. Although the bulk composition of flax fibres is mainly composited of cellulose, the same assumption about their surface composition might not be accurate [14,15]. For instance, the percentage of O/C on the surface of flax fibres has been shown to be 0.15 [14], which is below the 0.8 value of O/C for pure cellulose [16] based on X-ray photoelectron spectroscopy (XPS) analysis. Components such as fatty acids, proteins, pectin, and lignin are often available on the surface of flax fibres besides cellulose [14].

The outstanding quasi-static tensile properties of elementary flax fibres are summarised in Table 1 in comparison to other natural fibres. Due to the natural inhomogeneities and defects within the fibre, there is a considerable variation in the tensile properties of single natural fibres [13,17]. However, such variations can be significantly reduced by careful control over the supply chain of fibres and their characterisation methods [18]. One alternative method to assess the tensile properties of natural fibres, which is more representative of their performance in composites, is impregnated fibre bundle testing (IFBT) [19–21]. IFBT is a tensile test based on epoxy-reinforced UD natural fibre continuous yarns, which provides optimum fibre alignment and fibre volume fraction per specimen. The epoxy resin is often used in IFBT to assure good adhesion between fibre and matrix. Fibre properties are back-calculated based on the rule of mixtures which has a minor statistical error margin. Based on the IFBT method, flax fibres have an elastic modulus of 58 ± 6 GPa, a tensile strength of 530 ± 44 MPa, compressive strength of 237 ± 29 MPa, and a tensile strain failure of 1.08 ± 0.13% at a low density of 1.4 g/cm^3 [20]. Regardless of good elastic modulus, tensile and compressive strength, flax fibres are brittle, which limits the performance of composites, especially under

loading conditions such as impact and fatigue. The main reasons for the brittle nature of flax fibres are their low MFA which limits their elongation at failure [5], in addition to voids and defects such as kink bands along fibres [22,23].

Table 1. Properties of natural fibres and a reference glass fibre.

Fibre	ρ_f (g/cm^3)	E (GPa)	S (MPa)	ε (%)	Reference
Flax	1.4−1.5	40−60	500−1500	1−2	[18,24]
Hemp	1.4−1.5	14−44	500−800	2−4	[13,24]
Jute	1.3−1.5	30−31	300−600	1−2	[13,24,25]
Bamboo	1.4−1.5	33−48	400−500	1−5	[26]
Sisal	1.3−1.5	9−25	300−500	2−5	[27]
Silk	1.2−1.3	16−19	600−750	17−20	[28–30]
Wood	0.1−0.9	15−27	500−1300	3−7	[13]
E-glass	2.4−2.7	70−85	2000−3000	2−3	[24,30]

Besides low MFA angle and defects along fibres, moisture and temperature influence the tensile properties of flax fibres, especially elastic modulus and elongation at failure [31,32]. Flax fibres are hydrophilic and naturally contain water molecules. For instance, at the ambient condition of 65% RH (21 °C), water comprises 7% of total fibre weight [33]. The intrinsic water molecules bound to natural fibres act as a natural plasticiser. For instance, the tensile strain at failure of the elementary flax fibres conditioned at 50% RH (23 °C) is 2.93 ± 0.74%, which decreases by 29% to 2.07 ± 0.31% by oven-drying at 105 °C for 4 hours [34]. Based on the normal stress analysis, it is estimated that the shear strength of the S2 cell wall of flax fibres is 45 MPa at 50% RH (23 °C), whereas the shear strength of only 9 MPa is estimated for oven-dried fibres [34]. However, natural fibres are often dried in the oven to avoid moisture evaporation and void formation and to prevent potential negative effects of moisture on the curing process of polymeric resins during the manufacturing of composites [14,35,36].

Drying and heat treatment can also alter the chemical structure of flax fibres. The isothermal thermogravimetric analysis (TGA) of flax fibres conducted in an air atmosphere for 60 min results in the removal of water and loss in surface waxes at 120 °C (90−94% residual mass). The complete evaporation of strongly linked water molecules to the polysaccharide matrix within flax fibres is realised at 150 °C [34]. Pectin, which holds elementary fibres together, degrades at 180 °C (87−91% residual mass) [37]. The hemicellulose, which acts as the matrix for cellulose microfibrils of

flax fibres, degrades within the 200−230 °C temperature range [37]. Depolymerisation of polysaccharides is realised within the 250−400 °C range. The aromatic and non-cellulosic substances degrade above 400 °C [37]. Therefore, polymer matrix systems with processing temperatures below 200 °C should be preferred for manufacturing natural fibre composites to avoid the physical degradation of fibres.

From the environmental perspective, natural fibres such as flax and hemp hold a particular advantage over synthetic fibres such as E-glass. The non-renewable energy required for the production of flax fibres is within the 9−12 GJ/tonne range [38] compared to 45−55 GJ/tonne for glass fibres [39]. Flax and hemp have an average yield of 5−8 tonnes per hectare and absorb 1.4−1.6 tonnes of CO_2 per tonne [2]. Compared to glass fibre, the production of flax fibre imposes lower pressure on abiotic depletion (−90%), photochemical oxidation (−88%), and human toxicity (−98%). However, flax fibres have higher eutrophication (+17) and land-use indices compared to glass fibres [38]. Due to the potential threats in land-use and eutrophication, the production of natural flax fibres is limited compared to synthetic fibres. Therefore, the research in the field of natural fibres has been focused on improving the quality and consistency of flax fibres in terms of yield, extraction process and physical quality of fibres to enhance their versatility, durability and reliability for engineering applications [2,40,41].

In summary, this section briefly introduced flax fibres' production and extraction, their morphological and chemo-physical properties, and their environmental merits. Flax fibres provide a combination of low density and good mechanical properties comparable to glass fibres. Compared to other natural fibres, the mechanical performance of flax fibres is outstanding, which is attributed to the high cellulose content and low microfibril angle within the S2 cell wall. However, flax fibres are brittle which is partly related to their low microfibril angle, and defects along fibres which are intrinsic features of fibres or created during the fibre extraction. The inherent moisture bound to the flax fibres acts as a natural plasticiser and enhances the ductility of fibres. The brittle nature of flax fibres can negatively affect their composites' long-term durability, especially under impact and fatigue loading conditions. The following section will provide a brief overview of flax fibre composites, state of the art on their impact resistance and fatigue tolerance.

3.2 Introduction to impact and fatigue behaviour of flax fibre reinforced composites

The main markets for flax fibre composites are sporting goods, leisure boats, secondary and interior parts of automobiles. In such applications, structures experience cyclic mechanical loads (fatigue) and low-velocity impact loads, such as falling tools and projectile hits, to name a few. An invisible impact-induced internal damage can negatively affect the long-term durability of composites subjected to fatigue loading. Therefore, fatigue performance and impact resistance are critical for structural flax fibre composites. However, achieving synergy between fatigue and impact resistance can be challenging. For instance, impact-resistant composites with a toughened polymer matrix or poor interfacial adhesion might have poor fatigue performance. The core aim of this section is to elaborate on the reasoning behind the limited impact resistance and fatigue performance of flax fibre composites.

This introduction describes the effect of reinforcement properties and architecture, polymer matrix type, toughening of polymers, and interlaminar toughness on low-velocity drop-weight impact and tension-tension fatigue resistance of flax fibre composites. In the literature, the understanding and number of studies focusing on fibre surface modification strategies and their effect on the impact and fatigue performance of composites are very limited. However, the existing literature on interfacial toughening methods is discussed in each section.

3.2.1 Low-velocity impact behaviour of flax fibre reinforced composites

Low-velocity impact refers to impact incidents where the contact time is such that the whole structure has time to respond to the loading and creates through-thickness damage. This type of impact is one of the most common incidents during the service-life of structural composites, which can cause critical visible or invisible damages. Impact resistance is the ability of a composite to sustain a given impact loading with the minimum extent of internal damage. Impact damage tolerance is the ability to sustain a given level of damage with minimum effect on the structural performance (e.g., compression after impact). So, the two characteristics, namely impact resistance and impact damage tolerance, are not necessarily mutually inclusive. Therefore, the term 'impact tolerance' combines impact resistance and impact damage tolerance [42].

In general, composites absorb the low-velocity impact energy through matrix cracking, interfacial debonding and delamination, ply splitting, and especially fibre failure [43]. The typical internal damage patterns of composites after low-velocity impact testing are presented in Figure 3. Matrix cracking results from longitudinal stress on the upper and lower surfaces of composites beam, which form due to property mismatch between fibre and matrix and are usually oriented in planes parallel to the fibre direction in unidirectional layers [44]. Impact-induced delamination results from the bending stiffness mismatch between adjacent layers with different fibre orientations, where the highest mismatch prevails between 0/90 layers [45]. In 0/90 cross-ply lay-ups, impact-induced delamination initiates as a mode I fracture due to high out-of-plane normal stresses caused by matrix cracks and high interlaminar shear stresses between ply interfaces [46]. Fibres have the most bearing on the impact response of composites and occur under the impactor due to high local stresses and indentation effects governed by shear forces [44]. Fibres can either fail in tension due to the membrane forces generated during the impact or by shear-out during the penetration of the impactor [42]. The ability of fibres to elastically store energy is a fundamental parameter for the low-velocity impact resistance of composites [47]. Therefore, fibre ductility and stiffness are critical parameters for the impact resistance of composites [44].

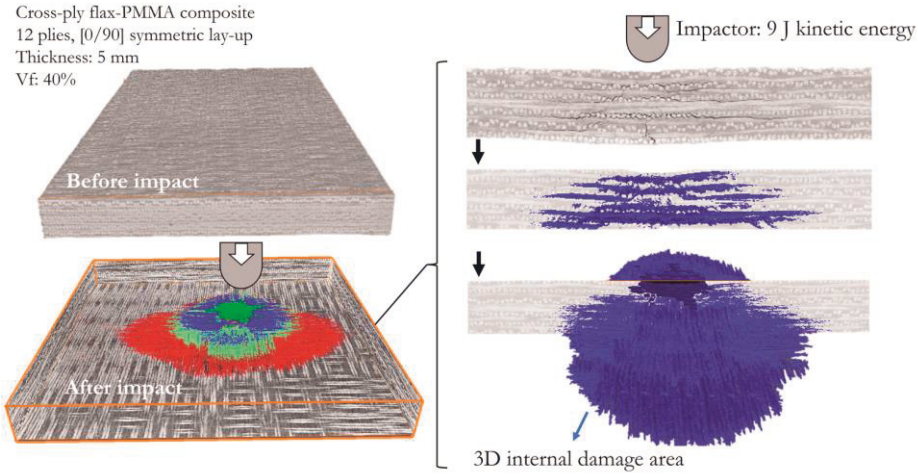

Fig 3. Typical internal damage patterns of composites after the low-velocity impact testing.

Due to the brittle nature of flax fibres, the low-velocity impact resistance of flax fibre composites is inferior compared to glass fibre composites. For instance, the impact perforation energy of cross-ply flax-epoxy composites is 4J/mm [48,49], which is 80% lower than the similar value for cross-ply glass-epoxy composites [50]. Contrary to the glass fibre composites, flax fibre composites' internal impact damage patterns are often dominated by fibre failure with limited delamination, which limits the impact energy dissipation capacity of flax fibre composites [49,51]. The brittle characteristic of flax fibre composites is presented in Figure 4. Half of the plies failed by a crack initiating from the tension side of the specimen (rear surface) when subject to 9 J kinetic energy, which is notably below its perforation energy (21 J). Therefore, the brittle characteristic of flax fibre composites should be addressed to enhance their reliability and durability for structural applications. The essential material parameters and strategies that can alter the impact behaviour of flax fibre composites are discussed in the following paragraphs.

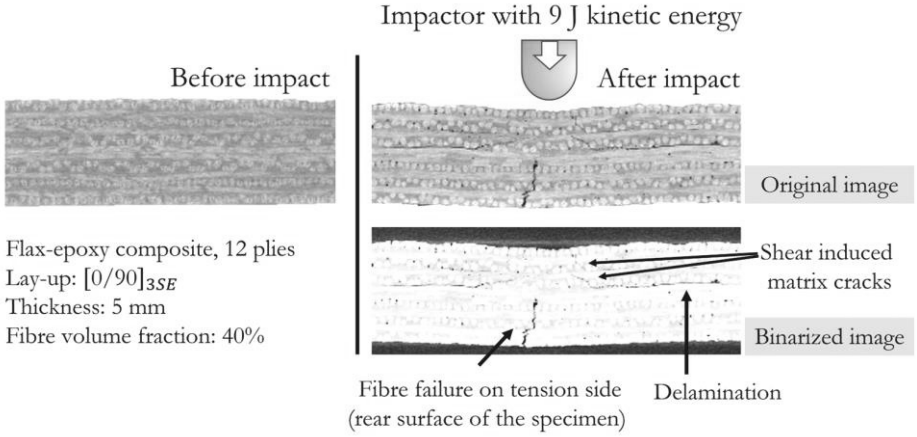

Fig 4. The typical low-velocity impact failure modes of flax fibre composites with kinetic energy far below the perforation [modified from Paper II].

The lay-up and architecture of reinforcements can alter the impact performance of composites in terms of damage area and perforation energy. Cross-ply flax fibre composites based on UD plies absorb higher impact energies than woven plies due to the higher in-plane strength of cross-ply composites based on UD plies [49,52]. Impact energy absorption by delamination is highest for cross-ply composites due to the mismatch of bending stiffness between adjacent plies [45]. Nevertheless, cross-ply composites based on woven reinforcements exhibit limited damage compared to cross-ply laminates based on UD plies and thus tend to have better properties after impact (damage tolerance) [49]. This is due to the coarse fibre

bundles within the woven fabrics that act as crack-stoppers and reduced delamination due to the nesting of the woven fabrics, which enforces crack propagation through a tortuous path. Bensadoun et al. [49] studied the low-velocity impact behaviour of flax fibre composites with different fibre architectures, namely plain weave, 2 × 2 twill (including low, medium, and high twist yarns), and 0/90 lay-up based on UD fabrics. In terms of impact energy absorption, the performances of composites reinforced with plain weave, twill, and 0/90 lay-up based on UD fabrics were similar. However, at a non-perforation impact energy of 3 J (for 2 mm thick laminates), woven composites had, on average, 20% less damage area than cross-ply composites based on the plain weave and UD fabrics. Among twill fabric reinforced composites, those with the lowest crimp and yarn twist had the highest absorbed energy at the perforation. The in-plane strength of composites is essential for the impact perforation energy, as fibre failure is the dominant failure mode. It is known that the in-plane strength of composites decreases by the twist level in yarns. Also, the stiffness in composites (which is directly related to the impact resistance [44]) is inversely proportional to the crimp (tortuosity) level of fabrics. The crimp level in fabrics increases by the twist angle of yarns. From a processing point of view, a high twist angle in yarns can have a negative effect on wetting and resin impregnation. An alternative helicoidal ply stacking configuration with a ply angle of 9° was proposed by Chew et al. [53]. The helicoidal configuration enhanced the impact energy absorption capacity of flax-epoxy composites by enabling systematic matrix crack propagation through extensive spiral paths. The fibre-dominant failure mode of composites was altered. The maximum contact force of helicoidal composites was respectively 72% and 52% higher than similar composites with quasi-isotropic and cross-ply lay-ups. The thickness-normalised impact perforation energy of flax-epoxy composites with helicoidal lay-up (7 J/mm) was respectively 16% and 40% higher than quasi-isotropic (6 J/mm) and cross-ply (5 J/mm) lay-up. However, the final thickness of helicoidal flax fibre composites seems to be high (minimum 8.5 mm), and the effect of such ply configurations on other properties of composites, such as fatigue, is yet to be studied.

The toughness and ductility of the polymer matrix system influence impact energy absorption and damage volume through plastic flow, crack blunting, and void coalescence. The selection of polymer matrix systems is limited to those with processing temperatures below 200 °C due to the thermal degradation of flax fibres at elevated temperatures. For example, substituting a brittle epoxy matrix with maleic anhydride grafted polypropylene (MAPP) increases the absorbed energy at the

perforation of cross-ply and woven flax fibre composites by 22% and 50%, respectively [49]. This is often related to the higher elongation at failure of thermoplastic polymers (e.g., ε_f of 474% for MAPP[49]) compared to brittle polymer matrix systems such as epoxies with elongation at failure of 3−5%. However, based on the literature the type of the matrix (thermoplastic or thermoset) and matrix toughening have a minor or no effect on the perforation energy of flax fibre composites [51]. For instance, inclusion of nanosized particles such as reduced graphene oxide and TiO_2 enhance the interfacial adhesion between fibre and matrix and fracture toughness of composites such as flax-epoxy [54–56]. At kinetic energies below perforation, the toughening of polymer matrix with nanoparticles alters the impact performance of flax fibre composites in terms of maximum contact force due to better interfacial adhesion between fibre-matrix and limits extend of matrix cracking [55,56]. Although tough thermoplastic polymers can increase fracture toughness by an order of magnitude over brittle thermoset composites [57], the presence of brittle flax fibres prevents the growth of plastic zones in the matrix [47]. Therefore, matrix toughening strategies might not be sufficient to modify the limited impact perforation energy of flax fibre composites.

Interlaminar toughening can limit the delamination growth in composites when subjected to impact loads. Thermoplastic film or nonwoven mat interleaving between plies can control damage growth (e.g., by limiting the delamination growth close to the mid-plane) and create a synergy between energy dissipation and after-impact residual mechanical performance of composites. For instance, Yasaee et al. [43] reduced the delamination area of glass fibre reinforced epoxy composites by 38% by interleaving 50 μm thick polyimide thermoplastic films. Consequently, the compression after impact strength of composites was modified by 18%. Studies on interlaminar toughening of natural fibre composites are currently limited to two research papers on carbon nanotube buckypaper [58] and through-thickness stitching [59] of flax-epoxy composites. Chen et al. [58] enhanced the G_{IC} of flax-epoxy composites by 22%−50% by interleaving 140 μm thick multiwall carbon nanotube (MWCNT) buckypapers. Therefore, the Charpy impact strength of flax-epoxy composites was enhanced by 16%. However, the authors did not study the effect of CNT interleaving on low-velocity impact performance or other critical properties such as fatigue. Ravandi et al. [59] studied the effect of through-thickness stitching of flax fabrics on the impact behaviour of cross-ply flax-epoxy composites. The stitching method negatively affected the energy absorption and perforation energy due to defects such as fibre distortion and resin pockets. Further

investigations are required to understand the effect of various interlaminar toughening methods on the impact resistance and tolerance of flax fibre composites. As described before, the internal impact damage traces of flax fibre composites in the literature are dominated by fibre failure due to the brittle nature of fibres and minor delamination. Therefore, the interlaminar toughening might have a minor effect on the impact resistance of natural fibre composites.

Surface modification of fibres can modify the interfacial shear strength and fracture toughness of natural fibre composites. The main fibre surface modification strategies for natural fibre composites are plasma treatment, extraction of lipophilic compounds from fibre surfaces, deposition of functional nanoparticles, and chemical grafting of coupling agents [60]. For instance, plasma treatment of natural fibres at atmospheric pressure (with air, helium, or argon gas) enhances the surface roughness of fibres and increases the O/C ratio on the fibre surface by creating C=O and O–C=O functional group [61]. The enhanced surface roughness of fibres promotes the mechanical adhesion between fibre and matrix, while the oxygen-containing functional groups promote hydrogen bonding with polar polymer matrix systems and reactive resins such as epoxy [61]. The extraction of waxes from fibre surfaces (e.g., by ethanol treatment [62]), introducing coupling agents (e.g., amino silanes [63]), and depositing functionalised nanoparticles (e.g., TiO_2 [64], GO [25]) on fibres have essentially similar effects as plasma treatment which are enhancing the O/C ratio and surface roughness of fibres. However, some treatments, such as alkali modification [62], and plasma treatment with argon [65], can reduce the tensile strength of natural fibres due to chemical adjustments (e.g., by removing the hemicellulose and pectin from fibre microstructure) or physical adjustments (e.g., creating defects and cavities within fibres). The embrittlement of fibres due to surface modification strategies might have a negative effect on the impact and fatigue tolerance of composites. However, the studies in the literature are mainly focused on the interfacial shear strength and quasi-static mechanical performance of natural fibre composites. Further investigations on macroscale composites and their fatigue and low-velocity impact performance are required to understand the potential of proposed fibre surface modifications in the literature. Also, the contribution of the proposed fibre modification strategies on the interfacial toughness between fibre and matrix is somewhat overlooked in the literature. Interfacial toughening can be a suitable strategy for modulating the impact tolerance of composites with brittle fibres. Coating fibres with a ductile phase compatible with polymer matrix can enhance the elongation at failure and toughness of composites. Ductile and tough

interphase can potentially reduce the extent of impact-induced fibre failure by promoting energy dissipation through interfacial sliding between fibre and matrix. Interfacial toughening can be realised by depositing fibrous or multi-layer nanomaterials onto the fibre [66–68], coating fibres with elastomer or tough polymer coating [69,70], creating long chain entanglement between fibre-matrix [71]. For instance, growing carbon nanotubes on carbon fibres through chemical vapour deposition has been shown to improve the Izod impact strength of carbon-epoxy composites by 34% without negatively affecting the quasi-static mechanical properties of composites [68]. Lin et al. [69] improved the interfacial shear strength between aramid fibre and epoxy by 67.7% with 1.39% fibre sizing content of thermoplastic polyurethane. The quasi-static tensile strength and elongation at failure of toughened composites were increased by 10%, while the fracture toughness was enhanced by 126%. The authors ascribed the tough nature of polyurethane-modified composites to the presence of a ductile interface which delayed the debonding by crack deflection. However, the effect of interfacial toughness on low-velocity impact and fatigue resistance of natural fibre composites is not yet studied.

3.2.2 Fatigue behaviour of flax fibre reinforced composites

Every structural material experiences in-service cyclic mechanical load, which fluctuates over time and creates time-varying stresses below the quasi-static strength of the material. The time-varying fatigue loading is localised at the material or geometrical discontinuities. Natural fibres such as flax are hierarchical cellulosic materials with inhomogeneities in fibre geometry, morphology, and chemistry. Therefore, fatigue performance is critical for the long-term durability of flax fibre reinforced composites.

Fatigue loading of composites creates multi-staged damage. Matrix cracks develop in the early stage of the fatigue process along fibres in the tensile loading direction. The crack density increases by cyclic loads and reaches a saturation point where stress redistribution limits the initiation of new cracks. However, the macroscopic size matrix cracks can create stress concentration and other damage modes such as fibre-matrix interfacial debonding, delamination, and fibre failure. Therefore, the fatigue performance of flax fibre composites can be tailored based on the toughness of polymer matrix systems, good interfacial adhesion and interfacial toughness between fibre and matrix, ductility of fibres, and fibre architecture.

As described in the previous section, cross-ply composites based on woven or unidirectional fabrics provide the best impact resistance for flax fibre composites. The type of weave and fabric geometry are essential parameters in the fatigue performance of woven composites. Asgharinia et al. [72] found that the resistance of woven flax-epoxy to fatigue damage increases by decreasing the crimp in the yarns. Flatter and yet denser yarns reduce the crimp of fabrics. The authors studied flax-epoxy composites reinforced with twill-weave fabrics with areal densities of 224 g/m^2 and 550 g/m^2. The quasi-static tensile properties of both composites were similar. However, the number of cycles to failure at every stress level for flax-epoxy composites with 224 g/m^2 areal density was notably higher than 550 g/m^2. The better fatigue performance of flax-epoxy composites with a lower areal density of fabrics was ascribed to the lower level of transverse cracks and delamination due to the lower crimp index of fabrics. Bensadoun et al. [73] studied flax-epoxy composites with various fibre architectures. Composites with the highest quasi-static tensile stiffness and strength values also had longer fatigue life and less damage accumulation, which was demonstrated by smaller hysteresis loop area, lower strain shifts and plastic deformations. The longer fatigue life in ascending order was found for flax-epoxy composites with [0], [0/90], quasi-isotropic, woven, short fibre, and [90] fibre lay-ups [74]. Mahboob et al. [75] studied the fatigue performance of flax-epoxy and glass-epoxy composites with various lay-up configurations based on strain-controlled (constant strain-amplitude) cycling testing. The strain-controlled cyclic testing was shown to eliminate the apparent modulus alteration reported for flax fibre composites by several stress-controlled studies [74]. Authors found that the fatigue performance of flax-epoxy composites (at indoor conditions) is comparable to their glass-epoxy counterparts with all lay-up configurations. Also, flax-epoxy composites showed superior resistance to stiffness loss and lower residual inelastic strains than glass-epoxy composites.

Interfacial adhesion is critical for effective stress transfer between fibre and matrix. Under cyclic loading conditions, interfacial adhesion mainly affects the off-axis and shear properties of composites and corresponding damage developments [76]. For instance, composites with poor interfacial adhesion show an early reduction in stiffness, a high damage growth rate, and low fatigue damage tolerance [76]. The main fibre surface treatment strategies are lipophilic treatments for natural fibres, depositing nanocrystals such as GO, coating ductile thermoplastic layer on fibres, and chemical grafting of coupling agents on fibres [76]. For instance, Towo and Ansel [77] investigated the effect of lipophilic extraction from jute fibres based on

NaOH alkali treatment. Due to the higher surface roughness and free hydroxyl groups of alkali-modified jute fibres, the in-plane quasi-static tensile strength of jute-polyester composites was increased by 25%. However, the alkali treatment negatively affected the fatigue performance of composites due to the embrittlement of fibres [77,78]. Deng and Ye [79] studied the effect of applying electrochemically oxidation and epoxy sizing (0.4 wt%) on the interfacial shear strength based on the single fibre pull-out test and tension-tension fatigue performance of unidirectional carbon fibre-epoxy composites. The interfacial shear strength of carbon-epoxy was enhanced by 33% with the proposed fibre surface modification. In the quasi-static tests, the longitudinal and transverse strain to failure of UD carbon-epoxy composites were improved by 8% and 65%, respectively. Under cyclic loading, modified composites had longer fatigue life (i.e., a higher number of cycles to failure) at high applied stresses. However, the effect of interfacial adhesion was less pronounced at low-stress levels. In other words, the slope of stress-cycles to failure (*S-N*) graphs of the composites increased by the fibre modification which shows the fatigue behaviour is closely related to the interfacial adhesion. Broyles et al. [80] studied the fatigue performance of carbon fibre-vinyl ester composites with ductile thermoplastic sizing of carbon fibre based on polyhydroxy ether (phenoxy resin). The ductile sizing reduced the *S-N* slope of composites and enhanced the fatigue limit by 60% compared to unmodified carbon fibre-vinyl ester specimens. Authors concluded the significant effect of interfacial toughness on the fatigue performance of composites with brittle fibres. Overall, the interfacial adhesion and interfacial toughness have an influence of fatigue performance of composites. However, the effect of surface modifications for natural fibre composites are mainly focused on the quasi-static mechanical properties [60] which does not necessary correlate with the fatigue performance of composites [76].

4 MATERIALS AND METHODS

4.1 Materials

4.1.1 Flax fibres and polymer matrices

Flax fibres were selected as the reinforcement in this thesis work due to their outstanding mechanical performance (compared to other natural fibres), which is desired in structural applications. This selection is geographically relevant as 70% of flax's global production is realised in Europe (specifically in France). Also, flax fibre fabrics are the only commercially available continuous natural fibre in the market. Non-crimp flax fabrics (ampliTex) of unidirectional and twill 2 × 2 types with an areal density of 300 g/m^2 were provided by Bcomp (Fribourg, Switzerland). The manufacturer treated the flax fibres with a standard boiling water procedure to remove waxes from the surface. A thin polyester weft thread connected the yarns of the UD flax fabrics. The average tensile properties of oven-dried flax fibre bundles (at 115 °C for 2 hours) are summarised in Table 2. The tensile properties of flax fibre bundles were back-calculated from the impregnated fibre bundle test (IFBT) results of flax-epoxy composites [21].

Table 2. The average tensile properties of ampliTex flax fibre bundles [21].

Property	Dry fibre
Elastic modulus within 0−0.1% strain range (GPa)	57 ± 3
Elastic modulus within 0.3−0.5% strain range (GPa)	38 ± 2
Failure strength along fibres (MPa)	600 ± 40
Elongation at failure (%)	1.0 ± 0.1

The thermoset and thermoplastic polymer matrix systems in the thesis work were epoxy and poly (methyl methacrylate) (PMMA) resins, respectively. The epoxy was a standard resin (Epopox A-28, Amroy Europe, Lahti, Finland) polymerised by a polyether diamine hardener (Jeffamine D-23, Hunstman, Texas, USA) with a 35 wt% hardener to epoxy ratio. The PMMA was in-situ polymerised at the ambient

conditions by mixing a liquid methyl methacrylate thermoplastic resin (Elium 188, Arkema, Colombes, France) and dibenzoyl peroxide initiator (BP-50-FT1, United Initiators GmbH, Pullach, Germany) with 3 wt% initiator to resin ratio. The average tensile properties of the polymer resin systems are summarised in Table 3. The testing data and specifications are available in the following reference link [81].

Table 3. The average tensile properties of polymer matrix systems [81].

Property	Epoxy	PMMA
Tensile modulus (GPa)	2.3 ± 0.1	2.6 ± 0.1
Tensile strength (MPa)	53.7 ± 1.1	63.5 ± 0.3
Elongation at break (MPa)	6.1 ± 0.4	6.6 ± 0.3

4.1.2 Flax fibre modification methods

To promote the interfacial adhesion and interfacial toughness between flax-epoxy, the surface of flax fibres was modified by multi-layer graphene oxide (GO) crystals and cellulose acetate thermoplastic coating based on the dip-coating method. The fibre modification strategy for PMMA-based composites was based on the environmental precondition of fibres at 50% and 90% RH (23 °C). The motivation to use preconditioned fibres was to enhance the ductility and toughness of composites.

Surface modification of flax fibres with graphene oxide

The graphene oxide (GO) surface modification was realised by dip-coating flax fibres in a 1.2 wt% aqueous dispersion of GO (for 24 hours at 23 °C). The 1.2 wt% GO concentration was selected as it provided the optimum interfacial adhesion between flax-epoxy in the preliminary studies. The GO concentrations in the preliminary studies were 0.65 wt%, 1.2 wt%, and 2 wt% GO. After dip-coating, the flax fibres were rinsed in deionised water to remove the excess (unbound) graphene oxide from the fibre surfaces and then oven-dried at 60 °C overnight. Two types of GO dispersions (with similar concentrations) were used. In Paper I, the flax fibres were modified by in-house synthesised GO-dispersion according to Hummer's method [82]. In Paper II, a commercial GO-dispersion was used due to the macro-scale nature of the study. The GO surface modification did not have any meaningful

effect on the tensile performance of single flax fibres [see Paper I, Table 2]. It should be noted that in Paper I, both unmodified and GO-modified flax fibres were immersed in de-ionised water for 24 h at 23 °C and dried at 50 °C overnight to account for the potential effect of water. However, in Paper II, the unmodified flax fabrics were used as received without water immersion.

For the graphene oxide synthesis, a 500 mL round bottom flask was placed on a magnetic stirrer in an ice bath (0 °C). A 46 mL of H_2SO_4 (VWR, VWR International Oy, Helsinki, Finland) was transferred to the flask and continuously stirred by a magnetic bar. 1 g of $NaNO_3$ (Sigma-Aldrich, Burlington, United states) and 2 g of graphite powder (type TIMREX KS44, TIMCAL Graphite & Carbon, Bodio, Switzerland) were added to the H_2SO_4. Then, 6 g of $KMnO_4$ (≥ 99.0%, Merck, Darmstadt, Germany) was gradually added to the reaction, maintaining the mixture's temperature below 5 °C. After 10 minutes, the ice bath was removed, and the reaction was continuously stirred for 6 hours at 23 °C, which finally turned into a viscous paste. Afterwards, 92 mL and 280 mL of distilled water were added to the reaction with 30 minutes gap in between. Also, 10 mL of hydrogen peroxide was added to the flask. After the GO synthesis, an aqueous dispersion of GO was sonicated for exfoliation and further centrifuged to remove the acid used in the process and the non-exfoliated GO sheets. The obtained brown suspension was dried in an oven at 50 °C for 24 hours to achieve a GO film. A 1.2 wt% aqueous dispersion of GO was prepared by mixing GO film with deionised water in a mortar and further sonication. Flax yarns were dip-coated in this dispersion for 24 hours at 23 °C and dried at 50 °C overnight. The reference flax yarns were immersed in deionised water for 24 hours at 23 °C and dried at 50 °C overnight to account for the potential effect of water.

The commercial graphene oxide was based on a stable aqueous dispersion of graphene oxide (Graphenea, Gipuzkoa, Spain) with a GO concentration of 1.2 wt%, pH of 1.8–2, and particle size of 14–17 μm. Flax fabrics were coated with GO by dip-coating for 10 minutes (at 23 °C). The dip-coated fabrics were rinsed in deionised water to remove the excess unbound GO particles from the surface. The GO-modified fabrics were oven-dried at 50 °C for 24 hours.

As stated in the literature review section, various thermoplastic and elastomeric coatings, such as polyurethane [69], can be used for the interfacial toughening of composites. However, this study aimed to use a biobased thermoplastic coating. The potential of a few biobased thermoplastic polymers, such as cellulose acetate, methyl cellulose, polyvinyl acetate, and nanocellulose was investigated for selecting suitable fibre coating. Based on the initial quasi-static tensile tests (unidirectional and transverse), the cellulose acetate coating resulted in a more uniform coating of flax fabrics, good interfacial strength between flax-epoxy, and the best combination of stiffness and ductility for flax-epoxy composites. Therefore, cellulose acetate was selected as the fibre coating for this study.

Pure cellulose acetate (CA) powder with average molecular weight of 100,000 (g/mol) was supplied by Acros Organics (New Jersey, United States). The degree of substitution of CA was 1.3. Based on the acetyl content and degree of substitution of the cellulose acetate, it can be dissolved in various solvents such as acetone, chloroform, 2-methoxyethanol, and dichloromethane. In this study, acetone was selected as a solvent, based on an extensive review of the green solvent guides by Byrne et al. [83], which categorised solvents into six subgroups from green (e.g. ethanol, water), between green and problematic (e.g. acetone), problematic (e.g. DMSO), between problematic and hazardous (e.g. dichloromethane), hazardous (e.g., 2-methoxyethanol), and highly hazardous (e.g. chloroform). Compared to other CA-solvents, acetone has the best environmental, health, safety, and energy demand indices [83]. Technical acetone by Kiilto Oy (Lempäälä, Finland) was used as a solvent for CA powder.

Flax fabrics were modified with CA by dip-coating into a CA-acetone solution (for 5 seconds, at 23 °C) with a CA concentration of 5 g CA in 100 mL acetone. The CA-modified fabrics were oven-dried at 115 °C for 2 hours. CA coating comprised the 4 ± 1 wt% of the modified fabrics. The thickness of the formed coating on flax fabrics was in the range of 3 μm. The CA concentration was selected by preliminary studies on quasi-static transverse tensile and Charpy impact testing of flax-epoxy composites. Among different CA concentrations (namely 2.5 gr, 5 gr, and 10 gr per 100 mL of acetone), the CA-modified flax-epoxy with 5 g CA/100 mL acetone concentration had the best performance and therefore was selected for the primary studies. It should be noted that the immersion of fibres in acetone (for 5 seconds, at

23 °C) did not alter the tensile performance of single flax fibres. The single fibre tensile testing data and specifications are available in the following reference link [84]. Further data on the mechanical properties of CA-modified flax yarns and fabrics are provided in Paper III [see Supplementary data in Paper III].

Moisture preconditioning of flax fibres for non-dry flax-PMMA composites

Flax fibres were preconditioned at three different environmental conditions before the resin infusion of composites. Based on the preconditioning methods, flax fabrics were labelled as Dry, RT, and RH.

Dry fabrics were oven-dried at 115 °C (for 2 hours), RT fabrics were conditioned at 50% RH (23 °C, for 24 hours), and RH fabrics were conditioned at 90% RH (23 °C, 24 hours). The moisture content of fibres was measured by an analytical balance (model GR-202, A&D Ltd, Tokyo, Japan). The average weight for three pieces of fabrics (10 mm × 10 mm; width × length) was measured consecutively after oven-drying and humidity conditioning. Compared to oven-dried (Dry) fabrics, the weight gains of RT and RH fabrics after conditioning were 8.1 ± 0.2 wt% and 16.8 ± 0.2 wt%, respectively. The environmental preconditionings for fabrics were done in a humidity chamber (model VC 0018, Vötschtechnik, Balingen, Germany).

4.1.3 Manufacturing of composites

Flax-epoxy composites for the quasi-static mechanical tests were manufactured based on hand lay-up followed by vacuum bagging. Flax-epoxy composites for cyclic loading and low-velocity impact testing were manufactured using vacuum-assisted resin infusion. Before manufacturing, flax fibres were oven-dried at 115 °C (for 2 hours). The amounts of fibres and the number of plies were estimated based on ISO 14127:2008 standard and $V_f = (m_f/\rho_f)/(V_c)$ formula. The V_f for all composites was aimed at 40%. In the formula, m_f is the mass of the fibres, V_c is the volume of the composite, and ρ_f is the density of flax fibres (1.4 g/cm^3), assuming a pore-free composite. The general overview of the vacuum-assisted resin infusion process is presented in Figure 5. The epoxy resin was degassed for 5 min before the resin infusion. Steel-made spacers were used to tailor the final thickness of the composites and their fibre volume fractions. After the resin infiltration, the vacuum-bagged setup was placed in a hot press to ensure that the final thickness of the composites

was the same as the steel spacers. Based on the manufacturer's recommendation, the composite laminates were cured at 90 °C for 24 hours and post-cured at 150 °C for 1 hour. The 40 ± 2% fibre volume fraction value of all manufactured composites was confirmed by X-CT analysis. The volume fraction values of porosities for flax-epoxy, GO-flax-epoxy, and CA-flax-epoxy composites were 2.4%, 0.04%, and 3.4%, respectively. After manufacturing, flax-epoxy composites were stored in a controlled environment (50% RH, 23 °C) for 3−4 weeks to reach equilibrium.

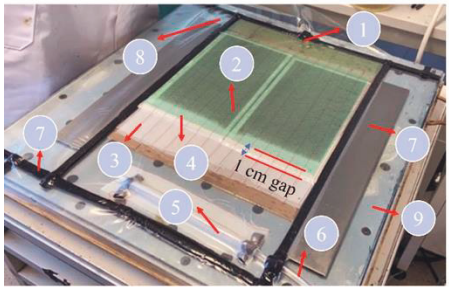

1. Resin inlet
2. Flax preforms (stack of fibres)
3. Peel ply sheet on both ends of flax preforms
4. Resin flow media
5. Spiral tube connected to vccuum line
6. Vaccuum line conected to a pump
7. Sealant tape
8. Vaccuum bag
9. Infusion table covered with a glass sheet

Fig 5. A snapshot from vacuum-assisted resin infusion process.

All flax-PMMA composites were manufactured by vacuum-assisted resin infusion with a 40% fibre volume fraction. The flax-PMMA composites were categorised into three groups: Dry, RT, and RH. The resin infusion and the in-situ polymerisation of flax-PMMA composites were realised at 23 °C. After the resin infiltration, the vacuum-bagged setup was placed in a hydraulic press constrained with steel-made spacers to ensure 40% V_f for composites. After manufacturing, flax-PMMA composites (Dry, RT, RH) were stored in a controlled environment (50% RH, 23 °C) for three months to reach equilibrium before further characterisation. The weight gain values of Dry and RT composites at equilibrium were respectively 2.3 ± 0.1 wt% and 0.2 ± 0.1 wt%. The weight of RH-type composites was reduced by 4.1 ± 0.2 wt% upon reaching an equilibrium due to moisture desorption of swollen fibres. The relative humidity (RH) conditionings were performed by a humidity chamber (model VC 0018, Vötschtechnik, Balingen, Germany). After reaching the equilibrium, the volumetric fraction of porosities for Dry and RT composites was 0.2 ± 0.05% and RH-type composites had an average porosity of 4.33 ± 0.29%. The fibre volume fractions of composites were 41.91 ± 1.92% (for Dry), 39.27 ± 1.72% (for RT), and 45.02 ± 3.05% (for RH). The volume fraction of fibres and porosities were analysed with X-ray computed tomography (UniTom HR, TESCAN, Ghent, Belgium) with a voxel size of 800 nm.

A band sawing machine (model RBS904, Ryobi, Hiroshima, Japan) was used to cut fabricated laminates into standard specimen dimensions. Specimen edges were polished to a final finish so that fibres in each ply were observable in a visible light microscope.

4.2 Characterisation methods

4.2.1 Spectroscopy analysis

The surface chemistries of modified and unmodified flax fibres were analysed by Fourier transform infrared (FTIR) spectroscopy and X-ray photoelectron spectroscopy (XPS).

The FTIR device was Perkin-Elmer Spectrum One (Perkin-Elmer, Beaconsfield, UK) equipped with the Universal Attenuated Total Reflectance (ATR) sampling accessory. The sampling accessory had a Diamond/ZeSe crystal with a 1.66 μm depth of penetration. Transmittance spectra were recorded within the 4000 to 600 cm^{-1} range and a 0.5 cm^{-1} resolution.

The XPS analysis was performed by employing a non-monochromatic Al Kα X-ray source and VG Microtech CLAM 4 hemispherical electron spectrometer. The spectra were collected on a circular analysis area with 0.6 mm in diameter in the following order C 1s, O 1s, survey scan, Na 1s, S 2p. The C 1s were repeated to check the possible X-ray-induced damage. The background-subtracted XPS spectra were least-squares fitted with a combination of symmetric Gaussian Lorentzian component line shapes. The binding energy scale was calibrated according to C 1s C–C/H peak at 284.8 eV. The relative atomic concentrations were calculated using Scofield photoionisation cross-sections.

4.2.2 Interfacial adhesion: Microbond testing

The effect of fibre surface modifications on the apparent interfacial shear strength (IFSS) between flax fibres and epoxy resin was studied with the microbond technique. For the test specimen preparation, single flax fibres were extracted from

flax fabrics by tweezers under an optical microscope and fixed on a stainless-steel sample holder with epoxy glue. The average diameter of single flax fibres was 15 ± 3 μm. The flax fibres were oven-dried (115 °C for 2 hours) before droplet deposition. Droplets of different sizes were deposited on flax fibres with FIBRODrop (Fibrobotics Oy, Tampere, Finland) device based on the resin dip method. The average embedded length of the droplets was 75 ± 17 μm. Droplets that had a higher volume than the single flax fibre were selected for testing. The microbond measurements were performed with FIBRObond (Fibrobotics Oy, Tampere, Finland) [85] device with 1 N load cell and 0.008 mm/s loading rate. The diameter of the fibres and the embedded length of the droplets were captured before each measurement with an optical microscope (model UI-3370SE, IDS, Germany) of the FIBRObond device. During the test, microvices sheared the droplets until complete debonding. The linear regression slope of the maximum debonding force of individual droplets versus the embedded area was considered the apparent IFSS. In total, 20 individual droplets were tested for each series of fibres.

4.2.3 Interfacial adhesion: In-plane shear and transverse tensile/flexural testing of composites

The effect of fibre modifications on the interfacial adhesion between fibre-matrix at the macroscale level was assessed by quasi-static tensile and flexural testing of composites with a universal testing machine (model 5967, Instron, MA, USA). The average mechanical properties of seven successful quasi-static test results, which failed within the specimen's gauge length, were reported for each composite system.

The in-plane shear testing of composites with $[+45/-45]_{SE}$ lay-ups was performed according to the ASTM D3518 testing standard by 30 kN load cell and 5 mm/min displacement rate. The specimens contained four plies of unidirectional flax fibres with a 40% fibre volume fraction. The specimens were prepared in a rectangular shape with dimensions of 250 mm × 25 mm × 2 mm (length × width × thickness). The stress value at the 5% engineering shear strain was reported as the maximum in-plane shear strength (τ_{12}^{max}) of composites. The in-plane shear stress was calculated based on the $\tau_{12} = F/(2A)$ formula, where F is the applied force, and A is the average cross-sectional area measured from three points along the gauge length of the specimens. The engineering shear strain was calculated based on the $\gamma_{12i} = \varepsilon_{Li} - \varepsilon_{Ti}$ formula, where γ_{12i} is the engineering shear strain at the i-th data point, ε_{Li} is the longitudinal normal strain at the i-th data point, and ε_{Ti} is the lateral normal

strain at the i-th data point. The shear chord modulus of elasticity was determined based on the $G_{12}^{chord} = \Delta\tau_{12}/\ \Delta\gamma_{12}$ formula. The $\Delta\tau_{12}$ is the difference in applied engineering shear stress between the two shear strain points, and $\Delta\gamma_{12}$ is the difference between the two engineering shear strain points (nominally 0 to 0.004).

The tensile performance of unidirectional composites with $[90]_4$ lay-up was assessed with 500 N load cell and 1 mm/min displacement rate according to the ASTM D3039 testing standard. The specimens were prepared in a rectangular shape with dimensions of 175 mm × 25 mm × 2 mm (length × width × thickness) and 40% fibre volume fraction. The transverse chord modulus of elasticity of composite specimens was calculated within the 0 to 0.001 absolute strain range according to the ASTM D3039 testing standard.

To ensure tensile failure within the gauge length of the specimens, glass fibre-epoxy tabs were applied with two-component epoxy glue (DP 460 Scotch-Weld, 3M, Minnesota, USA). Tabs had a $[+45/-45]_{SE}$ lay-up configuration and were 2 mm thick. Tabs were tapered at 45° to provide a smooth transition from the specimen to the tabbing area and avoid stress concentration.

The tensile tests were monitored with a stereo optical extensometer (StrainMaster Compact, LaVision, Göttingen, Germany) comprising two fixed optical cameras and an integrated LED illumination source. The full-field strain evolution during the tests was analysed using Digital Image Correlation (DIC) method. The cameras had a 5 MP resolution, a field-of-view of 120 × 140 mm^2, a spatial resolution of 52 μm/pixel, and a fixed working distance of 250 mm. Given that the position of the cameras was fixed with one another, a permanent spatial calibration was used to calibrate both intrinsic and extrinsic parameters of the system. The data was evaluated using the StrainMaster DIC software package (LaVision). During testing, the force data were simultaneously acquired using an analogue to digital converter to be associated with the deformation measured using DIC.

The transverse flexural performance of unidirectional composites was assessed with a 5 kN load cell and 2 mm/min displacement rate according to the ASTM D7264 testing standard. The specimens were prepared in a rectangular shape with dimensions of 153 mm × 13 mm × 4 mm (length × width × thickness) and 40% fibre volume fraction. For these four-point bending tests, only the failure strength of composites was reported, as the beam deflection was not monitored with an extensometer.

4.2.4 Quasi-static in-plane tensile testing of composites

Quasi-static in-plane tensile testing of composites was carried out with a universal tester (model 5967, Instron, MA, USA) according to the ASTM D3039 standard. The load cell and displacement rate were 30 kN and 2 mm/min, respectively. Depending on the study, composites had either $[0]_4$ lay-ups or $[(0,90)]_4$ lay-ups. The $[0]_4$ lay-up was composed of four unidirectional flax fibre plies with specimen dimensions of 250 mm × 15 mm × 2 mm. The $[(0,90)]_4$ lay-up was composed of four twill 2 × 2 woven fabric plies with specimen dimensions of 250 mm × 25 mm × 2 mm (length × width × thickness). The fibre volume fraction of composites was 40%. Tapered glass-epoxy tabs were applied to the specimens. The tensile tests were monitored with a stereo optical extensometer (StrainMaster Compact, LaVision, Göttingen, Germany). The composites' longitudinal chord modulus of elasticity was calculated within the 0 to 0.001 absolute strain range according to the ASTM D3039. An average of seven test results were reported for each material system.

4.2.5 Fatigue testing of composites

The fatigue performance of composites was evaluated by performing cyclic loading tests following the ASTM D3479 standard. The lay-up and fibre volume fraction of composites were $[(0,90)]_4$ and 40%, respectively. The $[(0,90)]_4$ lay-up was composed of four twill 2 × 2 woven fabric plies with specimen dimensions of 250 mm × 25 mm × 2 mm (length × width × thickness). Tapered glass-epoxy tabs were used to reduce the stress concentration at the gripped section of the specimens. The tests were performed with a servo-hydraulic tester (MTS 180, Minnesota, USA) equipped with a 100 kN load cell and a gauge length of 150 mm. A constant-load amplitude and a sinusoidal wave shape were applied at a frequency of 5 Hz. The loading frequency of 5 Hz was chosen to avoid any temperature rise above 10 °C (see ASTM D3479). The stress ratio (R) of the nominal minimum to maximum applied stress was 0.1. Stress-cycles to failure (S-N) graphs were acquired by registering the number of cycles to failure and the nominal maximum stress for each specimen. The load levels (90%, 80%, 70%, and 50%) for the low-cycle fatigue tests were defined with respect to the ultimate tensile strength (S_0). Three specimens per load level (excluding any grip failure) were reported. The surface temperature of the specimens during testing was monitored by a longwave IR camera (model Ti400, Fluke, Washington, USA) with thermal sensitivity of 0.05 °C at 30 °C. The specimens were stored for one week in the fatigue testing ambient for environmental stabilisation.

4.2.6 Low-velocity impact testing of composites

The low-velocity impact performance was studied with an instrumented drop-weight tester (Type 5, Rosand, Ohio, USA) without rebound impacts per ASTM D7136 and ASTM D5628 standards. The flax fibre reinforced composites had a cross-ply configuration with a $[0/90]_{3SE}$ lay-up, comprised of 12 unidirectional fabric layers. Rectangular-shaped specimens with dimensions of 60 mm × 60 mm × 5 mm (length × width × thickness) were clamped between two steel fixtures with a circular test area (diameter 40 mm) representing fixed support. The drop height of the impactor (2772 gr) was adjusted to, e.g., 0.33 m to reach kinetic energies of 9 J. The impact performance of composites was studied in a wide range of kinetic energies starting from 3 J up to complete perforation by 3 J sequences. A hemispherical steel-made indenter (diameter 12.7 mm) was fixed to the impactor. The contact force was measured using a load sensor (60 kN) between the head and the impactor structure. The force data were recorded at a 180 kHz frequency. The displacement of the impactor was numerically integrated from the measured contact force-time curve. For each impact energy level, three composite specimens were tested.

The rear surfaces of composites (opposite to the impacted surface) were in-situ monitored with synchronised high-speed optical camera (Fastcam SA-X2, Photron, Tokyo, Japan) and high-speed IR camera (Fast IR-1500 M2K, Telops, Quebec City, Canada). An unprotected gold mirror (PFSQ20-03-M03, THORLABS, Newton, United States) at 80 cm lens distance and a conventional mirror at 35 cm lens distance were placed at an angle below the impact specimen to reflect the IR electromagnetic radiation and full-field deformations respectively. The emissivity of the composites in the infrared range (ability to emit infrared energy) was measured to convert radiometric temperature to surface temperature. The schematic representation of the drop-weight impact testing setup coupled with high-speed optical and IR cameras is presented in Figure 6.

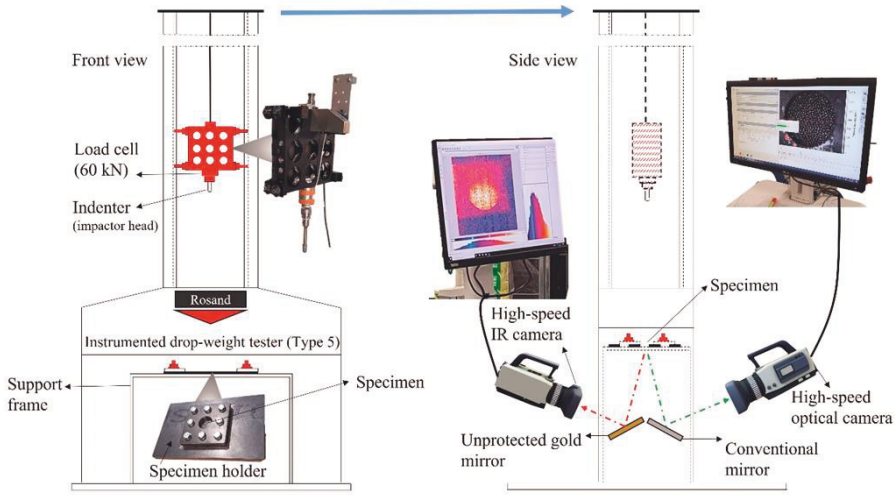

Fig 6. Schematic representation of the drop-weight impact testing setup coupled with high-speed optical and IR cameras [Paper IV, Supplementary data].

The infrared images were taken at an acquisition rate of 10000 Hz and an image resolution of 128 × 112 pixels. The IR camera measures radiometric temperature, which relies on the target being a black body or having user input emissivity values. The emissivities of the investigated composites were determined by coating half of the composite specimens with a thermographic paint (type HERP-HT-MWIR-BK-11, LabIR, Teslova, Czech Republic) to create a homogeneous reference layer with known emissivity. The surface of the specimen was heated by a heat gun until 50 °C. The reference painting allowed for the determination of surface temperature, which was compared to the radiometric measurements from the composite surface to determine its emissivity. The emissivity values determined for flax-PMMA and flax-epoxy composites were 0.95 and 0.88, respectively.

The unprotected gold mirror's reflectance was approximately 98% in the infrared wavelength range and was considered in the radiometric temperature calculation. The radiometric temperature of the specimens was then converted to surface temperature with the following equation $T^{\text{True}} = T^{\text{Radiometric}}/\sqrt[4]{\varepsilon}$ where ε is the emissivity [86]. The IR data analysis was performed with the Reveal software (Telops, Quebec City, Canada).

The full-field strain measurements were carried out using a high-speed optical camera (Fastcam SA-X2, Photron, Tokyo, Japan), which imaged the rear surface of the composite specimen through a conventional mirror. The optical cameras imaged

the specimen at a 35 cm lens distance. The specimen was illuminated using Ultra-Bright LED modules (Visual Instrumentation Corporation, Lancaster, United States). The optical images were acquired at a rate of 10000 Hz with a resolution of 768 × 640 pixels and an exposure time of 20 μs. The full-field strains were calculated using 2D-DIC with the commercial package DAVIS10 (LaVision, Göttingen, Germany). The optical images were processed with the subset size of 41 × 41 pixels, step size of 13 pixels, and virtual strain gauge (VSG) of 67 pixels for the results presented in this article. The matching process of the DIC analysis was performed using an affine shape function and a sixth-order spline sub-pixel image interpolation scheme with the zero-normalised sum of squared differences (ZNSSD) criteria.

The in-situ surface deformations on the rear surface of specimens during impact testing were plotted as von Misses strain maps and superimposed on high-speed optical images. Generally, the von Mises strain can be determined if a given material will yield or fracture. The von Mises strain condenses the three-dimensional strain state at any given point into an effective scalar strain value equivalent to the strain of a uniaxial load state. The equivalent von Mises strain was computed in the DaVis program or StrainMaster DIC. As the DIC imaging was performed in a 2D mode, the von Mises strain maps had similar values for both plane stress and plane strain analysis.

The acquisition on both optical and infrared systems was synchronised using a waveform generator (33500B, Keysight Technologies, Santa Rosa, United States). The trigger to start data acquisition on the camera systems was also recorded on the same oscilloscope that recorded load to allow for accurate temporal synchronisation of load with strain and temperature. More information on the synchronisation of high-speed optical and infrared systems can be found in the article by Soares et al. [87].

4.2.7 X-ray computed tomography (X-CT)

The volume fraction of fibres and porosities within composites were investigated by a high-resolution X-CT (UniTom HR, TESCAN, Ghent, Belgium). The scanner was equipped with a 160 kV/25 W nanofocus X-ray tube, a tungsten reflection target, a low radiation detector of 2916 × 2280 pixels, and a 75 μm pixel pitch. The scans were acquired at 60 kV and 0.7 W, with a voxel size of 800 nm. In total, 2800 radiographic projections were acquired over a 360º angle sample rotation, each with

an exposure time of 900 ms and frame averaging of 3 to reduce the projection's random noise. No physical filters were used for the acquisition of the projections.

The internal damage patterns of impact-tested composite specimens were characterised with a lower resolution X-CT (UniTOM XL, TESCAN, Ghent, Belgium). The scanner was equipped with a 230 kV/300 W microfocus X-ray tube, a tungsten reflection target, a 2856 × 2856 pixels detector, and a 150 μm pixel pitch. The scans were acquired at 60 kV and 35 W, with a voxel size of 35 μm. In total, 2877 radiographic projections were acquired over a 360º angle sample rotation, each with an exposure time of 67 ms and frame averaging of 3 to reduce the projection's random noise.

In both cases, the acquired radiographic projections were reconstructed into tomographic slices by applying a filter back-projection algorithm in the TESCAN reconstruction software Panthera. Image analysis and visualisation were performed in the software Avizo 3D v2021.1.

4.2.8 Optical and electron microscopy

The fracture surface analysis of composites was carried out with a ULTRAplus (Zeiss, Oberkochen, Germany) scanning electron microscope (SEM). A thin platinum-palladium (Pt-Pd) coating was used to ensure enough conductivity for the SEM samples.

The post-impact assessment of failure mechanisms in the impacted specimens was evaluated with a DM 2500 M (Leica, Wetzlar, Germany) optical microscope using a dark field mode. The specimens were embedded in an epoxy resin before polishing. The surface deformations on the rear surface of composites (opposite to the impacted surface after the drop-weight test) were inspected with three-dimensional optical profilometry with an InfiniteFocus G5 (Alicona, Graz, Austria).

5 RESULTS AND DISCUSSIONS

This chapter provides a coherent overview of the key results based on the appended journal articles. The chapter's primary focus is the effect of fibre surface modification strategies on the low-velocity impact and fatigue performance of flax-epoxy and flax-PMMA composites. For the supporting information, readers are referred to the appended journal articles.

The contribution of various surface modification strategies on the low-velocity impact perforation energy of flax-epoxy and flax-PMMA cross-ply composites are presented in Figure 7. Regardless of the matrix type, the perforation energy of flax-epoxy (4.2 J/mm), flax-PMMA (4.1 J/mm), and polylactic acid (PLA) based flax fibre composites (3.5 J/mm, [88]) are comparable. This shows the dominating effect of brittle flax fibres on the impact resistance of composites. As fibre rupture is the main limiting factor for perforation energy, composites processed with more ductile polymers can only enhance energy absorption [49,51,89]. However, the perforation energy of flax fibre reinforced polypropylene (PP) composites (4.9 J/mm) reported by Ramakrishnan et al. [51] is 14% higher than the flax-epoxy and flax-PMMA. The 14% higher perforation energy of flax-PP composites can be ascribed to the weak interfacial strength between flax and PP, which promotes energy dissipation through interfacial sliding [90]. Indeed, PP is highly non-polar and not compatible with the polar characteristic of flax fibres [57]. The apparent interfacial shear strength of flax-PP (4.9 ± 0.7 MPa [91]) is 69% and 67% lower than flax-epoxy (16.1 ± 0.8 MPa) and flax-PLA (15.3 ± 3.3 MPa) [92] respectively. The perforation energy of cross-ply glass-PP composite (5.1 J/mm [93]) is 6%, 21% higher than cross-ply flax-PP and flax-PMMA counterparts. The better impact resistance of glass fibre reinforced composites can be ascribed to the higher ductility of E-glass compared to flax fibres. However, the mechanical performance and competitiveness of flax fibre composites can be modulated by adjusting their interfacial adhesion and toughness. The effects of microscale fibre modification strategies on the impact and fatigue performance of flax fibre composites are discussed in the following subsections.

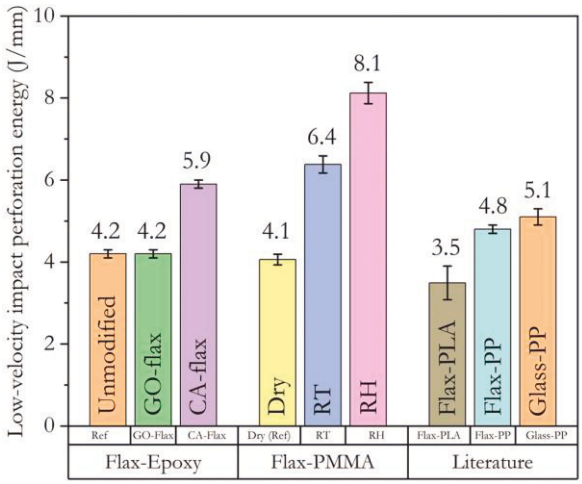

Fig 7. Thickness-normalised impact perforation energy of cross-ply flax fibre composites with 40% fibre volume fraction [modified from Papers II-IV]. The perforation energy of cross-ply flax-PLA [88], flax-PP [51], and Glass-PP [93] composites are provided from the literature.

5.1 Effect of graphene oxide fibre surface modification

This section describes the effect of interfacial strength on the fatigue performance and impact resistance of flax-epoxy composites based on the results from Paper I and Paper II. It was hypothesised that the surface functionalisation of flax fibres with oxygen-rich multilayer GO crystals could promote the interfacial adhesion and effective load transfer between flax fibres and epoxy resin which is promising for the fatigue performance of composites. However, increasing the interfacial strength might potentially embrittle the flax-epoxy composites and decrease their impact resistance. The following paragraphs elaborate on the effect of GO treatment on the microscopic and macroscopic properties of flax fibres and their composites.

The surface chemistry of fibres has a significant role in the interfacial adhesion between fibre and matrix. The XPS spectra of unmodified flax fibres (Flax), a graphene oxide film (GO), and GO-modified flax fibres (GO-flax) are presented in Figure 8. Based on the XPS analysis, the O/C ratio of unmodified flax is 0.4. The O/C ratio of 0.4 for unmodified flax is below the theoretical O/C ratio of 0.83 for pure cellulose and closer to the theoretical O/C ratio of 0.35 for lignin [16].

Therefore, the surface of flax is rich in aliphatic carbon components containing a greater portion of lignin and extractives rather than pure cellulose. Analysis of the aliphatic carbon region (C 1s in Figure 8 a, d) is necessary to understand the flax fibres' surface composition further. The 284.8 eV peak in Figure 8 (d) corresponds to unoxidised C–C bonding and hydrocarbons, while the peaks between 286 eV and 289 eV correspond to oxidised C species so that the oxidation state increases with the binding energy. The four components in C 1s of flax fibre (Figure 8 d) were explained by Fuentes et al. [14] as (1) C–(C, H) linkages of lignin and extractives (at 284.8 eV peak); (2) CC–OH groups of cellulose, pectin, lignin and extractives, as well as CC–OC–C linkages of lignin and extractives (at 286.4 eV peak); (3) C=O groups in lignin and extractives, as well as OC–CC–O linkages in cellulose and hemicelluloses (at 287.4 eV peak); (4) COOH groups of hemicelluloses, as well as COOC and COOH groups of extractives (at 288.6 eV peak). Considering the XPS analysis, surface modification of flax fibres with oxygen-rich GO crystals might promote further interactions between flax and epoxy resin by enhancing the O/C ratio or the ratio of oxidised C in flax fibres.

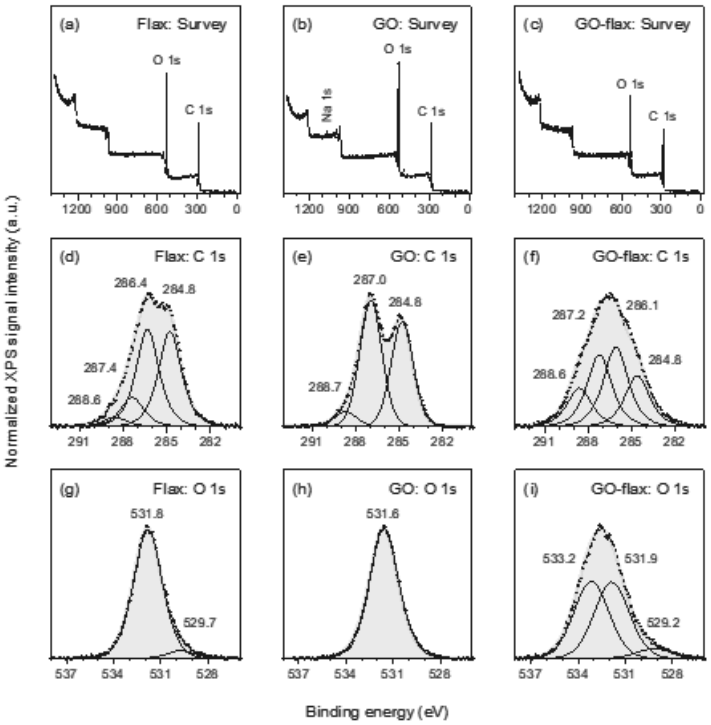

Fig 8. XPS spectra of flax, GO, and GO-flax. (a)–(c) survey scans, (d)–(f) C 1s, and (g)–(i) O 1s core level spectra [Paper II].

It is often reported that the O/C ratio for natural fibres decreases by GO-modification due to the presence of oxygen-containing groups in GO [25]. Contrary to common expectations, the overall O/C ratio of GO and GO-modified flax fibres is similar to the unmodified flax fibres and near 0.4. However, the GO-modified flax contains 50% more oxidised C than flax fibre and GO. The O 1s transition shows one prominent peak below 532 eV on flax and GO, representing O–C and O=C bonds. An interesting change is observed in O 1s on GO-modified flax fibres. A new component/peak appears at 533.2 eV that is not present in unmodified flax or the graphene oxide film. Overall, the C 1s and O 1s spectra of GO-flax cannot be fitted using a combination of the line shapes of flax and GO, suggesting bond formation between flax and GO. One explanation for the new high binding energy component in O 1s is that hydrogen bonding is formed between GO and flax, as the detected binding energy corresponds, e.g., to water or C–OH [94]. The observed changes in the O 1s component ratios show that when the flax fibres are dip-coated in the aqueous dispersion of graphene oxide, about half of the oxygen in O–C/=C is reacting to C/H–O–H (see Table 1 in Paper II: concentration of O 1s: O–C/=C). At the same time, the relative amount of (H–)O–C=O increased in C 1s. The higher degree of oxidised C can promote the further formation of hydrogen bonds between flax fibres and epoxy functional groups of the resin. For instance, the C−N bond can form between amine hardener and GO-treated flax fibres by ring-opening polymerisation.

The contribution of graphene oxide treatment of flax fibres on the fibre-matrix adhesion is presented in Figure 9. The slope-based results (linear regression) in Figure 9 suggest an apparent interfacial shear strength (τ^{app}) of 33 ± 3 MPa for GO-flax-epoxy which is 43% higher than 23 ± 3 MPa for flax-epoxy. The higher τ^{app} of GO-modified fibres is related to their higher degree of oxidised C, which creates additional hydrogen and covalent bonds between flax and epoxy. The mechanical interlocking between wrinkled GO crystals and epoxy resin is an additional factor which can potentially contribute to the interfacial adhesion between flax fibres and epoxy resin. Another observation in Paper I (Figure 5 in Paper I) was the movement of the failure onset locus towards the matrix in the microbond test.

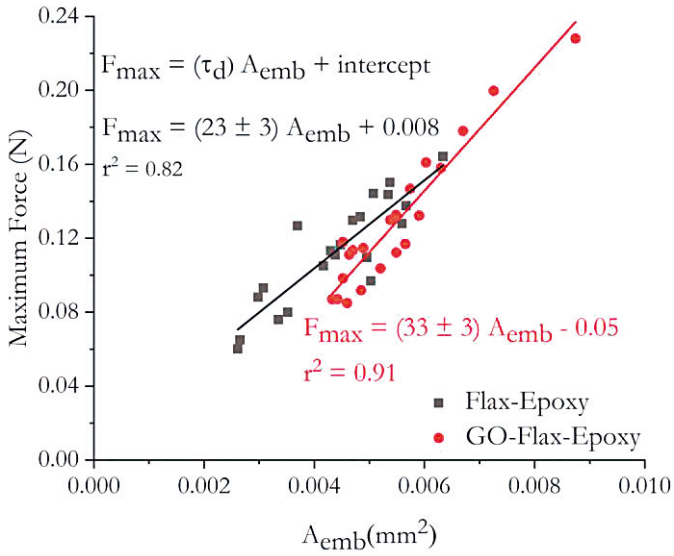

Fig 9. Microbond test results for flax-epoxy and GO-flax-epoxy [Paper I].

The better interfacial adhesion with GO-modified fibres can benefit the macroscopic performance of flax-epoxy composites, especially when subjected to fatigue loading. The collected *S-N* data and normalised fatigue data from flax-epoxy specimens with $[(0,90)]_4$ lay-ups are presented in Figure 10 (A) and Figure 10 (B), respectively.

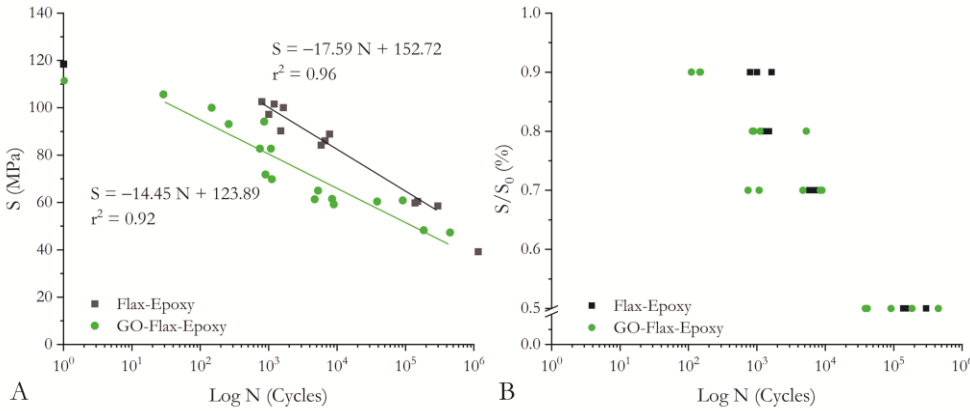

Fig 10. Collected *S-N* data (A) and normalised fatigue data (B) of flax-epoxy composites with $[(0,90)]_4$ lay-up [Paper II].

In Figure 10 (A), the average tensile strength of GO-modified composites at the first cycle (S_0 = 110 ± 3 MPa), is 8% lower than the unmodified flax-epoxy composites

(S_0 = 120 ± 5 MPa), which is also reflected in the fatigue results. The relatively lower S values of GO-modified specimens in Figure 10 (A) can be related to the effect of water immersion on the tensile performance of flax fibres. Indeed, the pectin and hemicellulose within flax fibres can be partially dissolved in water during the GO fibre modification and alter the tensile performance of fibres [62]. At the 90% loading ratio (in Figure 10 B), the number of cycles to failure of GO-modified specimens (10^2 cycles) is one order of magnitude lower than unmodified flax-epoxy (10^3 cycles). However, at a loading range of 50%–80%, both series are comparable in terms of cycles to failure. Therefore, the S-N slope of GO-modified composite (−14.45) is less steep than unmodified flax-epoxy (−17.59), indicating a 17% slower fatigue strength degradation rate within the loading range of 50%–90% for GO-flax-epoxy. The more stable fatigue performance of GO-modified specimens can be ascribed to their low void content (less than 0.04% compared to 2.41% for unmodified flax-epoxy [Paper II, Paper I]) and 40% higher interfacial adhesion with epoxy resin which was studied through microbond tests. The more ductile behaviour of GO-modified specimens within the 50%–80% loading range (compared to the quasi-static and 90% loading cases) can be related to the sliding within multilayer GO crystals which is promoted by cyclic loading and friction between fibre and matrix [66]. Also, under cyclic fatigue loading, the epoxy functional groups of graphene oxide can potentially transform into ether groups [95]. The bond angle within ether groups (R–C–R) can alter and contribute to energy dissipation under cyclic loading conditions [95]. The fracture surface investigations after fatigue testing of specimens are provided in Paper II (see Figure 5 and Figure 6 in Paper II). The fracture surface of cross-ply flax-epoxy composites after fatigue failure was dominated by brittle fibre failure with smooth fibre surfaces. However, fibre pull-outs and resin residues on fibres were captured in the fracture surface of GO-flax-epoxy specimens after fatigue testing. The traces of fibre pull-out suggested that the GO-modification enhances the energy dissipation of composites through fibre-matrix sliding and shearing. The resin residues on fibres demonstrated good compatibility between the epoxy resin and GO-modified fibres.

From the fatigue design point of view, larger specimen sets with different loading conditions (e.g., compression-tension) and information about the expected in-service life are required. However, the preliminary fatigue testing data presented in Figure 10 provides design insights about the fatigue performance of flax-epoxy specimens with $[(0,90)]_4$ lay-ups. In Figure 10 (B), the variation in the number of cycles until failure for flax-epoxy is small, which is promising. However, coating flax

fibres with GO has increased the variation in the data, which might be related to the inhomogeneous nature of GO crystals (e.g., degree of functionality) and the nonuniform distribution of GO on fibres. The run-out threshold for flax-epoxy specimens was at the 30% load level, where the specimens did not fail up to 10^6 cycles. Also, at 50% load level, GO-modified and unmodified specimens do not fail until 10^5–10^6 cycles, suggesting reliable and long service life.

The impact kinetic energy-time histories of cross-ply flax-epoxy composites with $[0/90]_{3SE}$ lay-up are outlined in Figure 11. The impact energy is partly recovered at kinetic energies below the perforation energy, as shown in Figure 11 (A). At 21 J kinetic energy, the impactor perforates the specimens, and almost all the impact energy is absorbed by plastic deformations. In Figure 11 (B), the internal damage patterns of GO-flax-epoxy and flax-epoxy at perforation energy are similar and comprised of ply failure, delamination, and fibre pull-outs.

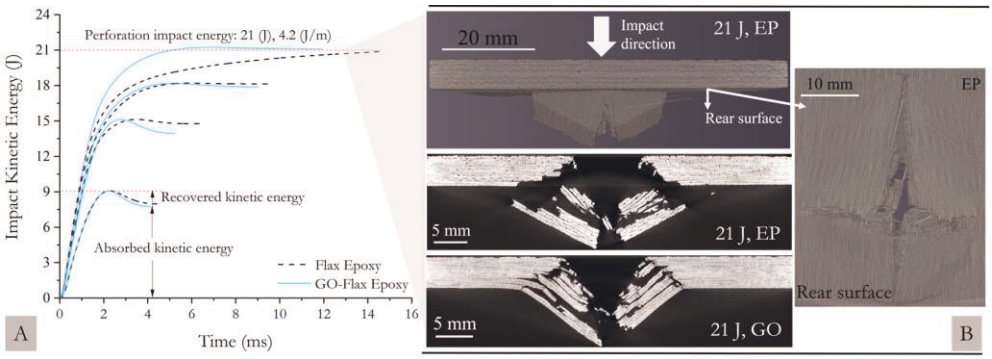

Fig 11. Effect of GO-modification on the energy-time history of composites (A) and internal damage patterns at perforation based on X-CT (B) [Paper II].

In Figure 11 (A), the thickness-normalised impact perforation energy for both GO-flax-epoxy and flax-epoxy composites is 4.2 ± 0.1 J/mm. The main reason for the limited perforation energy of flax fibre composites is the brittle nature of fibres. As a result, increasing the interfacial adhesion strength with GO-modification does not alter the limited perforation energy of flax-epoxy composites. Therefore, it is necessary to modify the ductility of fibres and interfacial toughness to achieve a better impact resistance for flax fibre composites. However, it should be noted that at kinetic energies below the perforation, GO-modification reduces the absorbed kinetic energy and enhance the recovered kinetic energy for flax-epoxy composites

(see Figure 11 A). This aspect is further discussed by considering the internal damage patterns of composites in Figure 12.

In Figure 12 (A), at the kinetic energy of 9 J (1.8 J/mm), half of the flax-epoxy plies have failed in a brittle manner with minor delamination. Compared to unmodified flax-epoxy, the crack length on the rear surface (tension side) of GO-modified composite is limited and travels through a more tortuous path. The cumulative lengths of delamination lines for GO-flax-epoxy at 9 J (43 mm) are 50% higher than the similar values for flax-epoxy at 9 J (21 mm). A similar observation is evident for 15 J kinetic energy in Figure 12 (B). The higher extent of delamination and energy dissipation in GO-modified composites can be related to the multi-layer nature of graphene oxide crystals. The shear strength in multilayer graphene oxide could be as low as 5.3 ± 3.2 MPa [96]. The weakly bonded graphene layers can potentially promote energy dissipation through interfacial sliding between fibre and matrix and sliding between individual graphene oxide layers within GO. A recent study showed that surface modification of carbon fibres with graphene oxide deposits (5–50 μm in diameter and composed of 5–10 GO layers) enhanced the interfacial damping performance of carbon-epoxy composites by 113% based on the loss factor acquired from dynamic mechanical analysis (DMA) [66]. Evidently, at kinetic energies below the perforation energy, the GO-modification reduces the extent of fibre failure in flax-epoxy composites by promoting interlaminar delaminations. Therefore, the GO-modified composites have higher elastically recovered kinetic energy values compared to unmodified flax-epoxy composites (see Figure 12 C). Further studies, such as compression after impact (CAI), are needed to understand better the contribution of GO-modification on the impact tolerance of flax-epoxy composites. However, GO-modification might have a positive effect on the impact tolerance of composites as it modifies the interfacial shear strength of composites.

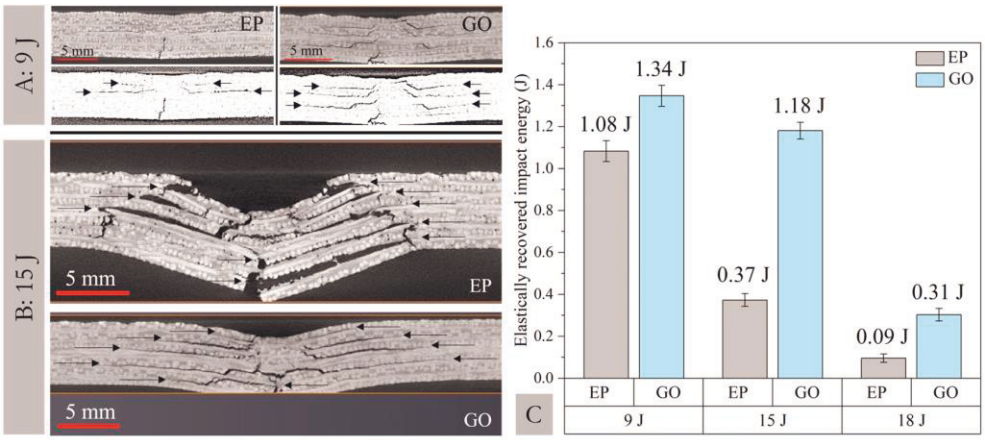

Fig 12. X-CT images of unmodified (EP) and GO-modified (GO) flax-epoxy composites tested at 9 J (A) and 15 J (B) kinetic energies and elastically recovered impact energy of composites (C) [modified from Paper II].

In summary, the effect of GO-modification on the microscale and macroscale properties of flax-epoxy was investigated. The XPS analysis showed that the surface chemistry of flax fibres is composed of lignin, pectin, and other extractives rather than pure cellulose. The GO-modification enhanced the oxidised C content of flax surfaces by 50%, which promoted hydrogen and covalent bond formation between flax and epoxy resin. As a result, the GO-modification enhanced the apparent interfacial shear strength of flax-epoxy by 40%. At 50% load level, GO-modified and unmodified specimens did not fail until 10^5–10^6 cycles, suggesting a reliable and long service life for flax-epoxy composites. The fatigue run-out threshold was 30% load level. The GO modification decreased the porosity of flax-epoxy composites, as described in Paper I–II. As a result, the GO-modification lowered the fatigue strength degradation rate within the loading range of 50%–90% by 17% without a negative effect on their impact resistance. The higher interfacial strength provided by GO-modification had a minor effect on the impact resistance of flax-epoxy composites. However, it was envisioned that GO-modification could positively affect the impact tolerance (e.g., CAI) of flax-epoxy composites by providing better interfacial strength. It was concluded that the interfacial toughness and ductility of flax fibres should be modified to address the limited perforation energy of flax fibre composites.

5.2 Effect of cellulose acetate fibre surface modification

Here, the effect of interfacial toughness on the impact resistance of flax-epoxy is studied based on the thermoplastic coating of flax fibres with cellulose acetate (CA). It was hypothesised that applying a ductile layer between fibre and matrix can enhance the ductility of brittle flax-epoxy composites and modify their limited impact resistance. The following paragraphs elaborate on the effect of CA-modification on the microscopic and macroscopic properties of flax fibre composites based on the results from Paper III.

The FTIR spectra (Figure 13 A) of pure CA have characteristic peaks at 1735 cm^{-1} and 1221 cm^{-1} related to the stretching vibration of the C=O bond of ester groups and the C−O bond of ether groups, respectively [97]. Those distinct peaks of CA are shifted to 1740 cm^{-1} and 1232 cm^{-1} in CA-modified flax fibres, indicating hydrogen bonding between C=O and C−O groups of CA and hydroxyl groups of flax fibre. The FTIR results indicate good compatibility and bonding between flax and CA. It is also shown that CA forms a uniform coating on flax fibres with an approximate thickness of 3 μm (see Paper III, Figure 2). The CA-coating decreases the apparent interfacial shear strength (τ^{app}) of flax-epoxy by 22% (Figure 13 B). The lower τ^{app} of CA-modified elementary flax fibres can be the uniform CA coating which reduces the effective contact area for chemical and physical bonds between epoxy and flax. However, the τ^{app} of 17 MPa can still provide sufficient bonding for effective load transfer between fibre-matrix.

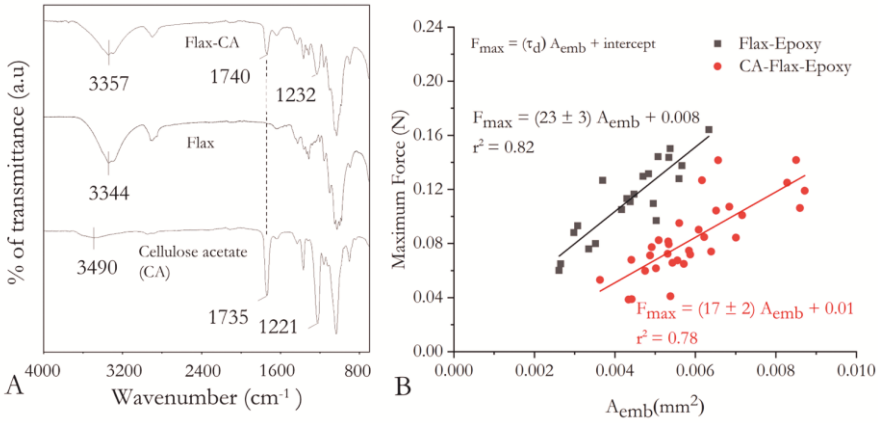

Fig 13. The FTIR spectra of CA-modified fibres [Paper III] (A) and the effect of CA modification on the microbond test results (B).

The contribution of CA-modification on the quasi-static tensile performance of flax-epoxy composites is presented in Table 4 and Figure 14. The UD flax-epoxy and CA-flax-epoxy composites have a comparable modulus of elasticity (within 0−0.1% strain range) in the range of 24 GPa and average tensile failure strength in the range of 260 MPa. The average in-plane shear strength of CA-modified composites is 22% lower than unmodified composites, which corroborates with the microbond results. However, the failure strains of CA-modified laminates with $[0]_4$ and $[+45/-45]_{SE}$ lay-ups are 13% and 52% higher than the flax-epoxy values. Despite the 22% decrease in the interfacial strength, the increase in strain at failure of CA-modified composites has enhanced their toughness by 22% (for $[+45/-45]_{SE}$ lay-up) and 11% (for $[0]_4$ lay-up) compared to the unmodified flax-epoxy.

Table 4. The average quasi-static tensile properties of flax-epoxy composites with and without CA-modification [Paper III].

Lay-up	Fibre	$E^{(0.1\%)}$ (GPa)	$\sigma^{failure}$ (MPa)	$\varepsilon^{failure}$ (%)	Toughness (MJ/m³)
$[0]_4$	Flax	24.98 ± 0.85	260 ± 7	1.66 ± 0.04	23.8 ± 1.1
	CA-Flax	24.55 ± 0.56	260 ± 11	1.88 ± 0.07	26.6 ± 1.6
$[+45/-45]_{SE}$	Flax	5.21 ± 0.25	67 ± 2	3.72 ± 0.49	19.2 ± 4.5
	CA-Flax	4.82 ± 0.43	52 ± 5	5.64 ± 0.37	23.6 ± 4.3

The contribution of CA-modification on the toughness of flax-epoxy composites is also evident in the tensile failure mode of composites (see Figure 14). The brittle failure mode of flax-epoxy composites (transverse to fibre direction) is altered to ductile failure dominated by shear bands and shear-type failure along the fibre direction in CA-modified composites. Compared to the unmodified flax-epoxy, the higher toughness of CA-modified composites can be ascribed to their higher elongation at failure and plasticity by the inclusion of the thermoplastic phase (CA). Further data on the quasi-static tensile tests and fractographic observations are provided in the appended Paper III.

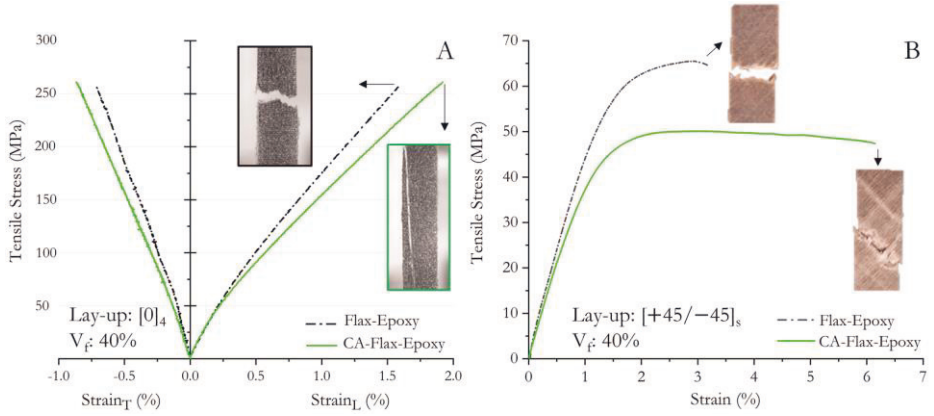

Fig 14. The representative (average) in-plane tensile (A) and in-plane shear stress-strain plots (B) of composites [Paper III].

The impact kinetic energy-time histories of cross-ply composites with $[0/90]_{3SE}$ lay-up are presented in Figure 15. The CA-modification has enhanced the perforation energy of flax-epoxy composites by 40%. The thickness-normalised perforation energy of the tough and ductile CA-modified flax-epoxy (5.9 ± 0.1 J/mm) is higher than the corresponding flax-PLA (by 69%) [88], flax-PP (by 23%) [51], and Glass-PP (by 15%) [93] composites with similar composite and testing configurations. The quasi-static tensile and low-velocity impact results show that interfacial toughening is a promising strategy to achieve a new class of stiff and tough natural fibre composites as environmentally superior alternatives for glass fibre composites.

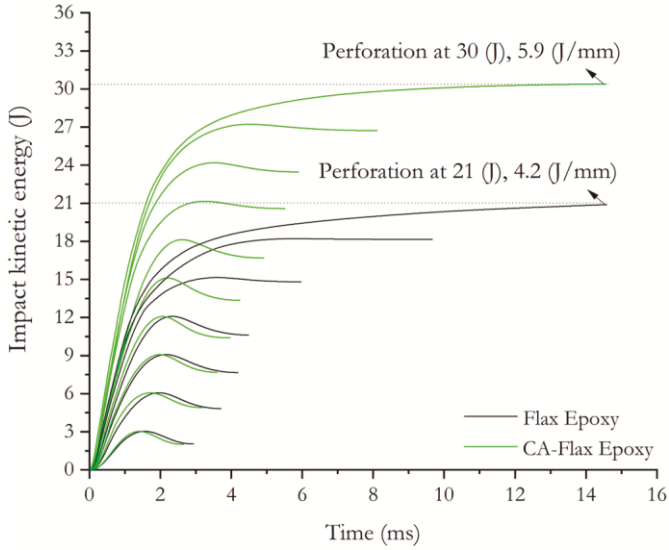

Fig 15. The effect of CA on the energy-time history of composites [Paper III].

The contribution of CA-modification on the impact resistance of flax-epoxy composites at non-perforation kinetic energies is discussed based on the contact force-displacement curves (Figure 16) and internal damage patterns (Figure 17). In general, the contact-force curve in drop-weight impact tests is comprised of three phases: (i) initial linear loading phase, (ii) damage progression in a plateau-type region, and (iii) rebound of the impactor. At maximum contact force by the end of phase-I, the damage initiates on the rear surface of composites as matrix cracking and ply-splitting. These phases are captured and analysed by in-situ synchronised high-speed imaging in Paper IV (see Figure 8 and Figure 9 in Paper IV). The maximum contact force by the end of phase-I for CA-modified composites is higher than unmodified flax-epoxy composites at different kinetic energies (Figure 16 A-C). The higher contact force in CA-modified specimens is related to their enhanced ductility and toughness, which can delay damage initiation and progression. The length of phase-II (penetration phase) is limited in CA-modified specimens compared to unmodified flax-epoxy, which indicates better damage resistance of interfacially toughened composites. In Figure 16 (D), the recovered kinetic energy (the area under the phase-III) of CA-modified composites is higher than unmodified flax-epoxy, which can be ascribed to their higher ductility.

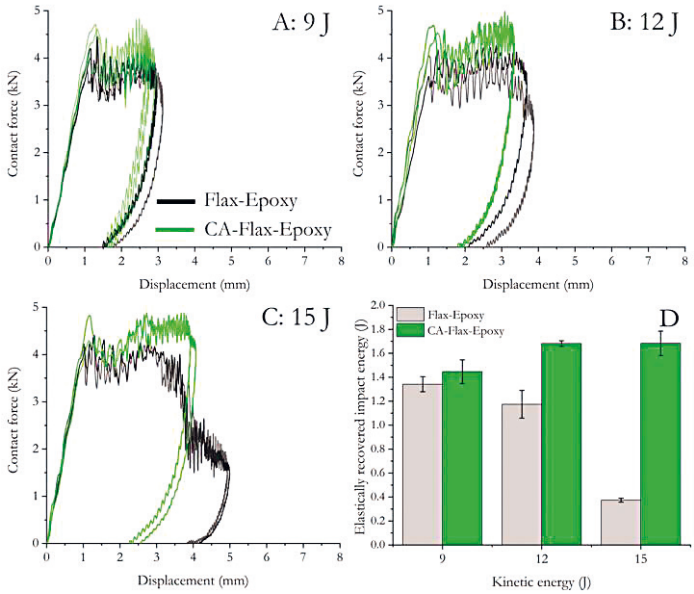

Fig 16. Effect of CA-modification on the contact force-displacement curves (A-C) and recovered kinetic energies of composites (D) [modified from Paper III].

The better impact resistance of interfacially toughened flax-epoxy composites is demonstrated in Figure 17 based on microscopy images from the surface and internal damage patterns of specimens after impact testing. Figure 17 (A) shows the permanent surface deformation maps on the rear surface (tension side) of cross-ply specimens with $[0/90]_{3SE}$ lay-up. These deformation maps were acquired by the profilometry measurements after impact testing. The maps were then superimposed on the rear surface of the composites. Compared to the unmodified flax-epoxy, CA-modified composites have a lower extent of permanent surface deformation and damage at non-perforation kinetic energies. The internal damage patterns of flax-epoxy composites at 15 J kinetic energy are provided in Figure 17 (B-C). The CA-modification of flax fibres has altered the brittle and fibre-dominant failure mode of flax-epoxy composites to interfacial debonding between fibre and matrix.

In summary, the results here showed that the CA-modified composites offer a scarce combination of stiffness and ductility, which enhanced the impact resistance of flax-epoxy composites by 40%. Also, the impact resistance of CA-modified specimens was 14% higher than their glass fibre composite counterparts.

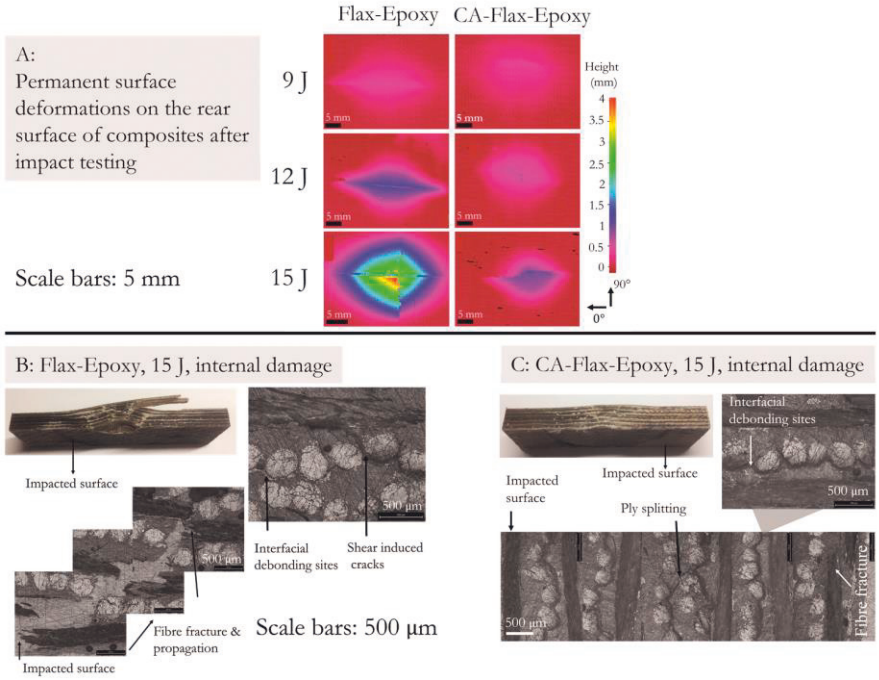

Fig 17. Effect of CA-modification on the rear surface deformation and internal damage patterns of composites [modified from Paper III].

5.3 Effect of environmental preconditioning of fibres

The intrinsic water molecules bound to natural fibres act as a natural plasticiser. For instance, the tensile strain at failure of the flax fibres conditioned at 50% RH (23 °C) decreases by 29% due to oven-drying of fibres, which is a necessary protocol for manufacturing natural fibre composites [34]. This section investigates the effect of environmental preconditioning of flax fibres on the interfacial adhesion and toughness of flax-PMMA composites. It was hypothesised that the moisture-insensitive in-situ polymerisation of flax-PMMA composites with ductile non-dry fibres could modify the limited impact resistance of composites without compromising their good fatigue performance. The following paragraphs elaborate on the microscopic and macroscopic properties of non-dry flax-PMMA composites based on the results from Paper IV.

The internal microstructures of flax-PMMA composites after three months of stabilisation at 50% RH (23 °C) are presented in Figure 18. It should be reminded

that the flax-PMMA composites were processed with oven-dried (Dry) and precondition fibres (RT: at 50% RH, RH: at 90% RH). Based on the X-CT analysis, the volume fraction of porosities is 0.2 ± 0.05% for Dry and RT composites and 4.33 ± 0.29% for the RH-type composites. The fibre volume fractions of composites are 41.91 ± 1.92% (for Dry), 39.27 ± 1.72% (for RT), and 45.02 ± 3.05% (for RH).

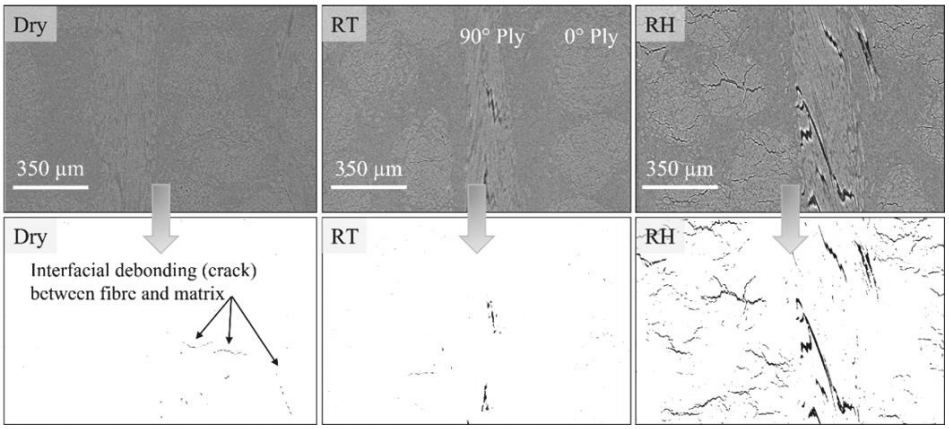

Fig 18. X-CT tomography of flax-PMMA composites after environmental stabilisation at 50% RH (23 °C, for 3 months) [Paper IV].

The similar amount of void content in Dry and RT composites suggests that the extent of fibre swelling and shrinkage for RT composites is limited. Therefore, in Table 5, the transverse tensile strength, which is highly dependent on the interfacial adhesion between fibre and matrix and porosities, is in the same range for RT and Dry composites. In Table 5, the transverse elastic modulus, which is highly dependent on the elastic modulus of the resin matrix, is similar for RT and Dry composites. Their similar transverse tensile modulus confirms that the in-situ polymerisation of PMMA is not sensitive to fibre moisture during manufacturing. However, the transverse elastic modulus and strength of RH specimens are 48% and 38% lower than the Dry, mainly due to the higher porosity of RH composites. Indeed, the RH fibres (preconditioning at 90% RH) have shrunk during the composites' stabilisation at 50% RH and created interfacial crack openings of 9.7 ± 3.1 µm in width (see Figure 18). The tensile elastic modulus and failure strength values for cross-ply composites with $[(0,90)]_4$ lay-ups follow a similar trend as transverse tensile tests (see Table 5). However, the average elongation at failure values for RT and RH specimens with $[(0,90)]_4$ lay-ups are 13% and 50% higher than

the reference Dry specimens, respectively. The more ductile nature of RT and RH specimens compared to Dry was also evident through in-plane shear tests provided in Paper IV. For instance, the elongation at failure (γ_{12}) of RT and RH specimens with $[+45/-45]_{SE}$ lay-ups were 42% and 77% higher than Dry, respectively [Table 1, Paper IV]. The ductile behaviour of non-dry composites is related to the plasticising effect of moisture bound to the internal microstructure of fibres and 38% lower transverse tensile strength (i.e., interfacial adhesion) of RH compared to Dry (see Table 5). The RT composite is especially promising as it provides similar interfacial adhesion and stiffness as the Dry composite but with notably higher toughness.

Table 5. Quasi-static tensile properties of the flax-PMMA composites [Paper IV].

Composite, lay-up	E^{chord}, (GPa)	σ^{failure}, (MPa)	$\varepsilon^{\text{failure}}$, (%)
Dry, $[90]_4$	3.1 ± 0.3	14.5 ± 0.3	0.41 ± 0.05
RT, $[90]_4$	3.1 ± 0.2	13.7 ± 0.7	0.42 ± 0.02
RH, $[90]_4$	1.6 ± 0.1	8.9 ± 0.6	0.72 ± 0.01
Dry, $[(0,90)]_4$	11.7 ± 0.2	110.2 ± 1.8	1.62 ± 0.06
RT, $[(0,90)]_4$	11.4 ± 0.1	105.2 ± 1.2	1.83 ± 0.05
RH, $[(0,90)]_4$	8.4 ± 0.1	94.5 ± 1.4	2.44 ± 0.08

The fatigue performance of flax-PMMA composites is presented in Figure 19. In Figure 19 (A), the *S-N* slope of RH (−12.45) is less steep compared to Dry (−15.87), which indicates a 21% slower fatigue strength degradation rate within the loading range of 50%–80% for RH composites that had 50% higher elongation at failure compared to Dry specimens (see Table 5, $[(0,90)]_4$ lay-up). The *S-N* slope of Dry and RT composites are similar, which can be explained by their similar level of interfacial shear strength based on in-plane shear and transverse tensile tests. In Figure 19 (B), the number of cycles to failure of Dry, RT, and RH specimens within the 50%–90% loading range are comparable. Also, in terms of the number of cycles to failure, the performance of flax-PMMA specimens is comparable to their flax-epoxy counterparts (see Figure 19 B and Figure 10 B). The flax-PMMA specimens reach the run-out threshold (10^6 cycles before failure) at a 50% load level. The results in Figure 19 indicate that processing flax-PMMA composites with non-dry fibres especially in the case of RT (preconditioned at 50% RH) does not negatively affect

their fatigue performance, which is promising. The fracture surfaces of non-dry specimens (in Paper IV) are dominated by fibre pull-out traces, indicating their higher level of ductility than the reference Dry specimens.

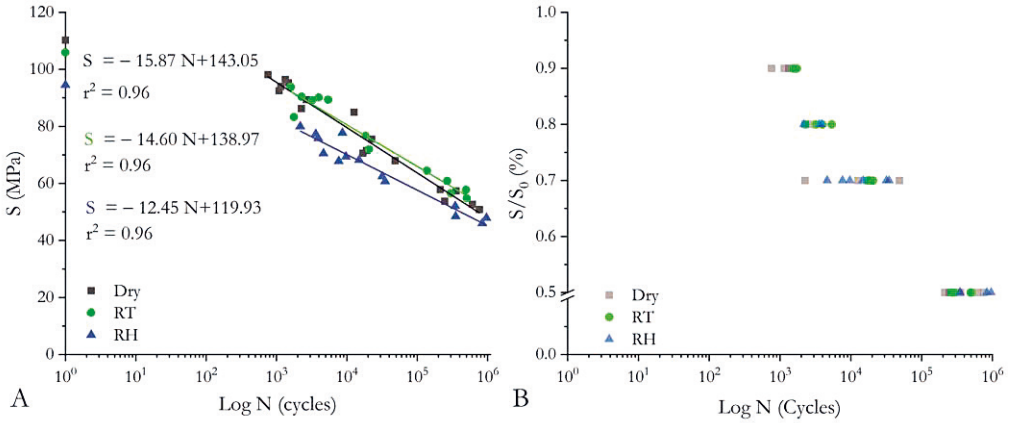

Fig 19. Collected *S-N* data (A) and normalised fatigue data (B) of cross-ply flax-PMMA composites with $[(0,90)]_4$ lay-up [Paper IV].

The impact kinetic energy-time histories of cross-ply composites with $[0/90]_{3SE}$ lay-up are presented in Figure 20. The impact perforation energy of Dry flax-PMMA composites has been enhanced by using ductile non-dry fibres up to 57% (for RT) and 100% (for RH). The RT composites are especially promising as they offer good interfacial adhesion, stiffness, fatigue performance, and outstanding impact resistance. For instance, the thickness-normalised impact perforation energy of RT (6.4 ± 0.2 J/mm) is higher than the corresponding flax-epoxy (by 52%), flax-PLA (by 83%), flax-PP (by 33%), and glass-PP (by 25%) composites with similar composite and testing configurations. It is beneficial to revisit the quasi-static tensile test results of non-dry composites to justify their better impact resistance than the Dry specimens. The in-plane shear toughness values of non-dry specimens were similar. Also, the interfacial strength of the RT was as good as the Dry specimens, while the interfacial strength of the RH was 38% lower than Dry. Therefore, the main reasons for better impact resistance of the RT and RH specimens compared to the Dry composites are the ductility of non-dry fibres and lower interfacial adhesion in the case of RH specimens.

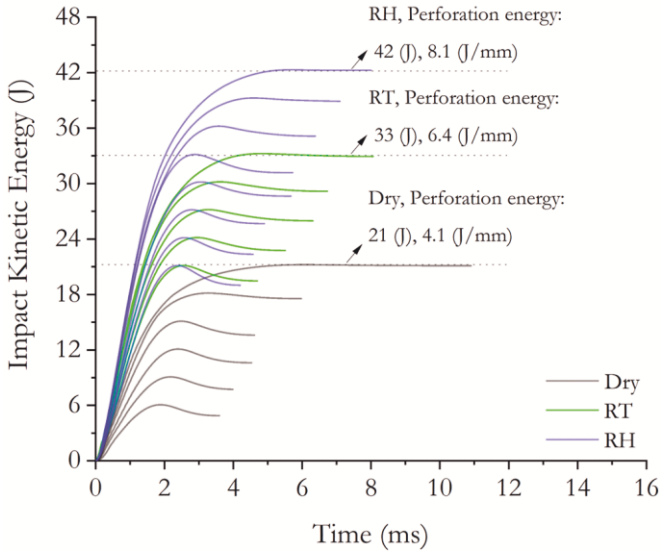

Fig 20. The energy-time history of flax-PMMA composites [Paper IV].

The internal damage patterns of the perforated Dry specimen at 21 J kinetic energy are presented in Figure 21. At the same impact kinetic energy, the non-dry specimens have reduced the extent of fibre failure due to their higher ductility and by promoting energy dissipation through shear-induced damages such as ply-splitting and delaminations. The cumulative length of delaminations in the RT specimen (112.56 mm) is 37% higher than in the RH specimen (82.05 mm). Also, the ply splitting, one of the RT's dominant damage modes, is very limited in the RH specimen.

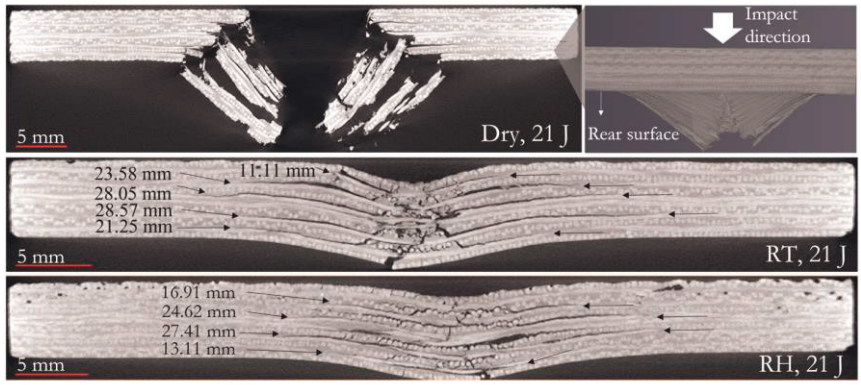

Fig 21. Damage patterns of flax-PMMA composites based on X-CT [Paper IV].

Figure 22 (A) shows the contact force-displacement histories of the flax-PMMA specimens at 21 J kinetic energy. The maximum contact force (F^{max}) of the RT and RH composites at 21 J kinetic energy are respectively 13% and 19% above the similar value for the Dry specimens (see Figure 22 B). This can be explained by the limited degree of ply failure within non-dry composites at 21 J kinetic energy (as shown in Figure 21), which enhances the load-bearing capacity of the RT and RH specimens. Also, the average displacement values at F^{max} for RT and RH are respectively 45% and 61% higher than those for Dry (Figure 22 C). The higher displacement values suggest that the non-dry specimens present more ductile resistance against the impactor. Further discussions on the in-situ impact response of flax-PMMA composites are provided in Paper IV.

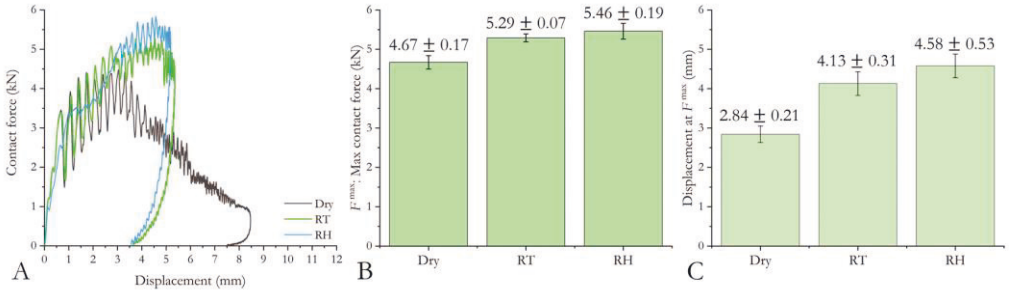

Fig 22. Contact force-displacement curves of flax-PMMA composites at 21 J (4.1 J/mm) impact kinetic energy (A), average values for the maximum contact forces (B), and displacement at maximum contact force (C) [Paper IV].

In summary, the results in this section showed that the brittle characteristic of flax-PMMA composites could be modified by harnessing the hydrophilic nature of natural fibres. The effect of moisture during manufacturing and the environmental preconditioning of flax fibres on the impact resistance and fatigue performance of flax-PMMA composites was addressed. The in-situ polymerisation of PMMA was not sensitive to moisture during manufacturing. By using the non-dry (preconditioned) fibres, the impact resistance of flax-PMMA composites enhanced between 50%−100% without a negative effect on their fatigue performance. The non-dry flax-PMMA composites can find various applications in industrial/structural fields as they offer unique combinations of stiffness and toughness, impact resistance and fatigue tolerance.

6 CONCLUSIONS

Engineering natural fibres such as flax are sustainable and low density structural materials which offer a unique combination of stiffness and damping properties. The market capacity and use cases of flax fibre reinforced composites have grown tremendously in recent years, especially in the sports and automotive sectors. In such applications, impact and fatigue resistance are essential for the long-term durability and sustainability of flax fibre composites. However, the brittle nature of flax fibres limits their resistance against dynamic loads such as impact. This thesis investigated the effect of interfacial adhesion and toughness on the impact and fatigue performance of flax-epoxy and flax-PMMA composites.

6.1 Overview

The results showed that it is possible to produce stiff and tough flax fibre composites which have comparable or even higher impact resistance than glass fibre reinforced composites. The proposed interfacial toughening methods enhanced the impact resistance of flax-epoxy (up to 40%) and flax-PMMA (up to 100%) without or with minor compromise on their interfacial strength and fatigue performance. The interfacial sliding/debonding between fibre and matrix, and the ductility of fibres had a significant role in modifying the damage modes and impact resistance of composites. In the following sections, the effects of each microscale fibre modification on the macroscale mechanical performance of composites are described in relation to research questions I–III.

Interfacial strength

The effect of interfacial strength on the fatigue and impact performance of flax-epoxy composites was studied based on graphene oxide (GO) fibre surface

modification. The GO-modified fibres enhanced the interfacial strength between flax and epoxy by 40% based on the microbond tests. This enhancement was ascribed to the 50% higher degree of oxidised carbon (C-C/H) on GO-modified flax fibres compared to unmodified fibres. As a result, the GO-modified fibres were more reactive towards the epoxy resin, and their composites were less porous compared to unmodified flax-epoxy (0.04% vs. 2.41%). Therefore, the GO-modified fibres enhanced the cyclic loading performance of flax-epoxy composites by 17%. At impact kinetic energies below the perforation limit, the GO modification limited the extent of fibre failure by promoting energy dissipation through interlaminar delamination. This observation was attributed to the weakly bonded sheets of GO within multilayer GO crystals. It was concluded that the GO-modification could potentially enhance the impact tolerance (e.g., CAI) of flax-epoxy composites by providing better interfacial strength. Nevertheless, the surface treatment did not positively or negatively affect the limited perforation energy of flax-epoxy composites. As was observed in Paper I, the enhanced interfacial adhesion in GO-modified composites limits the ductility of flax-epoxy specimens. Overall, the GO-modification created a synergy between fatigue and impact performance of flax-epoxy composites.

Interfacial toughness

The CA-modified fibres enhanced the low-velocity impact perforation energy of cross-ply flax-epoxy composites by 40% without compromising the in-plane mechanical performance of composites. Also, in Paper III, the Charpy impact strength of CA-modified specimens with $[0]_4$ lay-up was 40% higher than the unmodified flax-epoxy. The CA-modification reduced the apparent interfacial shear strength between flax-epoxy (based on microbond tests) and the in-plane shear strength of composites by 22%. As a result, the quasi-static tensile toughness values of CA-modified composites with $[+45/-45]_{SE}$ and $[0]_4$ lay-ups were respectively 22% and 11% higher than the unmodified flax-epoxy specimens. Interestingly, the CA-modification enhanced the ductility of flax-epoxy composites without negatively affecting their elastic modulus. For instance, the elongation at failure of flax-epoxy specimens with $[+45/-45]_{SE}$ lay-up increased by 52% with CA-modification. It can be concluded that the 40% better impact resistance of modified composites was due to their stiff and tough nature. The CA-modification promoted energy dissipation

through interfacial sliding and debonding between flax and epoxy and limited the extent of fibre failure in impact tests.

Ductility of fibres and moisture during manufacturing of composites

Based on the quasi-static tensile results and morphology analysis of composites, it was concluded that the in-situ polymerisation of PMMA is not sensitive to moisture during manufacturing. The MMA monomers are often emulsion polymerised in an aqueous medium which might explain the moisture insensitivity of the polymerisation.

The Dry and RT composites had similar tensile moduli, transverse tensile strength, and in-plane shear strength. However, the tensile elongation at failure of RT specimens with $[(0,90)]_4$, $[+45/-45]_{SE}$ lay-ups were 13% and 42% higher than Dry. The better ductility of RT specimens was ascribed to the plasticising effect of water molecules, and it was described by previous findings in the literature [34]. The RT composites had a unique combination of good interfacial strength, stiffness, ductility and toughness. Therefore, the impact resistance and perforation energy of cross-ply RT specimens were 56% higher than Dry. Also, the fatigue performance of cross-ply RT specimens was as good as the Dry specimens.

The RH specimens experienced significant shrinkage and interfacial debonding between fibre and matrix during the stabilisation period. As a result, the transverse tensile and in-plane shear strength of RH specimens were −38% and −23% lower than the reference Dry specimens. Besides the plasticising effect of water molecules, the primary toughening mechanism for RH specimens was their low interfacial shear strength which enhanced their ductility. For instance, the in-plane shear strain to failure of RH specimens was 77% more than Dry. Therefore, the impact perforation energy of cross-ply RH specimens was 97% higher than Dry. The *S-N* slope of RH (−12.45) was 21% less steep compared to Dry (−15.87), which might yield a longer fatigue life for RH composites.

6.2 Research impact and industrial implications

Designing lightweight composites with contrasting properties such as stiffness and toughness can be challenging. The proposed fibre modification strategies in this

thesis resolved this challenge without compromising the other properties of composites. For instance, the CA-modified composites were as stiff and strong as flax-epoxy and had more impact resistance than flax-PP thermoplastic composites. The impact resistance of CA-modified flax-epoxy and non-dry flax-PMMA composites was competitive with glass-PP counterparts. The results showed that interfacial toughening could effectively create a synergy between fatigue and impact resistance of natural fibre composites.

Also, it was shown that the moisture affinity of natural fibres could be harnessed as a toughening method for their composites by using moisture-insensitive polymerisation methods. Naturally, such polymerisation methods can save processing time and energy by eliminating the common oven-drying step in manufacturing natural fibre composites. Additionally, processing composites with moist (non-dry) fibres can reduce the swelling and shrinkage of natural fibre composites in wet environments.

Overall, the findings in this thesis can promote the in-service durability of natural fibre composites and enhance their competitiveness for structural applications which require a combination of the following properties: stiffness and toughness, good interfacial adhesion and ductility, fatigue tolerance and impact resistance, hydrothermal stability, durability, and recyclability.

REFERENCES

[1] Musio S, Müssig J, Amaducci S. Optimizing hemp fiber production for high performance composite applications.
Front Plant Sci 2018;871:1702.h
https://doi.org/10.3389/FPLS.2018.01702/XML/NLM.

[2] Gabrion X, Koolen G, Grégoire M, Musio S, Bar M, Botturi D, et al. Influence of industrial processing parameters on the effective properties of long aligned European hemp fibres in composite materials.
Compos PartA Appl Sci Manuf 2022;157:106915.
https://doi.org/10.1016/J.COMPOSITESA.2022.106915.

[3] Corbin A-C, Sala B, Soulat D, Ferreira M, Labanieh A-R, Placet V. Development of quasi-unidirectional fabrics with hemp fiber: A competitive reinforcement for composite materials.
J Compos Mater 2021;55:551–64.
https://doi.org/10.1177/0021998320954230.

[4] Rong MZ, Zhang MQ, Liu Y, Yang GC, Zeng HM. The effect of fiber treatment on the mechanical properties of unidirectional sisal-reinforced epoxy composites.
Compos Sci Technol 2001;61:1437–47.
https://doi.org/10.1016/S0266-3538(01)00046-X.

[5] Bourmaud A, Morvan C, Bouali A, Placet V, Perré P, Baley C. Relationships between micro-fibrillar angle, mechanical properties and biochemical composition of flax fibers.
Ind Crops Prod 2013;44:343–51.
https://doi.org/10.1016/j.indcrop.2012.11.031.

[6] Wang C, Wang N, Liu S, Choo-Smith L, Zhang H, Zhi Z. Investigation of microfibril angle of flax fibers using X-ray diffraction and scanning electron microscopy.
J. Nat. Fibres, 17 (7) (2018), pp. 1001-1010.
https://doi.org/10.1080/15440478.2018.1546639.

[7] Khodayari A, Thielemans W, Hirn U, Van Vuure AW, Seveno D. Cellulose-hemicellulose interactions - A nanoscale view.
Carbohydr Polym 2021;270:118364.
https://doi.org/10.1016/J.CARBPOL.2021.118364.

[8] Roach MJ, Mokshina NY, Badhan A, Snegireva A V., Hobson N, Deyholos MK, et al. Development of Cellulosic Secondary Walls in Flax Fibers Requires β-Galactosidase.
Plant Physiol 2011;156:1351–63.
https://doi.org/10.1104/PP.111.172676.

[9] Bos HL, Van Den Oever MJA, Peters OCJJ. Tensile and compressive properties of flax fibres for natural fibre reinforced composites.
J Mater Sci 2002;37:1683–92.
https://doi.org/10.1023/A:1014925621252.

[10] Khodayari A, Van Vuure AW, Hirn U, Seveno D. Tensile behaviour of dislocated/crystalline cellulose fibrils at the nano scale.
Carbohydr Polym 2020;235:115946.
https://doi.org/10.1016/J.CARBPOL.2020.115946.

[11] Melelli A, Jamme F, Legland D, Beaugrand J, Bourmaud A. Microfibril angle of elementary flax fibres investigated with polarised second harmonic generation microscopy.
Ind Crops Prod 2020;156:112847.
https://doi.org/10.1016/J.INDCROP.2020.112847.

[12] Beaugrand J, Goudenhooft C, Alvarado C, Devaux MF, Rivard C, Durand S, et al. Evolution of the flax cell wall composition during development and after gravitropism by synchrotron fluorescence imaging.
Ind Crops Prod 2022;175:114256.
https://doi.org/10.1016/J.INDCROP.2021.114256.

[13] Bourmaud A, Beaugrand J, Shah DU, Placet V, Baley C. Towards the design of high-performance plant fibre composites.
Prog Mater Sci, 97 (2018), pp. 347-408.
https://doi.org/10.1016/j.pmatsci.2018.05.005.

[14] Fuentes CA, Ting KW, Dupont-Gillain C, Steensma M, Talma AG, Zuijderduin R, et al. Effect of humidity during manufacturing on the interfacial strength of non-pre-dried flax fibre/unsaturated polyester composites.
Compos Part A Appl Sci Manuf 2016;84:209–15.

https://doi.org/10.1016/J.COMPOSITESA.2016.01.023.

[15] Fuentes CA, Tran LQN, Dupont-Gillain C, Vanderlinden W, De Feyter S, Van Vuure AW, et al. Wetting behaviour and surface properties of technical bamboo fibres.
Colloids Surfaces A Physicochem Eng Asp 2011;380:89–99.
https://doi.org/10.1016/J.COLSURFA.2011.02.032.

[16] Johansson LS, Campbell JM, Koljonen K, Stenius P. Evaluation of surface lignin on cellulose fibers with XPS.
Appl Surf Sci 1999;144–145:92–5.
https://doi.org/10.1016/S0169-4332(98)00920-9.

[17] Zhang Z, Cai S, Li Y, Wang Z, Long Y, Yu T, et al. High performances of plant fiber reinforced composites—A new insight from hierarchical microstructures.
Compos Sci Technol 2020;194:108151.
https://doi.org/10.1016/j.compscitech.2020.108151.

[18] Baley C, Gomina M, Breard J, Bourmaud A, Davies P. Variability of mechanical properties of flax fibres for composite reinforcement. A review.
Ind Crops Prod 2020;145:111984.
https://doi.org/10.1016/J.INDCROP.2019.111984.

[19] Bensadoun F, Verpoest I, Baets J, Müssig J, Graupner N, Davies P, et al. Impregnated fibre bundle test for natural fibres used in composites.
J Reinf Plast Compos 2017;36:942–57.
https://doi.org/10.1177/0731684417695461.

[20] Prapavesis A, Tojaga V, Östlund S, Willem van Vuure A. Back calculated compressive properties of flax fibers utilizing the Impregnated Fiber Bundle Test (IFBT).
Compos Part A Appl Sci Manuf 2020;135:105930.
https://doi.org/10.1016/J.COMPOSITESA.2020.105930.

[21] Javanshour F. Tensile Properties of Flax Fibre Bundles with Graphene Oxide Coating 2019.
https://doi.org/10.5281/ZENODO.3382823.

[22] Bourmaud A, Pinsard L, Guillou E, De Luycker E, Fazzini M, Perrin J, et al. Elucidating the formation of structural defects in flax fibres through synchrotron X-ray phase-contrast microtomography.
Ind Crops Prod 2022;184:115048.

https://doi.org/10.1016/J.INDCROP.2022.115048.

[23] Melelli A, Durand S, Arnould O, Richely E, Guessasma S, Jamme F, et al. Extensive investigation of the ultrastructure of kink-bands in flax fibres. Ind Crops Prod 2021;164:113368. https://doi.org/10.1016/J.INDCROP.2021.113368.

[24] Pickering KL, Efendy MGA, Le TM. A review of recent developments in natural fibre composites and their mechanical performance. Compos Part A Appl Sci Manuf 2016;83:98–112. https://doi.org/10.1016/j.compositesa.2015.08.038.

[25] Sarker F, Karim N, Afroj S, Koncherry V, Novoselov KS, Potluri P. High-Performance Graphene-Based Natural Fiber Composites. ACS Appl Mater Interfaces 2018;10:34502–12. https://doi.org/10.1021/acsami.8b13018.

[26] Dessalegn Y, Singh B, Van Vuure AW, Rajhi AA, Mohammed G, Ahmed S, et al. Influence of Age and Harvesting Season on The Tensile Strength of Bamboo-Fibre-Reinforced Epoxy Composites. Mater 2022, Vol 15, Page 4144 2022;15:4144. https://doi.org/10.3390/MA15124144.

[27] Pickering KL, Efendy MGA, Le TM. A review of recent developments in natural fibre composites and their mechanical performance. Compos Part A Appl Sci Manuf 2016. https://doi.org/10.1016/j.compositesa.2015.08.038.

[28] Van Vuure AW, Vanderbeke J, Mosleh Y, Verpoest I, El-Asmar N. Ductile woven silk fibre thermoplastic composites with quasi-isotropic strength. Compos Part A Appl Sci Manuf 2021;147:106442. https://doi.org/10.1016/J.COMPOSITESA.2021.106442.

[29] Pérez-Rigueiro J, Viney C, Llorca J, Elices M. Mechanical properties of silkworm silk in liquid media. Polymer; 2000;41:8433–9. https://doi.org/10.1016/S0032-3861(00)00179-8.

[30] Shah DU, Porter D, Vollrath F. Can silk become an effective reinforcing fibre? A property comparison with flax and glass reinforced composites. Compos Sci Technol 2014;101:173–83. https://doi.org/10.1016/J.COMPSCITECH.2014.07.015.

[31] Placet V, Cisse O, Boubakar ML. Influence of environmental relative humidity on the tensile and rotational behaviour of hemp fibres.
J Mater Sci 2012;47:3435–46.
https://doi.org/10.1007/S10853-011-6191-3/FIGURES/9.

[32] Thuault A, Eve S, Blond D, Bréard J, Gomina M. Effects of the hygrothermal environment on the mechanical properties of flax fibres.
J Compos Mater 2014;48 (14):1699–707.
https://doi.org/10.1177/0021998313490217.

[33] Faruk O, Bledzki AK, Fink HP, Sain M. Biocomposites reinforced with natural fibers: 2000–2010.
Prog polym Sci, 2012; 37 (11), pp. 1552-1596.
https://doi.org/10.1016/j.progpolymsci.2012.04.003.

[34] Baley C, Le Duigou A, Bourmaud A, Davies P. Influence of drying on the mechanical behaviour of flax fibres and their unidirectional composites.
Compos Part A Appl Sci Manuf 2012;43:1226–33.
https://doi.org/10.1016/j.compositesa.2012.03.005.

[35] Zhang D, Milanovic NR, Zhang Y, Su F, Miao M. Effects of humidity conditions at fabrication on the interfacial shear strength of flax/unsaturated polyester composites.
Compos Part B Eng 2014;60:186–92.
https://doi.org/10.1016/J.COMPOSITESB.2013.12.031.

[36] Virtanen S, Wikström L, Immonen K, Anttila U, Retulainen E, Virtanen S, et al. Cellulose kraft pulp reinforced polylactic acid (PLA) composites: effect of fibre moisture content.
AIMS Mater Sci 2016 3756 2016;3:756–69.
https://doi.org/10.3934/MATERSCI.2016.3.756.

[37] Van de Velde K, Baetens E. Thermal and mechanical properties of flax fibres as potential composite reinforcement.
Macromol Mater Eng, 2001; 286 (6): pp. 342-349.
https://doi.org/10.1002/1439-2054(20010601)286:6<342::AID-MAME342>3.0.CO;2-P.

[38] Le Duigou A, Davies P, Baley C. Environmental impact analysis of the production of flax fibres to be used as composite material reinforcement.
J Biobased Mater Bioenergy 2011;5:153–65.
https://doi.org/10.1166/jbmb.2011.1116.

[39] Bensadoun F, Vanderfeesten B, Verpoest I, Van Vuure AW, Van Acker K. Environmental impact assessment of end of life options for flax-MAPP composites.
Ind Crops Prod 2016;94:327–41.
https://doi.org/10.1016/j.indcrop.2016.09.006.

[40] Müssig J, Amaducci S, Bourmaud A, Beaugrand J, Shah DU. Transdisciplinary top-down review of hemp fibre composites: From an advanced product design to crop variety selection.
Compos Part C Open Access 2020;2:100010.
https://doi.org/10.1016/J.JCOMC.2020.100010.

[41] Haag K, Padovani J, Fita S, Trouvé JP, Pineau C, Hawkins S, et al. Influence of flax fibre variety and year-to-year variability on composite properties.
Ind Crops Prod 2017;98:1–9.
https://doi.org/10.1016/J.INDCROP.2016.12.028.

[42] Greenhalgh E, Hiley M. The assessment of novel materials and processes for the impact tolerant design of stiffened composite aerospace structures.
Compos Part A Appl Sci Manuf 2003;34:151–61.
https://doi.org/10.1016/S1359-835X(02)00188-4.

[43] Yasaee M, Bond IP, Trask RS, Greenhalgh ES. Damage control using discrete thermoplastic film inserts.
Compos Part A Appl Sci Manuf 2012;43:978–89.
https://doi.org/10.1016/j.compositesa.2012.01.011.

[44] Richardson MOW, Wisheart MJ. Review of low-velocity impact properties of composite materials.
Compos Part A Appl Sci Manuf 1996;27:1123–31.
https://doi.org/10.1016/1359-835X(96)00074-7.

[45] Liu D. Impact-Induced Delamination—A View of Bending Stiffness Mismatching.
J Compos Mater 1988;22:674–92.
https://doi.org/10.1177/002199838802200706.

[46] Chang FK, Choi HY, Jeng ST. Study on impact damage in laminated composites.
Mech Mater, 1990; 10: pp. 83-95.
https://doi.org/10.1016/0167-6636(90)90019-C.

[47] Cantwell W, Morton J. The impact resistance of composite materials—a review.
Compos Mater, 1991; 22: pp. 347-362.
https://doi.org/10.1016/0010-4361(91)90549-V.

[48] Sarasini F, Tirillò J, Lampani L, Barbero E, Sánchez-Sáez S, Valente T, Gaudenzi P, Scarponi C. Impact behavior of sandwich structures made of flax/epoxy face sheets and agglomerated cork.
J. Nat. Fibres, 17 (2) (2020), pp. 1544-0478.
https://doi.org/10.1080/15440478.2018.1477084.

[49] Bensadoun F, Depuydt D, Baets J, Verpoest I, van Vuure AW. Low velocity impact properties of flax composites.
Compos Struct 2017;176:933–44.
https://doi.org/10.1016/j.compstruct.2017.05.005.

[50] Mosleh Y, Clemens D, Gorbatikh L, Verpoest I, Van Vuure AW. Penetration impact resistance of novel tough steel fibre-reinforced polymer composites.
J Reinf Plast Compos 2015;34 (8):624–635.
https://doi.org/10.1177/0731684415574538.

[51] Ramakrishnan KR, Corn S, Le Moigne N, Ienny P, Slangen P. Experimental assessment of low velocity impact damage in flax fabrics reinforced biocomposites by coupled high-speed imaging and DIC analysis.
Compos Part A Appl Sci Manuf 2021;140:106137.
https://doi.org/10.1016/j.compositesa.2020.106137.

[52] Panzera TH, Jeannin T, Gabrion X, Placet V, Remillat C, Farrow I, et al. Static, fatigue and impact behaviour of an autoclaved flax fibre reinforced composite for aerospace engineering.
Compos Part B Eng 2020;197:108049.
https://doi.org/10.1016/j.compositesb.2020.108049.

[53] Chew E, Liu JL, Tay TE, Tran LQN, Tan VBC. Improving the mechanical properties of natural fibre reinforced laminates composites through Biomimicry.
Compos Struct 2021;258:113208.
https://doi.org/10.1016/j.compstruct.2020.113208.

[54] Prasad V, Sekar K, Varghese S, Joseph MA. Enhancing Mode I and Mode II interlaminar fracture toughness of flax fibre reinforced epoxy composites with nano TiO2.
Compos Part A Appl Sci Manuf, 124 (2019), p.10550.

10.1016/j.compositesa.2019.105505.

[55] Pereira AC, Monteiro SN, Simonassi NT, Vieira CMF, Lima AM, Costa UO, et al. Enhancement of impact toughness using graphene oxide in epoxy composite reinforced with ramie fabric.
Compos Struct 2022;282:115023.
https://doi.org/10.1016/J.COMPSTRUCT.2021.115023.

[56] Alipour A, Lin R, Jayaraman K. Effects of graphene network formation on microstructure and mechanical properties of flax/epoxy nanocomposites.
J Mater Res Technol 2021;15:4610–22.
https://doi.org/10.1016/J.JMRT.2021.10.082.

[57] Woigk W, Fuentes CA, Rion J, Hegemann D, van Vuure AW, Dransfeld C, et al. Interface properties and their effect on the mechanical performance of flax fibre thermoplastic composites.
Compos Part A Appl Sci Manuf 2019;122:8–17.
https://doi.org/10.1016/j.compositesa.2019.04.015.

[58] Chen C, Li Y, Yu T. Interlaminar toughening in flax fiber-reinforced composites interleaved with carbon nanotube buckypaper.
J Reinf Plast Compos 2014;33:1859–68.
https://doi.org/10.1177/0731684414548084.

[59] Ravandi M, Teo WS, Tran LQN, Yong MS, Tay TE. Low velocity impact performance of stitched flax/epoxy composite laminates.
Compos Part B Eng 2017;117:89–100.
https://doi.org/10.1016/j.compositesb.2017.02.003.

[60] Mohammed M, Rasidi M, Mohammed A, Rahman R, Osman A, Adam T, et al. Interfacial bonding mechanisms of natural fibre-matrix composites: An overview.
BioResources 2022;17 (4), 7031-7090.
https://doi.org/10.15376/BIORES.17.4.MOHAMMED.

[61] Gupta US, Dhamarikar M, Dharkar A, Chaturvedi S, Kumrawat A, Giri N, et al. Plasma modification of natural fiber: A review.
Mater Today Proc 2021;43:451–7.
https://doi.org/10.1016/J.MATPR.2020.11.973.

[62] Acera Fernández J, Le Moigne N, Caro-Bretelle AS, El Hage R, Le Duc A, Lozachmeur M, et al. Role of flax cell wall components on the microstructure and transverse mechanical behaviour of flax fabrics reinforced epoxy-

biocomposites.
Ind Crops Prod 2016;85:93–108.
https://doi.org/10.1016/j.indcrop.2016.02.047.

[63] Van de Weyenberg I, Ivens J, De Coster B, Kino E, Baetens E, Verpoest I. Influence of processing and chemical treatment of flax fibres on their composites.
Compos Sci Technol, 63 (2003); pp.
https://doi.org/10.1016/S0266-3538(03)00093-9.

[64] Wang H, Xian G, Li H. Grafting of nano-TiO2 onto flax fibers and the enhancement of the mechanical properties of the flax fiber and flax fiber/epoxy composite.
Compos Part A Appl Sci Manuf 2015;76:172–80.
https://doi.org/10.1016/j.compositesa.2015.05.027.

[65] Seghini MC, Touchard F, Sarasini F, Chocinski-Arnault L, Tirillò J, Bracciale MP, et al. Effects of oxygen and tetravinylsilane plasma treatments on mechanical and interfacial properties of flax yarns in thermoset matrix composites.
Cellulose 2020;27:511–30.
https://doi.org/10.1007/s10570-019-02785-3.

[66] Gong L, Zhang F, Peng X, Scarpa F, Huang Z, Tao G, et al. Improving the damping properties of carbon fiber reinforced polymer composites by interfacial sliding of oriented multilayer graphene oxide.
Compos Sci Technol 2022;224:109309.
https://doi.org/10.1016/J.COMPSCITECH.2022.109309.

[67] Shirvanimoghaddam K, Balaji K V., Yadav R, Zabihi O, Ahmadi M, Adetunji P, et al. Balancing the toughness and strength in polypropylene composites.
Compos Part B Eng 2021;223:109121.
https://doi.org/10.1016/J.COMPOSITESB.2021.109121.

[68] Rahmanian S, Thean KS, Suraya AR, Shazed MA, Mohd Salleh MA, Yusoff HM. Carbon and glass hierarchical fibers: Influence of carbon nanotubes on tensile, flexural and impact properties of short fiber reinforced composites.
Mater Des 2013;43:10–6.
https://doi.org/10.1016/J.MATDES.2012.06.025.

[69] Lin J, Wang L, Liu L, Lu K, Li G, Yang X. Two-stage interface enhancement of aramid fiber composites: Establishment of hierarchical interphase with waterborne polyurethane sizing and oxazolidone-containing epoxy matrix.

Compos Sci Technol 2020;193:108114.
https://doi.org/10.1016/j.compscitech.2020.108114.

[70] Randall JD, Stojcevski F, Djordjevic N, Hendlmeier A, Dharmasiri B, Stanfield MK, et al. Carbon fiber polypropylene interphase modification as a route to improved toughness.
Compos Part A Appl Sci Manuf 2022;159:107001.
https://doi.org/10.1016/J.COMPOSITESA.2022.107001.

[71] Eyckens DJ, Demir B, Randall JD, Gengenbach TR, Servinis L, Walsh TR, et al. Using molecular entanglement as a strategy to enhance carbon fiber-epoxy composite interfaces.
Compos Sci Technol 2020;196:108225.
https://doi.org/10.1016/J.COMPSCITECH.2020.108225.

[72] Asgarinia S, Viriyasuthee C, Phillips S, Dubé M, Baets J, Van Vuure A, et al. Tension–tension fatigue behaviour of woven flax/epoxy composites.
J Reinf Plast Compos 2015;34:857–867.
https://doi.org/10.1177/0731684415581527.

[73] Bensadoun F, Vallons KAM, Lessard LB, Verpoest I, Van Vuure AW. Fatigue behaviour assessment of flax–epoxy composites.
Compos Part A Appl Sci Manuf 2016;82:253–66.
https://doi.org/10.1016/J.COMPOSITESA.2015.11.003.

[74] Mahboob Z, Bougherara H. Fatigue of flax-epoxy and other plant fibre composites: Critical review and analysis.
Compos Part A Appl Sci Manuf 2018;109:440–62.
https://doi.org/10.1016/J.COMPOSITESA.2018.03.034.

[75] Mahboob Z, Fawaz Z, Bougherara H. Fatigue behaviour and damage mechanisms under strain controlled cycling: Comparison of Flax–epoxy and Glass–epoxy composites.
Compos Part A Appl Sci Manuf 2022;159:107008.
https://doi.org/10.1016/J.COMPOSITESA.2022.107008.

[76] Galiotis C, Koimtzoglou C. The effect of the interface on the fatigue performance of fibre composites. In: Harris B, editor.
Fatigue Compos. 1st ed., Woodhead publishing limited; 2003, p. 170–98.

[77] Towo AN, Ansell MP. Fatigue evaluation and dynamic mechanical thermal analysis of sisal fibre–thermosetting resin composites.
Compos Sci Technol 2008;68:925–32.

https://doi.org/10.1016/J.COMPSCITECH.2007.08.022.

[78] Islam MS, Pickering KL, Foreman NJ. Influence of alkali fiber treatment and fiber processing on the mechanical properties of hemp/epoxy composites. J Appl Polym Sci 2011;119:3696–707. https://doi.org/10.1002/app.31335.

[79] Li M, Pu Y, Thomas VM, Yoo CG, Ozcan S, Deng Y, et al. Recent advancements of plant-based natural fiber–reinforced composites and their applications. Compos Part B Eng 2020;200:108254. https://doi.org/10.1016/j.compositesb.2020.108254.

[80] Broyles NS, Verghese KNE, Davis S V., Li H, Davis RM, Lesko JJ, et al. Fatigue performance of carbon fibre/vinyl ester composites: the effect of two dissimilar polymeric sizing agents. Polymer 1998;39:3417–24. https://doi.org/10.1016/S0032-3861(97)10078-7.

[81] Javanshour F. Quasi-static tensile properties of PMMA (Elium 188) and Epoxy (Epopox A-28) resins 2022. https://doi.org/10.5281/ZENODO.7381444.

[82] Hummers WS, Offeman RE. Preparation of Graphitic Oxide. J Am Chem Soc 1958;80:1339–1339. https://doi.org/10.1021/ja01539a017.

[83] Byrne FP, Jin S, Paggiola G, Petchey THM, Clark JH, Farmer TJ, et al. Tools and techniques for solvent selection: green solvent selection guides. Sustain Chem Process 2016;4. https://doi.org/10.1186/s40508-016-0051-z.

[84] Javanshour F. Effect of acetone on the tensile properties of single flax fibres 2023. https://doi.org/10.5281/ZENODO.7698687.

[85] Laurikainen P, Kakkonen M, von Essen M, Tanhuanpää O, Kallio P, Sarlin E. Identification and compensation of error sources in the microbond test utilising a reliable high-throughput device. Compos Part A Appl Sci Manuf 2020;137:105988. https://doi.org/10.1016/j.compositesa.2020.105988.

[86] Nie Y, Claus B, Gao J, Zhai X, Kedir N, Chu J, et al. In Situ Observation of Adiabatic Shear Band Formation in Aluminum Alloys.
Exp Mech 2020;60:153–63.
https://doi.org/10.1007/S11340-019-00544-W/FIGURES/13.

[87] Soares GC, Hokka M. Synchronized Full-Field Strain and Temperature Measurements of Commercially Pure Titanium under Tension at Elevated Temperatures and High Strain Rates.
Met 2022, Vol 12, Page 25 2021;12:25.
https://doi.org/10.3390/MET12010025.

[88] Fischer B, Sarasini F, Tirillò J, Touchard F, Chocinski-Arnault L, Mellier D, et al. Impact damage assessment in biocomposites by micro-CT and innovative air-coupled detection of laser-generated ultrasound.
Compos Struct 2019;210:922–31.
https://doi.org/10.1016/j.compstruct.2018.12.013.

[89] Yudhanto A, Wafai H, Lubineau G, Goutham S, Mulle M, Yaldiz R, et al. Revealing the effects of matrix behavior on low-velocity impact response of continuous fiber-reinforced thermoplastic laminates.
Compos Struct 2019;210:239–49.
https://doi.org/10.1016/J.COMPSTRUCT.2018.11.040.

[90] Liu T, Butaud P, Placet V, Ouisse M. Damping behavior of plant fiber composites: A review.
Compos Struct 2021;275:114392.
https://doi.org/10.1016/J.COMPSTRUCT.2021.114392.

[91] Merotte J, Duigou A Le, Kervoelen A, Bourmaud A, Behlouli O, O Sire, et al. Flax and hemp nonwoven composites: The contribution of interfacial bonding to improving tensile properties.
Polym. Test., 66 (2018), pp. 303-311.
10.1016/j.polymertesting.2018.01.019.

[92] Duigou A Le, Davies P, Baley C. Interfacial bonding of Flax fibre/Poly (l-lactide) bio-composites.
Compos Sci Technol 2010; 70 (2), pp. 231-239.
https://doi.org/10.1016/j.compscitech.2009.10.009.

[93] Fan J, Guan Z, Cantwell WJ. Modeling Perforation in Glass Fiber Reinforced Composites Subjected to Low Velocity Impact Loading.
Polym Compos 2011; 32: 1380-1388.
https://doi.org/10.1002/pc.21161.

[94] Kam CS, Leung TL, Liu F, Djurišić AB, Xie MH, Chan WK, et al. Lead removal from water – dependence on the form of carbon and surface functionalization.
RSC Adv 2018;8:18355–62.
https://doi.org/10.1039/C8RA02264J.

[95] Najafi F, Wang G, Cui T, Anand A, Mukherjee S, Filleter T, et al. Fatigue resistance of atomically thin graphene oxide.
Carbon N Y 2021;183:780–8.
https://doi.org/10.1016/J.CARBON.2021.07.062.

[96] Daly M, Cao C, Sun H, Sun Y, Filleter T, Singh CV. Interfacial Shear Strength of Multilayer Graphene Oxide Films.
ACS Nano 2016;10:1939–47.
https://doi.org/10.1021/acsnano.5b05771.

[97] Fei P, Liao L, Cheng B, Song J. Quantitative analysis of cellulose acetate with a high degree of substitution by FTIR and its application.
Anal Methods 2017;9:6194–201.
https://doi.org/10.1039/c7ay02165h.

APPENDED JOURNAL ARTICLES

PAPER I

Supplementary data is available through the online version provided by Elsevier.

Composites: Part A 142 (2021) 106270

Contents lists available at ScienceDirect

Composites Part A

journal homepage: www.elsevier.com/locate/compositesa

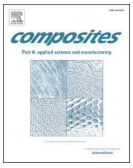

Effect of graphene oxide surface treatment on the interfacial adhesion and the tensile performance of flax epoxy composites

F. Javanshour [a,*], KR. Ramakrishnan [a,b], R.K. Layek [a,c], P. Laurikainen [a], A. Prapavesis [d], M. Kanerva [a], P. Kallio [e], A.W. Van Vuure [d], E. Sarlin [a]

[a] Faculty of Engineering and Natural Sciences, Tampere University, Tampere, Finland
[b] Department of Engineering Science, University of Oxford, UK
[c] Department of Separation Science, LUT University, Lahti, Finland
[d] Department of Materials Engineering, KU Leuven, B-3001, Heverlee, Belgium
[e] Faculty of Medicine and Health Technology, Tampere University, Tampere, Finland

ARTICLE INFO

Keywords:
A. Natural fibres
A. Graphene
B. Fibre/matrix bond
B. Strength

ABSTRACT

The high stiffness and damping properties of flax fibres promote the integration of biocomposites in structural applications. However, the strength of flax/epoxy composites is still limited compared to glass/epoxy composites. Graphene oxide (GO) has proved to be a promising building block for nanocomposites due to its high toughness, stiffness and tunable interfacial interactions with polymers. This study aims to understand the potential of GO-based surface treatment of flax fibres to modify the interfacial adhesion and tensile performance of flax fibre/epoxy composites. GO-modification improves the interfacial shear strength of elementary flax fibre/epoxy by 43%. The interfacial improvement is also established by the 40% higher transverse bending strength compared to untreated flax/epoxy composites. The tensile moduli of GO-modified flax/epoxy composites are on average 2 GPa higher than for untreated flax fibre/epoxy composites in all strain ranges. The quasi-static longitudinal tensile strength of unidirectional composites is not affected by GO-modification.

1. Introduction

Natural fibres, such as flax, with excellent stiffness to weight ratio and damping properties [1] are a green class of reinforcements for composites. Flax fibres can partially substitute glass fibre in weight critical applications. Although flax fibres in the market are more expensive than glass fibres [2], the non-renewable energy required to produce flax fibre mats (9.55 MJ/kg) is significantly lower than glass fibres (54.7 MJ/kg) [3]. Also, from the perspective of abiotic depletion, human toxicity, photochemical oxidation, and end of life options, flax fibres are environmentally superior to glass fibres [4]. Flax/epoxy and glass/epoxy composites demonstrate similar tensile modulus range [5].

Epoxy matrices are ideal for low-cost manufacturing of large structures such as wind turbine blades with resin infusion based on their intrinsic low viscosity. Also, epoxide and hydroxyl groups of epoxy resin can form hydrogen bonds with free hydroxyl groups on flax fibre that is essential for effective load transfer between fibre and matrix [6,7]. The excellent performance of flax/epoxy composites is mainly due to the intrinsic properties of flax fibres. Flax fibres with a high amount of cellulose (60–80 wt%), and low cellulose microfibril angle (10°) have the highest strength values (800–1000 MPa) among natural fibres [8]. Contrary to other bast fibres such as hemp and jute, retted flax bundles can result in a more extensive content of individual elementary fibres which means a higher surface area for load transfer inside a polymer matrix [8,9]. However, the ultimate performance of flax/epoxy composites in various loading conditions is still low compared to glass fibre/epoxy composites [5].

One of the strategies to enhance the strength of flax/epoxy composites is to improve the interfacial adhesion between fibres and matrix. Research efforts in this area focus on the selective extraction of waxy (lipophilic) compounds from the fibre surface [10,11] and development of coupling agents [12–19]. The removal of lipophilic compounds from the flax surface increases the surface roughness and the number of reactive hydroxyl groups leading to better adhesion [6,12,14,20]. The objective of functionalisation is to introduce new functional groups on the fibre surface which can promote interfacial adhesion or toughness [14]. Graphene oxide (GO), a nanoscale material, can significantly enhance the damage tolerance and interfacial interactions as an additive

* Corresponding author.
E-mail address: farzin.javanshour@tuni.fi (F. Javanshour).

https://doi.org/10.1016/j.compositesa.2020.106270
Received 28 May 2020; Received in revised form 19 December 2020; Accepted 25 December 2020
Available online 1 January 2021

for polymers or as a surface functionalisation of fibres [21–28]. GO is a derivative of graphene with oxygen-rich functional groups such as carboxyl, epoxide, and hydroxyl capable of hydrogen bonding or even covalent bonding [29,30]. The tensile modulus of GO sheets consisting of three or more layers (thickness range from 3 nm to 1 μm) is around 40 GPa [31,32]. Although in-plane mechanical properties of GO are inferior to those of graphene, the efficiency of load transfer from a polymer matrix to fibres is much higher for GO covered fibres [33–35]. For instance, Zhang et al. [25] improved the interfacial adhesion and tensile strength of commercially sized carbon fibre/epoxy composites by 36% and 34% with deposition of GO on carbon fibres. Chen et al. [24] reported a 16% improvement in the interlaminar shear strength of GO-treated glass fibre/epoxy composites. Sarker et al. [15] reported significant improvement of 89% in the apparent interfacial shear strength (IFSS) of jute/epoxy by GO-modification of technical jute fibres. In another study by Sarker et al. [13], they also enhanced the tensile strength and the tensile modulus of jute/epoxy composites by 110% and 324% respectively by a combination of alkali lipophilic extraction, combing of jute bundles to individual fibres, and GO-adsorption. Their study is the only work dedicated to the contribution of GO-modification to the mechanical performance of natural fibre/epoxy composites. The current state of literature highlights the need for further research to assess the potential of GO- nanomodification of high-performance bast fibres such as flax to achieve better composites strength.

This work investigates the effect of surface treatment of flax yarns with GO on the tensile behaviour of unidirectional (UD) flax fibre/epoxy composites. The contribution of GO- surface modification to the interfacial adhesion between flax fibres and epoxy is assessed by microbond and transverse bending tests. The transverse cross-section of UD composites is analysed by optical microscopy to understand the effect of GO-treatment on the porosity of composites and individualisation of flax fibre yarns to individual fibres.

2. Methodology

Bcomp®, Switzerland provided unidirectional, non-crimp flax yarn fabric of ampliTex® UD type 5009 with an areal density of 300 g/m^2 and density of 1350 kg/ m^3. AmpliTex® materials are a high-performance class of flax fibres with hot water lipophilic treatment and broad content of individual elementary fibres [36]. Based on the manufacture's datasheet, the tensile modulus, tensile strength and the strain to failure of flax fibres are 61 GPa, 580 MPa, and 1%, respectively. Also, based on the assessment by Bcomp®, 5009 ampliTex (300 g/m^2) can replace 500 g/m^2 glass fibre UD fabric to have the same tensile modulus. Their calculations assumed a glass fibre with a density of 2600 kg/ m^3 and tensile modulus of 70 GPa. The reported values for the mechanical properties of flax and glass fibres agree with the literature [8].

Graphite powder by TIMCAL Ltd., Switzerland, was used in the synthesis of graphene oxide (GO) by the modified Hummers method [30]. Hydrogen peroxide (30%) and sodium nitrate $NaNO_3$ ($\geq$ 99%) were purchased from Sigma-Aldrich, potassium permanganate $KMnO_4$ from Merck, and sulfuric acid H_2SO_4 ($\geq$ 98%) from VWR®. EPON 828® epoxy resin and a Jeffamine® hardener with 32 wt% hardener to the epoxy ratio were used as the matrix.

For the graphene oxide synthesis [30], a 500 mL round bottom flask was placed in an ice bath (0 °C) on a magnetic stirrer. 46 mL of H_2SO_4 was transferred to the flask and continuously stirred by a magnetic bar. 1 g of $NaNO_3$ and 2 g of graphite powder was added to the H_2SO_4. Then, 6 g of $KMnO_4$ was gradually added to the reaction maintaining the temperature of mixture bellow 5 °C. After 10 min, the ice bath was removed, and the reaction continuously stirred for 6 h at 23 °C, which finally turned into a viscous paste. Afterwards, 92 mL and 280 mL of distilled water were added to the reaction with 30 min gap in between. Also, 10 mL of hydrogen peroxide was added to the flask.

After the GO synthesis, an aqueous dispersion of GO was sonicated for exfoliation and further centrifuged to remove the acid used in the process and the non-exfoliated GO sheets. The obtained brown suspension was dried in an oven at 50 °C for 24 h to achieve a GO film. A 1.2 wt % aqueous dispersion of GO was prepared by mixing GO film with de-ionised water with a mortar and further sonication. Flax yarns were dip-coated in this dispersion for 24 h at 23 °C and dried at 60 °C overnight. The reference flax yarns were immersed in de-ionised water for 24 h at 23 °C and dried at 60 °C overnight to account for the potential effect of water.

The X-ray diffraction (XRD) pattern of the synthesised graphene oxide crystals was examined by a Panalytical Empyrean Multipurpose Diffractometer with zero background. X-ray diffraction measurements were prepared by attaching the GO film on an amorphous sample holder. The instrument was operated at 40 kV and 40 mA with a Kα ($\lambda = 0.154$ nm) radiation source. The X-ray diffraction measurements were performed from $2\theta = 5^\circ$ to 40° at a rate of 2° min^{-1}.

The outcome of the GO synthesis (GO crystals) and the surface treatment of flax fibres was studied and compared to untreated material by Fourier transform infrared (FTIR) spectroscopy using a PerkinElmer Spectrum One device with the wavenumbers ranging from 500 to 4000 cm^{-1} with a resolution of 0.5 cm^{-1}. Three scans were performed for each fibre type.

The tensile performance of untreated and GO-modified elementary flax fibres was measured by Textechno FAVIGRAPH® with 20 cN load cell. Tensile tests were performed with 20 mm gauge length and with a crosshead speed of 2 mm/min. A pretension of 0.6 cN/tex was applied before each measurement. Fibres were stored for one week at a controlled environment of RH 50% and 25 °C.

Microbond tests were performed with a FibroBond® device [37] with 1 N load cell on single elementary fibres of flax. The elementary flax fibres were extracted from flax fabrics by tweezer under an optical microscope. The average diameter of elementary flax fibres was $17 \pm 3\mu$m. Epoxy droplets were deposited by a FibDrop® device, which enables to form droplets of controlled size. All droplets were inspected under a microscope before testing, and samples with defects were rejected. To avoid fibre breakage during the microbond test, only droplets in the range of 70μ m to 100μ m were tested. The droplets were cured at 90 °C for 24 h and post cured at 150 °C for 2 h. During the test, microvices sheared the droplets while the fibres were fixed with glue on steel sample holders. Tests were observed with a microscope. The loading rate was 8μ m/s.

The interfacial shear strength denoted as τ_d [38] was evaluated from the linear regression (slope) of a dataset of maximum force of individual droplets versus embedded area as [37]:

$$\tau_d = \frac{dF_{max}}{dA_{emb}} \tag{1}$$

where F_{max} is the measured maximum force, and A_{emb} is the embedded area along the fibre in the resin. In total, 20 individual droplets were tested for each sample.

Unidirectional (UD) flax fibre/epoxy coupons with a 10 mm width, 2 mm thickness, 250 mm length and 40% fibre volume fraction were manufactured based on the hand-layup method followed by hot pressing. Spacers with a 2 mm thickness were used in the press to assure the final thickness of the samples. Samples were cured at 90 °C for 24 h and post cured at 150 °C for 2 h. The fibre volume fraction (V_f) was calculated according to the ISO 14127:2008 standard:

$$V_f = \frac{m_f/\rho_f}{V_c}, \tag{2}$$

where m_f is the mass of the fibres, V_c is the volume of the composite and ρ_f is the density of the fibres (1350 kg/m^3), assuming a pore-free composite.

To compare the porosity content in flax/epoxy and GO-modified flax/epoxy composites, the transverse area of UD composites was inspected by LEICA DM 2500 M optical microscope on a dark field mode.

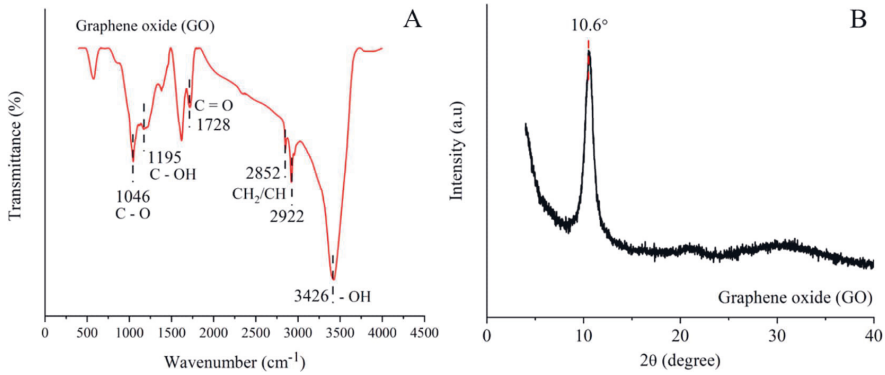

Fig. 1. The FTIR transmittance spectra (A) and XRD pattern (B) of graphene Oxide.

Samples were embedded in an epoxy resin before polishing. Images were processed using image processing software (ImageJ) to differentiate between porosity, fibre, lumen, and matrix. After thresholding on the grey level, a morphological analysis tool was applied to count the number and size of pores.

To study the interfacial adhesion at macroscale, transverse bending tests of composites were performed based on ASTM D7264. The flexural tests were performed on an Instron 5567 general-purpose mechanical testing machine with a 5 kN load cell. Composites were tested in a four-point bending condition with a crosshead speed of 2 mm/min. The strain was measured based on the load cell displacement.

Tensile tests were performed on the Instron 5567 testing machine with a 30 kN load cell and a crosshead speed of 2 mm/min based on ASTM D3039. The strain was measured using a clip-on extensometer (50 mm gauge length). Abrasive papers were placed without glue in between the testing clamps and the samples to avoid slipping. All samples were stored for two weeks before testing in a controlled environment of RH 50% and 22 °C. Average results from five samples per series are reported.

The fracture surfaces of tested composites and microbond test samples were examined with a Zeiss ULTRAplus scanning electron microscope (SEM). A thin carbon or gold coating was used to ensure sufficient conductivity for the samples.

3. Results and discussions

3.1. Characterisation of graphene oxide (GO)

Fig. 1a shows the FTIR spectra of graphene oxide (GO). The transmittance spectra of GO represents the various characteristic oxygen-rich functional groups. The strong and broad-band at 3426 cm^{-1} is related to the –OH stretching vibration of hydroxyl groups [39]. The existence of a few CH_2/CH groups can be noticed from bands at 2922 cm^{-1} and 2852 cm^{-1} [40]. The band around 1728 cm^{-1} is related to the C═O stretching vibration of carboxylic functional units [39]. Finally, the bands at 1195 cm^{-1} (C—OH stretching vibration) and 1046 cm^{-1} (C—O stretching vibration) testify the presence of epoxy functional groups [39]. Fig. 1b shows the sharp XRD peak at $2\theta = 10.6°$ which corresponds to 0.84 nm spacing between the graphene oxide sheets [40]. XRD pattern also indicates that the synthesised GO is free unreacted graphite (or unexfoliated) [41]. Based on our previous measurement with the atomic force microscope, the average thickness of single graphene oxide sheets was 0.84 nm [40]. In the same study, we also observed the wrinkled morphology of GO crystals which shows the flexible nature of GO. The results indicate the successful synthesis of GO with oxygen-rich functional groups.

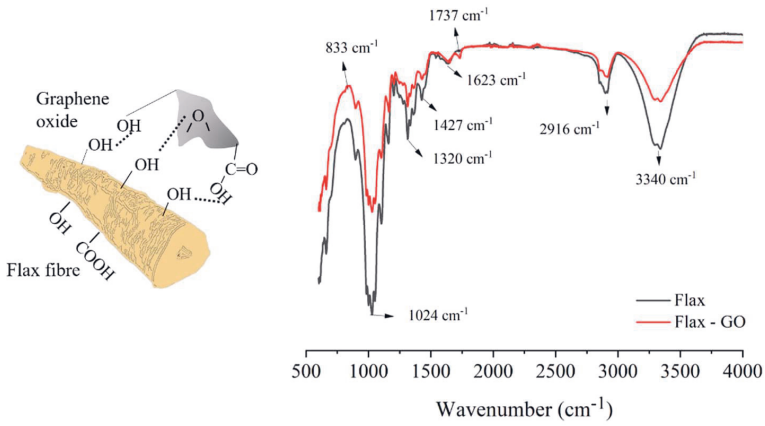

Fig. 2. The FTIR transmittance spectra of untreated flax and GO-modified flax fibres.

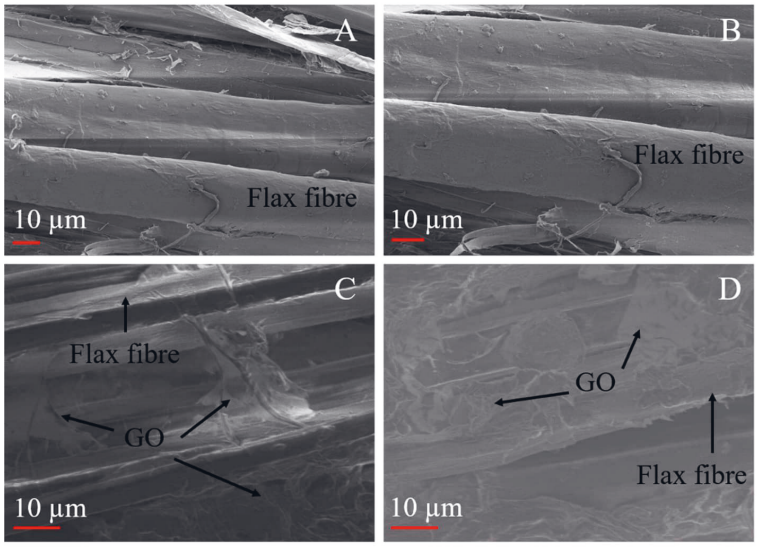

Fig. 3. Surface morphology of flax fibres (A, B) and GO-flax fibre (C, D).

Table 1
Summary of the tensile properties of elementary flax fibres.

Fibre	Breaking force cN	Elongation %	Tenacity cN/dtex	Linear density dtex
Flax	18 ± 6	3.1 ± 0.9	6.3 ± 2.7	3.2 ± 1.4
0.65 GO-flax	16 ± 6	2.9 ± 0.8	5.3 ± 2.7	3.6 ± 1.9
1.2 GO-flax	20 ± 5	3.6 ± 0.8	6.6 ± 2.7	3.5 ± 1.3
2 GO-flax	16 ± 6	2.9 ± 0.8	5.9 ± 2.4	2.9 ± 1.1

3.2. Surface characterisation of fibres

Fig. 2. shows the FTIR transmittance spectra of untreated flax and GO-modified flax fibres. The transmittance spectra of flax fibre show the typical band peaks of cellulose, hemicellulose, and lignin [11]. The band at 3340 cm^{-1} is related to the —OH stretching of hydroxyl groups mainly in cellulose and lignin [42]. The bands at 2849 cm^{-1} and 2916 cm^{-1} are usually related to the symmetric and asymmetric CH_2 stretching vibrations of cellulose and hemicellulose [42]. The band around 1632 cm^{-1} is ascribed to the O—H bending due to absorbed water [42,43]. The band groups at 1427 cm^{-1}, 1320 cm^{-1}, and 1024 cm^{-1} can be related to the C—H wagging vibration in cellulose and hemicellulose [43], the CH_2 rocking vibration at C6 in cellulose [42,44], and the C—O stretch vibrations of acetyl groups (lignin) [45]. The spectrum of the GO-modified flax exhibits a new band around 1737 cm^{-1} for the —C=O stretching vibrations of the —COOH groups of the GO [24,46]. FTIR results suggest successful adsorption of GO on the flax fibres by hydrogen bonding.

Fig. 3 compares the surface morphology of untreated flax fibres, and graphene oxide treated fibres. Fig. 3 a, b shows the rather smooth surface of flax fibres. Fig. 3 c, d represents the clear morphology difference between flax fibres and GO treated flax fibres. In Fig. 3 d the wrinkled nature of GO coating on the flax fibres is in agreement with our previous observation [40].

3.3. Tensile performance of elementary flax fibres

Table. 1 reports the average tensile properties of elementary flax fibres and GO treated flax fibres with three different concentrations (0.65 wt%, 1.2 wt%, 2 wt%). The breaking force, elongation at failure,

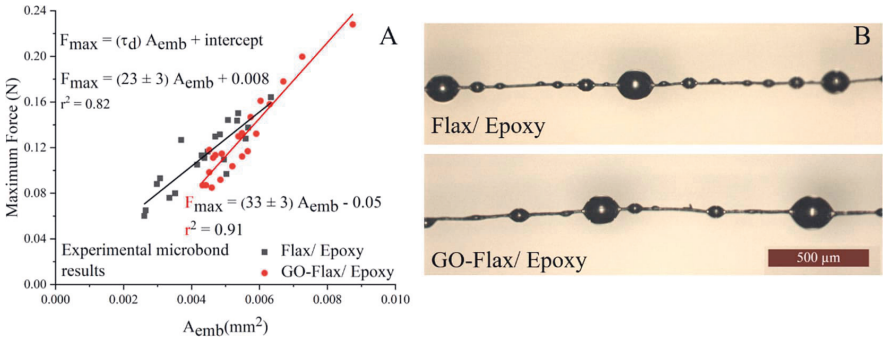

Fig. 4. Effect of GO-surface modification on the interfacial adhesion of elementary flax fibre/epoxy. (A) experimental microbond test results, (B) the shape of deposited epoxy droplets on the elementary flax and GO modified flax fibres.

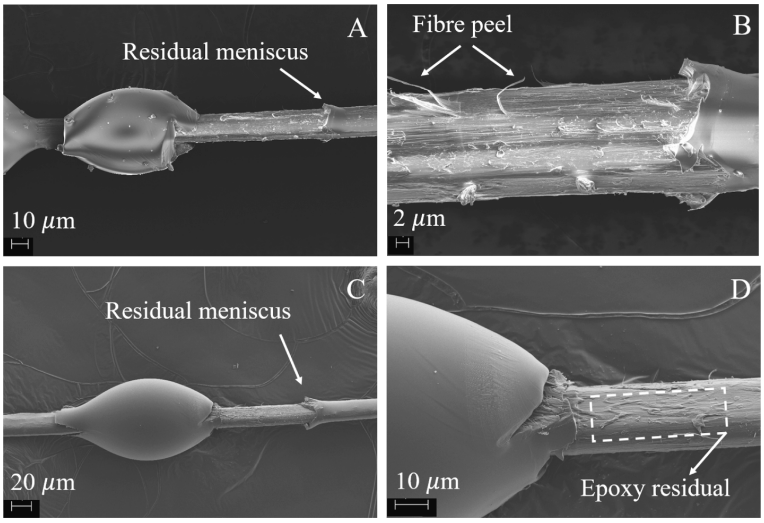

Fig. 5. Fracture surface analysis of untreated (A, B) and GO-treated (C, D) elementary flax fibre/epoxy after microbond test.

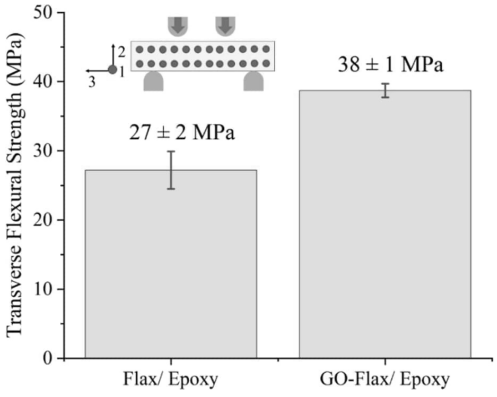

Fig. 6. Transverse four-point bending strength of untreated flax fibre/epoxy and GO-modified flax fibre/epoxy composites.

and tenacity of untreated elementary flax fibres are 18 ± 6 (cN), 3.1 ± 0.9 (%), and 6.3 ± 2.7 (cN/dtex) respectively. The variation from the average value is rather high which can be related to the inhomogeneous nature of natural fibres. The average tensile performance of elementary GO-flax fibres is in the range of untreated flax fibre regardless of the concentration. Also, the linear density of flax fibres is not affected by the graphene oxide surface modification. It can be concluded that there is no meaningful change in the tensile performance of single flax fibres after GO surface treatment. The detailed results are reported in the supplementary data 1.

3.4. Interfacial fibre/matrix adhesion

Fig. 4 presents the contribution of GO-treatment to the interfacial adhesion of elementary flax fibres with epoxy, as measured by the microbond test. The slope-based results (linear regression) in Fig. 4a suggest an interfacial shear strength (τ_d) of 33 ± 3 MPa for 1.2 wt% GO-flax/epoxy which is 43% higher than 23 ± 3 MPa for flax/epoxy. Microbond test assessment for 0.65 wt% GO-flax/epoxy and 2 wt% GO-flax/epoxy showed an interfacial shear strength of 25 ± 3 MPa and 20 ± 3 MPa respectively. The detailed results are reported in the supplementary data 2. The lower shear strength of 2 wt% GO-flax/epoxy can be potentially related to the formation of multi GO layers on the flax fibre acting as a weak spot against shear force. Daly et al. [47] showed that GO-to-GO shear strength in thicker multilayer graphene oxide could be as low as 5.3 ± 3.2 MPa. In the upcoming sections, performance of composites is based on 1.2 wt% GO-flax/epoxy which shows the best interfacial adhesion based on the microbond test.

Fig. 5 shows the fracture surfaces after the microbond test. The residual meniscus on the fibres (Fig. 5a, b) represents crack initiation in mode I close to the microvices followed by crack propagation along the interface, as was explained previously [48]. All droplets debonded with brittle failure. In Fig. 5b, d minor peelings of fibre cell-walls are evident after debonding. The sliver of fibre cell-walls indicates a better interfacial adhesion with epoxy compared to the internal fibre cohesion. In Fig. 5d resin residuals are visible on GO-modified elementary flax fibres after debonding, suggesting the failure onset locus has moved towards the epoxy matrix.

To further understand the effect of GO-modification on the interfacial adhesion of flax fibre/epoxy, Fig. 6 presents the transverse bending strength results of UD composites. Remarkably, the average transverse bending strength of the GO-flax/epoxy composites is 38 ± 1 MPa which is 40% higher than the corresponding value for flax/epoxy composite. The better transverse strength of GO-treated flax/epoxy composites suggests an improvement in the fibre/matrix adhesion. Better adhesion can be ascribed to the high amount of oxygen-containing functional groups of GO, namely hydroxyl (—OH), carboxyl (O—C═O), epoxide (C—O—C), and carbonyl (C═O), which can interact with the functional groups of epoxy [13,15,25]. C—N bond between amine hardener and GO treated flax fibres by ring opening polymerisation [13,49], and mechanical interlocking between wrinkled GO coating and epoxy is also possible [13]. The 43% improvement in the interfacial adhesion of flax fibre/epoxy composites by GO-surface modification, agrees with microbond results. Our findings agree with the previous reports on the effect of GO on the interfacial adhesion of glass and carbon fibres with epoxy, that GO can be used as an efficient interfacial coupler in fibrous composites [26,50].

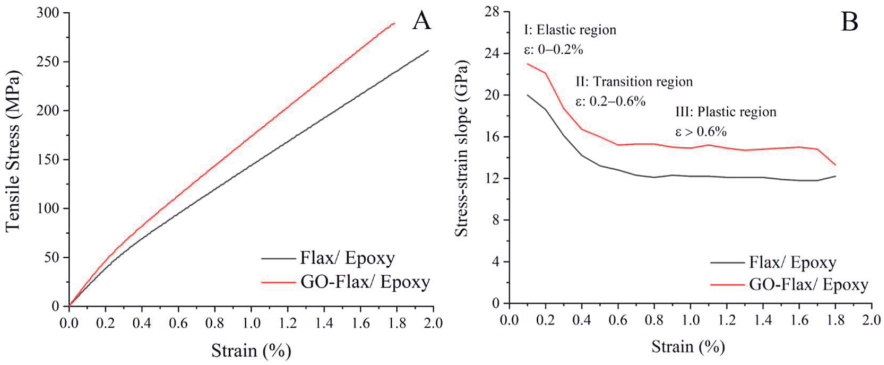

Fig. 7. Tensile behaviour of unidirectional flax/epoxy and GO-modified flax/epoxy. The graph A shows representative stress-strain results and the graph B shows the instantaneous stress-strain slope (stiffness) of the composite coupons for all strain ranges.

Table 2
Summary of the tensile properties of composites.

Sample	V_f	$E_{0.1\%}$	$E_{0.6\text{-}0.8\%}$	$\sigma_{tensile}$	$\varepsilon_{failure}$
	%	GPa	GPa	MPa	%
Flax/ Epoxy	40	20±1	13±1	260±21	1.86±0.07
GO-Flax/ Epoxy	40	23±1	15±1	275±14	1.70±0.05
Epoxy	–	2.2±0.05	–	53±1	5.1±0.1

3.5. Tensile behaviour of UD composites

Fig. 7a presents examples of the stress–strain curves related to the uniaxial tensile tests of flax/epoxy composites. Fig. 7b shows the trilinear development of tensile modulus with respect to strain. The nonlinearity at approximately 0.3% strain, is anticipated to be related to the viscoplastic deformation of the amorphous matrix of hemicellulose at the primary walls [51,52]. The tensile modulus of untreated flax fibre/epoxy and GO-treated flax fibre/epoxy composites are reported in Table. 2 for the initial strain range (until 0.1%) and between 0.6% and 0.8% strain range above the transition point. The tensile moduli (stiffness, E) of untreated flax fibre/epoxy composites at the initial and post-transition strain ranges are 20±1 GPa and 13±1 GPa respectively. In the similar strain ranges, GO-modified flax fibre composites have slightly higher (~2 GPa) modulus values of 23±1 GPa and 15±1 GPa. The difference in the tensile stiffness can be related to the better fibre/matrix adhesion with GO-treatment as reported in Fig. 6 by increased transverse flexural strength of composites. Better adhesion is often also associated with better fibre–matrix impregnation, which will lead to the increased modulus.

Additionally, Fig. 8 shows that the representative microstructure of GO-modified flax/epoxy composites is clearly less porous compared to

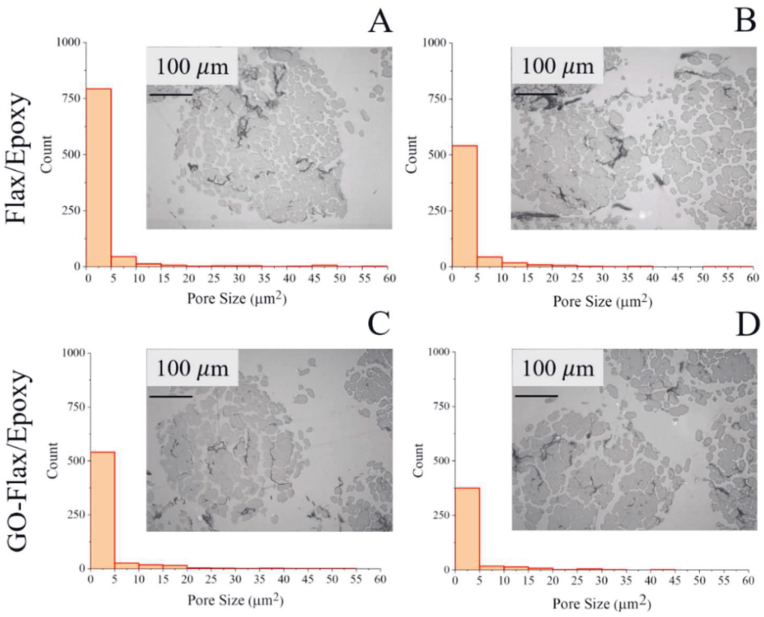

Fig. 8. The representative transverse cross-sectional micrographs of UD composites showing the microstructure of embedded fibre bundles of untreated flax fibre/epoxy (A, B) and GO- modified flax fibre/epoxy (C, D). The histograms show the number and size distribution of pores in each micrograph.

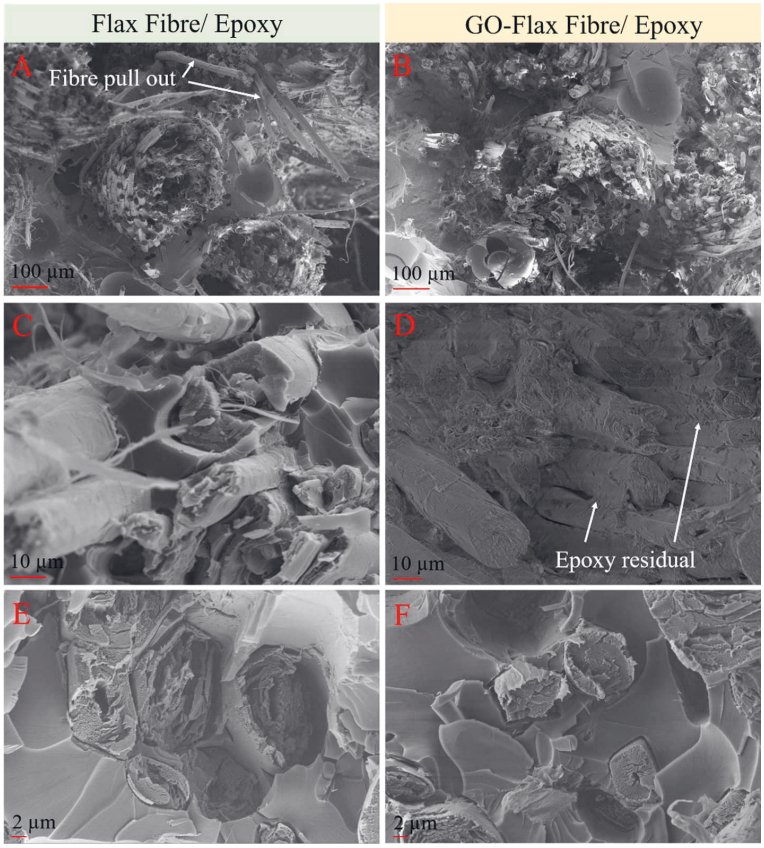

Fig. 9. The tensile fracture surface of flax/ epoxy (A, C, E) and GO-flax/ epoxy (B, D, F) composites.

reference flax/epoxy composites. The less porous nature of these GO-nanoengineered composites suggests a better fibre/matrix impregnation. The better fibre/matrix impregnation can be related to the improvement in fibre/matrix adhesion with GO treatment as discussed previously (in Section 3.4). Naturally, porosity in flax/epoxy would negatively affect the tensile stiffness [53] as well as ultimate performance. Due to the lower amount of porosity also at the fibre/matrix interface, GO-treated flax/epoxy demonstrates indeed better tensile stiffness (Table. 2). However, the tensile strength and the failure strain of both composites are at a similar level in this study. The failure process upon tensile test propagates fast and interfacial properties are not significantly shown – yet it is not clear if the GO-modification could not improve long-term dynamic (e.g. fatigue) performance in tensile mode.

The fracture surface of the flax/epoxy composite in Fig. 9a demonstrates that local failure in shear occurred along fibre/matrix interphases with long fibre pull-outs. The fracture surface of GO-modified flax/epoxy in Fig. 9b is essentially similar to the one of flax/epoxy except for the length of the fibre pull-outs. For GO-modified flax/epoxy, the pull-out lengths were observed shorter, which is known to indicate better load transfer and adhesion between the fibres and matrix of the composites. Also, Fig. 9c shows the relatively smooth fibre surfaces after flax/ epoxy fracture, whereas in Fig. 9d epoxy residual are evident on GO-modified flax fibres. Epoxy residuals on the fracture surface of GO-flax/epoxy composites show improved adhesion and affinity between fibre/matrix. Fig. 9 e, f indicates the brittle nature of the fracture surfaces for both untreated and modified composites.

Regardless of the 43% improvement in the microbond τ_d values, and 40% enhancement in the interfacial strength measured by transverse bending, our findings suggest that the extent of improvement in the longitudinal tensile strength of flax/epoxy composites by GO- modification of the high-performance flax fibres is not significant for quasi-static loadings. This observation is in line with the existing data. Merttote et al. [9] reported that in the case of high-performance flax yarns with large content of individual elementary fibres, even a 100% improvement in the interfacial adhesion does not significantly affect the longitudinal tensile strength of flax fibre reinforced composites. Also, a 110% improvement in tensile strength of jute/epoxy composites reported by Sarker et al. [13], was achieved by a combination of alkali lipophilic extraction, combing jute bundles to individual fibres, and GO-adsorption. Therefore, it can be argued that a significant improvement of the tensile strength in their work is mainly due to the removal of waxes and individualisation of pristine jute bundles.

Nevertheless, a significant improvement in transverse strength is very relevant to improve off-axis strength in multi-directional composites. In future work, the fatigue testing of flax/epoxy composites will have to be analysed to understand the interfacial effects on the dynamic load range. The fatigue testing of unidirectionally reinforced composites is still under development, due to the challenges related to the test specimen design that could reveal interfacial effects on the results [54,55].

4. Conclusions

This paper presents the potential of graphene oxide (GO) surface treatment to improve the interfacial adhesion and the tensile behaviour of flax fibre/epoxy composites. A GO-treatment is performed on a high-end flax fabric intended for structural applications rather than on green or unprocessed flax yarns to highlight the pure effect of GO-treatment. The microbond results indicated a 43% improvement in the interfacial shear strength of the elementary flax fibre/epoxy by GO-surface modification. The micrographs of the GO-treated flax fibres after the microbond test revealed a shift of the failure locus – the onset had shifted towards the matrix. The transverse strength of GO-modified flax fibre/epoxy composite outperformed the untreated flax fibre/epoxy by 40%. The better transverse strength of GO-flax/epoxy composites was ascribed to the enhanced interactions between oxygen-containing functional groups of GO adsorbed into flax fibres and epoxy (interface). A significant improvement in transverse strength of composites is very relevant to improve off-axis strength in multi-directional composites. The tensile stiffness of GO-modified flax fibre/epoxy composites was on average 2 GPa higher than untreated flax/epoxy composites for all strain ranges. The quasi-static longitudinal tensile ultimate strength and the failure strain were similar for the reference and modified version. Our findings suggest that the longitudinal tensile strength of UD flax/epoxy composites (with large content of individual elementary flax fibres) is not sensitive to the improvement in the fibre/matrix interfacial adhesion.

CRediT authorship contribution statement

F. Javanshour: Methodology, Formal analysis, Investigation, Writing - original draft, Project administration, Visualization. **KR. Ramakrishnan:** Writing - review & editing. **R.K. Layek:** Investigation, Writing - review & editing. **P. Laurikainen:** Software, Writing - review & editing. **A. Prapavesis:** Writing - review & editing, Project administration. **M. Kanerva:** Writing - review & editing. **P. Kallio:** Project administration, Funding acquisition, Supervision. **A.W. Van Vuure:** Supervision, Writing - review & editing, Funding acquisition. **E. Sarlin:** Supervision, Investigation, Writing - review & editing, Funding acquisition.

Declaration of Competing Interest

The authors declare that they have no known competing financial interests or personal relationships that could have appeared to influence the work reported in this paper.

Acknowledgements

This project is funded by the European Union's Horizon 2020 research and innovation programme under the Marie Skłodowska-Curie grant agreement No 764713 – FibreNet. This work made use of Tampere Microscopy Center facilities at Tampere University. The authors are grateful to Bcomp Ltd. and its CTO Dr Julien Rion for supplying the flax fabrics and providing valuable insights.

Appendix A. Supplementary data

Supplementary data to this article can be found online at https://doi.org/10.1016/j.compositesa.2020.106270.

References

[1] Duc F, Bourban PE, Plummer CJG, Månson J-AE. Damping of thermoset and thermoplastic flax fibre composites. Compos Part A Appl Sci Manuf 2014;64:115–23. https://doi.org/10.1016/j.compositesa.2014.04.016.

[2] Bourmaud A, Beaugrand J, Shah D, Placet V. Towards the design of high-performance plant fibre composites. Prog Mater Sci 2018;97:347–408. https://doi.org/10.1016/j.pmatsci.2018.05.005.

[3] Joshi S V, Drzal LT, Mohanty AK, Arora S. Are natural fiber composites environmentally superior to glass fiber reinforced composites? Compos. Part A Appl. Sci. Manuf., vol. 35, Elsevier; 2004, p. 371–6. http://doi.org/10.1016/j.compositesa.2003.09.016..

[4] Le Duigou A, Davies P, Baley C. Environmental impact analysis of the production of flax fibres to be used as composite material reinforcement. J Biobased Mater Bioenergy 2011;5:153–65. https://doi.org/10.1166/jbmb.2011.1116.

[5] Marrot L, Bourmaud A, Bono P, Baley C. Multi-scale study of the adhesion between flax fibers and biobased thermoset matrices. Mater Des 2014;62:47–56. https://doi.org/10.1016/j.matdes.2014.04.087.

[6] Islam MS, Pickering KL, Foreman NJ. Influence of alkali fiber treatment and fiber processing on the mechanical properties of hemp/epoxy composites. J Appl Polym Sci 2011;119:3696–707. https://doi.org/10.1002/app.31335.

[7] Matthews FL, Rawlings RD. Composite materials: engineering and science. Cambridge, England: Woodhead Publishing; 1999.

[8] Coroller G, Lefeuvre A, Le Duigou A, Bourmaud A, Ausias G, Gaudry T, et al. Effect of flax fibres individualisation on tensile failure of flax/epoxy unidirectional composite. Compos Part Appl Sci Manuf 2013;51:62–70.

[9] Merotte J, Le Duigou A, Kervoelen A, Bourmaud A, Behlouli K, Sire O, et al. Flax and hemp nonwoven composites: The contribution of interfacial bonding to improving tensile properties. Polym. Test. 2018;66:303–11. https://doi.org/10.1016/j.polymertesting.2018.01.019.

[10] Li Y, Pickering KL. Hemp fibre reinforced composites using chelator and enzyme treatments. Compos Sci Technol 2008;68:3293–8. https://doi.org/10.1016/j.compscitech.2008.08.022.

[11] Acera Fernández J, Le Moigne N, Caro-Bretelle AS, El Hage R, Le Duc A, Lozachmeur M, et al. Role of flax cell wall components on the microstructure and transverse mechanical behaviour of flax fabrics reinforced epoxy biocomposites. Ind Crops Prod 2016;85:93–108. https://doi.org/10.1016/j.indcrop.2016.02.047.

[12] Van de Weyenberg I, Ivens J, De Coster A, Kino B, Baetens E, Verpoest I. Influence of processing and chemical treatment of flax fibres on their composites. Compos Sci Technol 2003;63(9):1241–6.

[13] Sarker F, Potluri P, Afroj S, Koncherry V, Novoselov KS, Karim N. Ultrahigh Performance of Nanoengineered Graphene-Based Natural Jute Fiber Composites. ACS Appl Mater Interfaces 2019;11:21166–76. https://doi.org/10.1021/acsami.9b04696.

[14] Perremans D, Verpoest I, Dupont-Gillain C, Van Vuure AW. Investigation of the tensile behavior of treated flax fibre bio-composites at ambient humidity. Compos Sci Technol 2018;159:119–26.

[15] Sarker F, Karim N, Afroj S, Koncherry V, Novoselov KS, Potluri P. High-Performance Graphene-Based Natural Fiber Composites. ACS Appl Mater Interfaces 2018;10:34502–12. https://doi.org/10.1021/acsami.8b13018.

[16] Dang CY, Shen XJ, Nie HJ, Yang S, Shen JX, Yang XH, et al. Enhanced interlaminar shear strength of ramie fiber/polypropylene composites by optimal combination of graphene oxide size and content. Compos Part B Eng 2019;168:488–95. https://doi.org/10.1016/j.compositesb.2019.03.080.

[17] Seghini MC, Touchard F, Sarasini F, Chocinski-Arnault L, Tirillò J, Bracciale MP, et al. Effects of oxygen and tetravinylsilane plasma treatments on mechanical and interfacial properties of flax yarns in thermoset matrix composites. Cellulose 2020;27:511–30. https://doi.org/10.1007/s10570-019-02785-3.

[18] Wang H, Xian G, Li H. Grafting of nano-TiO2 onto flax fibers and the enhancement of the mechanical properties of the flax fiber and flax fiber/epoxy composite. Compos Part A Appl Sci Manuf 2015;76:172–80. https://doi.org/10.1016/j.compositesa.2015.05.027.

[19] Russo P, Vitiello L, Sbardella F, Santos JI, Tirillò J, Bracciale MP, et al. effect of carbon nanostructures and fatty acid treatment on the mechanical and thermal performances of flax/polypropylene composites. Polymers (Basel) 2020;12.. https://doi.org/10.3390/polym12020438.

[20] Van de Weyenberg I, Chi Truong T, Vangrimde B, Verpoest I. Improving the properties of UD flax fibre reinforced composites by applying an alkaline fibre treatment. Compos Part A Appl Sci Manuf 2006;37:1368–76. https://doi.org/10.1016/j.compositesa.2005.08.016.

[21] Wei X, Mao L, Soler-Crespo RA, Paci JT, Huang J, Nguyen ST, et al. Plasticity and ductility in graphene oxide through a mechanochemically induced damage tolerance mechanism. Nat Commun 2015;6:1–9. https://doi.org/10.1038/ncomms9029.

[22] Liu T, Zhao Z, Tjiu WW, Lv J, Wei C. Preparation and characterisation of epoxy nanocomposites containing surface-modified graphene oxide. J Appl Polym Sci 2014;131. https://doi.org/10.1002/app.40236. n/a-n/a.

[23] Toader G, Rusen E, Teodorescu M, Diacon A, Stanescu PO, Damian C, et al. New polyurea MWCNTs nanocomposite films with enhanced mechanical properties. J Appl Polym Sci 2017;134:45061. https://doi.org/10.1002/app.45061.

[24] Chen J, Zhao D, Jin X, Wang C, Wang D, Ge H. Modifying glass fibers with graphene oxide: Towards high-performance polymer composites. Compos Sci Technol 2014;97:41–5. https://doi.org/10.1016/j.compscitech.2014.03.023.

[25] Zhang X, Fan X, Yan C, Li H, Zhu Y, Li X, et al. Interfacial microstructure and properties of carbon fiber composites modified with graphene oxide. ACS Appl Mater Interfaces 2012;4:1543–52. https://doi.org/10.1021/am201757v.

[26] Zhang RL, Gao B, Ma QH, Zhang J, Cui HZ, Liu L. Directly grafting graphene oxide onto carbon fiber and the effect on the mechanical properties of carbon fiber composites. Mater Des 2016;93:364–9. https://doi.org/10.1016/J.MATDES.2016.01.003.

[27] Li F, Liu Y, Qu C-B, Xiao H-M, Hua Y, Sui G-X, et al. Enhanced mechanical properties of short carbon fiber reinforced polyethersulfone composites by graphene oxide coating. Polymer (Guildf) 2015;59:155–65. https://doi.org/10.1016/J.POLYMER.2014.12.067.
[28] Kamaraj M, Dodson EA, Datta S. Effect of graphene on the properties of flax fabric reinforced epoxy composites. Taylor Fr 2019. https://doi.org/10.1080/09243046.2019.1709679.
[29] Dreyer DR, Park S, Bielawski CW, Ruoff RS. The chemistry of graphene oxide. Chem Soc Rev 2010;39:228–40. https://doi.org/10.1039/b917103g.
[30] Hummers WS, Offeman RE. Preparation of Graphitic Oxide. J Am Chem Soc 1958;80:1339. https://doi.org/10.1021/ja01539a017.
[31] Dikin DA, Stankovich S, Zimney EJ, Piner RD, Dommett GHB, Evmenenko G, et al. Preparation and characterisation of graphene oxide paper. Nature 2007;448:457–60. https://doi.org/10.1038/nature06016.
[32] Compton OC, Cranford SW, Putz KW, An Z, Brinson LC, Buehler MJ, et al. Tuning the mechanical properties of graphene oxide paper and its associated polymer nanocomposites by controlling cooperative intersheet hydrogen bonding. ACS Nano 2012;6:2008–19. https://doi.org/10.1021/nn202928w.
[33] Pacilé D, Meyer JC, Fraile Rodríguez A, Papagno M, Gómez-Navarro C, Sundaram RS, et al. Electronic properties and atomic structure of graphene oxide membranes. Carbon N Y 2011;49:966–72. https://doi.org/10.1016/j.carbon.2010.09.063.
[34] Ramanathan T, Abdala AA, Stankovich S, Dikin DA, Herrera-Alonso M, Piner RD, et al. Functionalized graphene sheets for polymer nanocomposites. Nat Nanotechnol 2008;3:327–31.
[35] Ruiz L, Xia W, Meng Z, Keten S. A coarse-grained model for the mechanical behavior of multi-layer graphene. Carbon N Y 2015;82:103–15. https://doi.org/10.1016/j.carbon.2014.10.040.
[36] Sheet PD. Art . No . 5009 UD fabric Product description n.d.:1–2..
[37] Laurikainen P, Kakkonen M, von Essen M, Tanhuanpää O, Kallio P, Sarlin E. Identification and compensation of error sources in the microbond test utilising a reliable high-throughput device. Compos Part A Appl Sci Manuf 2020;137:105988. https://doi.org/10.1016/j.compositesa.2020.105988.
[38] Kang SK, Lee DB, Choi NS. Fiber/epoxy interfacial shear strength measured by the microdroplet test. Compos Sci Technol 2009;69:245–51. https://doi.org/10.1016/j.compscitech.2008.10.016.
[39] Stankovich S, Piner RD, Nguyen SBT, Ruoff RS. Synthesis and exfoliation of isocyanate-treated graphene oxide nanoplatelets. Carbon N Y 2006;44:3342–7. https://doi.org/10.1016/j.carbon.2006.06.004.
[40] Layek RK, Ramakrishnan KR, Sarlin E, Orell O, Kanerva M, Vuorinen J, et al. Layered structure graphene oxide/methylcellulose composites with enhanced mechanical and gas barrier properties. J Mater Chem A 2018;6:13203–14. https://doi.org/10.1039/c8ta03651a.
[41] Cote LJ, Cruz-Silva R, Huang J. Flash reduction and patterning of graphite oxide and its polymer composite. J Am Chem Soc 2009;131:11027–32. https://doi.org/10.1021/ja902348k.
[42] Rout SK, Tripathy BC, Padhi P, Kar BR, Mishra KG. A green approach to produce silver nano particles coated agro waste fibers for special applications. Surf Interfaces 2017;7:87–98. https://doi.org/10.1016/j.surfin.2017.03.004.
[43] Taha I, Steuernagel L, Ziegmann G. Optimization of the alkali treatment process of date palm fibres for polymeric composites. Compos. Interfac. 2007;14:669–84. https://doi.org/10.1163/156855407782106528.
[44] Sawpan MA, Pickering KL, Fernyhough A. Effect of various chemical treatments on the fibre structure and tensile properties of industrial hemp fibres. Compos Part A Appl Sci Manuf 2011;42:888–95. https://doi.org/10.1016/j.compositesa.2011.03.008.
[45] Roy A, Chakraborty S, Kundu SP, Basak RK, Basu Majumder S, Adhikari B. Improvement in mechanical properties of jute fibres through mild alkali treatment as demonstrated by utilisation of the Weibull distribution model. Bioresour Technol 2012;107:222–8. https://doi.org/10.1016/j.biortech.2011.11.073.
[46] Costa UO, Nascimento LFC, Garcia JM, Monteiro SN, da Luz FS, Pinheiro WA, et al. Effect of graphene oxide coating on natural fiber composite for multilayered ballistic armor. Polymers (Basel) 2019;11.. https://doi.org/10.3390/polym11081356.
[47] Daly M, Cao C, Sun H, Sun Y, Filleter T, Singh CV. Interfacial Shear Strength of Multilayer Graphene Oxide Films. ACS Nano 2016;10:1939–47. https://doi.org/10.1021/acsnano.5b05771.
[48] Dsouza R, Antunes P, Kakkonen M, Jokinen J, Sarlin E, Kallio P, et al. 3D interfacial debonding during microbond testing: Advantages of local strain recording. Compos Sci Technol 2020;195:108163. https://doi.org/10.1016/j.compscitech.2020.108163.
[49] Yang H, Shan C, Li F, Zhang Q, Han D, Niu L. Convenient preparation of tunably loaded chemically converted graphene oxide/epoxy resin nanocomposites from graphene oxide sheets through two-phase extraction. J Mater Chem 2009;19(46):8856–60.
[50] Chen J, Zhao D, Jin X, et al. Modifying glass fibers with graphene oxide: towards high-performance polymer composites. Compos Sci Technol 2014;97:41–5.
[51] Giancane S, Panella FW, Dattoma V. Characterization of fatigue damage in long fiber epoxy composite laminates. Int J Fatigue 2010;32(1):46–53.
[52] Bensadoun F, Verpoest I, Baets J, Müssig J, Graupner N, Davies P, et al. Impregnated fibre bundle test for natural fibres used in composites. J Reinf Plast Compos 2017;36:942–57. https://doi.org/10.1177/0731684417695461.
[53] Madsen B, Thygesen A, Lilholt H. Plant fibre composites–porosity and stiffness. Compos Sci Technol, 69 (7–8) (2009), pp. 1057–1069..
[54] Korkiakoski S, Brøndsted P, Sarlin E, Saarela O. Influence of specimen type and reinforcement on measured tension-tension fatigue life of unidirectional GFRP laminates. Int J Fatigue 2016;85:114–29. https://doi.org/10.1016/j.ijfatigue.2015.12.008.
[55] Korkiakoski S, Sarlin E, Suihkonen R, Saarela O. Influence of reinforcement positioning on tension-tension fatigue performance of quasi-unidirectional GFRP laminates made of stitched fabrics. Compos Part B Eng 2017;112:38–48. https://doi.org/10.1016/j.compositesb.2016.12.017.

PAPER II

UNPUBLISHED MANUSCRIPT

The peer-reviewed version is published by Elsevier in the journal of Composites Part C: Open Access (2023).

Effect of graphene oxide fibre surface modification on low-velocity impact and fatigue performance of flax fibre reinforced composites

F. Javanshour [1*], A. Prapavesis [2], K. Lahtonen [3], N. Pournoori [1], T. Pärnänen [1], M. Kanerva [1], A. W. Van Vuure [2], E. Sarlin [1]

[1] Unit of Materials Sciences and Environmental Engineering, Tampere University, Tampere, Finland

[2] Department of Materials Engineering, Composite Materials Group, KU Leuven, Leuven, Belgium

[3] Faculty of Engineering and Natural Sciences, Tampere University, P.O. Box 692, FI-33014 Tampere, Finland

* Corresponding author. Email address: farzin.javanshour@tuni.fi

Abstract

Fatigue and impact resistance are essential performance indicators for designing sustainable and durable natural fibre composites in structural applications. Here, flax fibres were modified with graphene oxide (GO) to stimulate energy dissipation through interfacial sliding between fibre and matrix and potentially between graphene layers. Based on the results, GO-modification reduced the slope of the *S-N* curve of flax-epoxy composites by 17%. The GO-modification of fibres altered the brittle fatigue failure mode of composites to ductile failure dominated by fibre pull-outs. According to the tomography assessments, GO-treatment promoted the dissipation of impact energy through delamination. Interestingly, GO-modification enhanced the capacity of composites to elastically restore part of the kinetic energy to the impactor and delayed the damage initiation. However, the GO-treatment of fibres did not alter the impact perforation energy of composites. The in-situ impact damage progression on the rear surface of composites was monitored with synchronised high-speed optical cameras.

Keywords

Natural fibers; Bicomposites; Surface treatments; Failure

1. Introduction

Natural fibres such as flax are a class of green engineering reinforcements for structural applications. Specifically, flax fibre bundles offer elastic modulus of 58 ± 6 GPa, tensile and compressive strength of 530 ± 44 MPa and 237 ± 29 MPa, respectively, tensile failure strain in the range of 1.08 ± 0.13%, and a low density of 1.4 g/cm^3 [1,2]. Polymeric composites reinforced with natural fibres are promising for sports and automotive applications [3–5], and they offer a unique combination of high stiffness and 2–3 times better damping than carbon fibre reinforced composites [6,7]. For those applications,

resistance against dynamic loads, which might onset fatigue and impact damage, is critical. Optimising these properties will allow design with natural fibre composites' to achieve both safety and sustainability.

The fatigue performance of composites reinforced with flax or hemp is comparable to conventional composites, such as glass fibre reinforced counterparts. For instance, composites produced with [0/90] cross-ply lay-up tested under strain-controlled cyclic load (5 Hz and strain ratio of 0.1) have shown comparable fatigue trend slopes for flax-epoxy and glass-epoxy composites [8]. However, the performance of natural fibre composites is not optimised in terms of impact resistance and perforation energy. Even at low-velocity impact energies far below the perforation energy, through-thickness fibre failure is the dominant damage mode for flax fibre composites [9,10]. It is essential to enhance the impact resistance of flax fibre reinforced composites without compromising their fatigue performance.

The interfacial toughness between flax fibre and matrix should be modified to allow energy dissipation through interfacial debonding and fibre pull-out to achieve better impact resistance [9–12]. Besides, the interfacial toughening strategy should also assure effective force transfer between fibre and matrix through optimum interfacial adhesion without or with minor compromises on the quasi-static performance of composites [9–11,13]. One of the effective methods is to deploy a thin ductile layer between fibre and matrix to promote interfacial toughness and fibre pull-out. For instance, cellulose acetate surface modification has been shown to reduce the impact-induced fibre-dominant failure and enhance the perforation energy of cross-ply flax-epoxy composites by 40% [9]. An alternative method can be to apply multilayer graphene oxide (GO) crystals on fibres and potentially promote energy dissipation through interfacial sliding between fibre and matrix and sliding between individual graphene oxide layers within GO [14]. A recent study showed that surface modification of carbon fibres with graphene oxide deposits (composed of 5–10 GO layers) enhanced the interfacial damping performance of carbon-epoxy composites by 113% based on the loss factor acquired from dynamic mechanical analysis (DMA) [14].

The effect of graphene oxide surface modification on the mechanical performance of natural fibre composites has been focused mainly on epoxy resins, where the fibre-matrix adhesion was studied based on microbond testing and quasi-static transverse tensile testing [15,16]. Usually, strong hydrogen and covalent bonds form between fibre and matrix by in-situ polymerisation of low viscosity and reactive resins such as epoxies and PMMA [17], where resin can also penetrate the fibre structures (with a penetration depth of 1.7–2.2 μm) [18]. Deposition of GO crystals with oxygen-containing functional groups (such as –OH, O–C=O, C–O–C, C=O) on fibres can further promote hydrogen bond formation between fibre and matrix [15,16]. For instance, flax fibres dip-coated in an aqueous dispersion with 1.2 wt% GO have shown 40% higher apparent interfacial shear strength and transverse flexural strength than unmodified flax-epoxy [15]. Interestingly, the fractographic studies of fibre and

droplets after microbond testing showed epoxy resin residue on GO-modified fibres suggesting the movement of failure onset locus towards the matrix [15]. Therefore, the surface modification of flax fibres with graphene oxide can be a potential toughening method against impact loads for macroscale composites.

The understanding of the effect of GO-surface modification of fibres on the impact and fatigue performance of composites is limited. Few studies are available on the impact performance of natural fibre composites with GO-dispersed epoxy resins [19,20] rather than GO-modified fibres. Alipour et al. [19] studied the low-velocity drop-weight impact behaviour at 18 J kinetic energy for flax-epoxy composites (2 × 2 twill woven fabrics, 0.1–0.7 wt% GO-dispersed epoxy resin, and 30% V_f). The best performance in terms of maximum impact contact force (+21%) and surface damage area on the rear surface (−68%, based on optical microscope images) was found for 0.5 wt% GO-modified composites. The higher contact force can be related to the 47% better quasi-static flexural strength of GO-modified composites compared to unmodified flax-epoxy in their study. However, the lower extent of surface damage area in their study is debatable as the internal damage area was not investigated.

Here, the synergistic effect of GO-fibre surface modification on the impact resistance and cyclic loading performance of flax-epoxy composites was investigated by applying tension-tension fatigue and low-velocity drop-weight impact tests. Epoxy resin was selected as the matrix due to its good mechanical properties and reactive nature, which provides strong interfacial adhesion between fibre and matrix [21], best durability under cyclic mechanical [22] and hygrothermal loading conditions [23–25], and wide industrial application. The motivation was to benefit from the potential energy dissipation through interfacial sliding between fibre and matrix, and inside graphene layers which were previously reported for GO-modified flax fibre-epoxy based on microbond testing and dynamic mechanical analysis [14,15,26]. After fatigue tests, the fracture surfaces of composites were investigated by scanning electron microscopy (SEM). The internal through-thickness damage of impacted composite specimens was studied by X-ray computed tomography.

2. Methodology

Non-crimp flax fabrics (ampliTex) of unidirectional and twill 2 × 2 types with an areal density of 300 g/m^2 were provided by Bcomp (Fribourg, Switzerland). The manufacturer treated the flax fibres with a standard boiling water procedure to remove waxes from the surface. A standard epoxy resin (Epopox A-28, Amroy Europe, Lahti, Finland) and a polyether diamine hardener (Jeffamine D-23, Hunstman, Texas, USA) with 35 wt% hardener to epoxy ratio were used as the polymer matrix system. A stable aqueous dispersion of graphene oxide (Graphenea, Gipuzkoa, Spain) with GO concentration of 1.2 wt%, pH of 1.8–2, and particle size of 14–17 μm was used for dip-coating flax fabrics for 10 minutes

(at 23 °C). The dip-coated fabrics were rinsed in deionised water to remove the excess unbound GO-particles from the surface. The GO-modified fabrics were oven-dried at 50 °C for 24 h. The selection of the GO concentration was with reference to the previous study, where the 1.2 wt% GO-modified flax fibres had the highest interfacial shear strength with epoxy resin [15].

The elemental surface compositions of GO films, unmodified flax, and GO-modified flax yarns were characterised based on X-ray photoelectron spectroscopy (XPS). The XPS analysis was performed by employing a non-monochromatic Al Kα X-ray source and VG Microtech CLAM 4 hemispherical electron spectrometer. The spectra were collected on a circular analysis area with 0.6 mm in diameter in the following order: C 1s, O 1s, survey scan, Na 1s, S 2p. The C 1s evaluation was repeated to check the possible X-ray-induced damage. The background-subtracted XPS spectra were least-squares fitted with a combination of symmetric Gaussian Lorentzian component line shapes. The binding energy scale was calibrated according to the C 1s C–C/H peak at 284.8 eV. The relative atomic concentrations were calculated using Scofield photoionisation cross-sections.

The effect of GO-modification on the polarity of flax fibres was investigated through a fibre-water contact angle with a high-precision tensiometer (K100SF, Krüss, Hamburg, Germany). Fibres were immersed in ultrapure water at a 1.5 mm/min velocity to measure the wetting forces exerted on the fibres. The contact angle was deduced from the Wilhelmy equation $F_{wet} = p\,\gamma_{LV}\cos\theta$ [27] where F_{wet} is the measured wetting force, p is the fibre perimeter, and γ_{LV} is the surface tension of water (72.8 mN/m). The wetted perimeters (p) of single fibres were deduced from the same formula with n-Hexane (99.6%, Acros Organics), assuming a perfectly wetting liquid ($\theta = 0°$ and $\gamma_{LV} = 18.4$ mN/m) [28].

Flax-epoxy composite panels with a fibre volume fraction (V_f) of 40% were manufactured based on the vacuum-assisted resin infusion method. The inherent moisture within flax fabrics was removed by oven-drying at 115 °C for 2 h before the resin infusion to minimise the void formation and possible hindrance of the curing process [10,29].

The fatigue performance of flax-epoxy composites was evaluated by performing cyclic loading tests of composites with $[(0,90)]_4$ lay-ups following the ASTM D3479 standard. Rectangular-shaped specimens were used with dimensions of 250 mm × 25 mm × 2 mm (length × width × thickness). Tapered glass-epoxy tabs were used to reduce the stress concentration at the gripped section of the specimens. The tests were performed with a servo-hydraulic tester (MTS 180, Minnesota, USA) equipped with a 100 kN load cell and a gauge length of 150 mm. A constant-load amplitude and a sinusoidal wave shape were applied at a frequency of 5 Hz. The loading frequency of 5 Hz was chosen to avoid any temperature rise above 10 °C (see ASTM D3479). The stress ratio (R) of the nominal minimum to maximum applied stress was 0.1. Stress-cycles to failure (S-N) graphs were acquired by registering the

number of cycles to failure and the nominal maximum stress for each specimen. The load levels (90%, 80%, 70%, and 50%) for the low-cycle fatigue tests were defined with respect to the ultimate tensile strength. Three specimens per load level (excluding any grip failure) were reported. The surface temperature of the specimens during testing was monitored by a longwave IR camera (model Ti400, Fluke, Washington, USA) with thermal sensitivity of 0.05 °C at 30 °C. The ambient conditions during tests were 23 °C and 50% RH. The fracture surface analysis of composites was carried out with a ULTRAplus (Zeiss, Oberkochen, Germany) scanning electron microscope (SEM). A thin platinum-palladium (Pt-Pd) coating was used to ensure enough conductivity for the SEM samples.

The low-velocity impact performance of flax-epoxy composites with a $[0/90]_{3S}$ lay-up was studied with an instrumented drop-weight tester (Type 5, Rosand, Ohio, USA) without rebound impacts per ASTM D7136 and ASTM D5628 standards. Rectangular-shaped specimens with dimensions of 60 mm × 60 mm × 5 mm (length × width × thickness) were clamped between two steel fixtures with a circular test area (diameter 40 mm) representing a fixed support. The drop height of the impactor (2772 g) was adjusted to 0.33, 0.55, 0.66, and 0.88 m to reach kinetic energies of 9, 15, 18, and 21 J, respectively. A hemispherical steel-made head (diameter 12.7 mm) was fixed to the impactor. The contact force was measured using a load sensor (60 kN) between the head and the impactor structure. The force data were recorded at a 180 kHz frequency. The displacement of the impactor was numerically integrated from the measured contact force-time curve. Three composite specimens were tested for each impact energy level. During the impact testing, the rear surfaces of composites (opposite to the impacted surface) were in-situ monitored via mirrors placed under the specimens with a synchronised high-speed optical camera (Fastcam SA-X2, Photron, Tokyo, Japan). A conventional mirror was placed at an angle with a 35 cm distance from the lens below the specimen to reflect the full-field deformations. The impact-induced internal damage of composites was studied with X-ray computed (X-CT) tomography (UniTOM XL, TESCAN, Ghent, Belgium) as a non-destructive inspection method.

3. Results and discussions

3. 1. Surface characterisation of fibres and morphology of composites

The XPS spectra of unmodified flax fibres (Flax), graphene oxide film (GO), and GO-modified flax fibres (GO-flax) is presented in Fig. 1 and Table 1. The GO and flax fibre surfaces contained only C and O, while GO also had trace amounts (<1 at. %) of Na and S. The surface characteristics of each series are investigated in the following paragraphs.

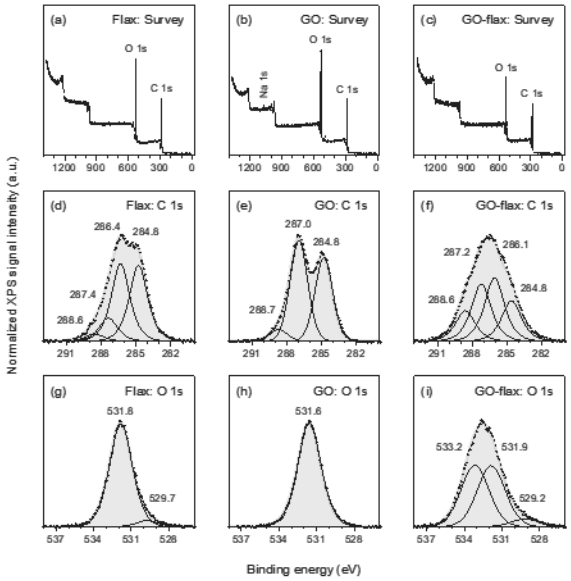

Fig 1. XPS spectra of flax, GO, and GO-flax. (a)–(c) survey scans, (d)–(f) C 1s, and (g)–(i) O 1s core level spectra.

Based on the XPS analysis, the overall O/C ratio of unmodified flax fibres (0.4) is below the theoretical O/C ratio of 0.83 for pure cellulose and closer to the theoretical O/C ratio of 0.35 for lignin [30]. Therefore, the surface of flax is rich in aliphatic carbon components containing a higher portion of lignin and extractives rather than pure cellulose. Analysis of the aliphatic carbon region (C 1s in Fig. 1 a, d) is necessary to further understand the flax fibres' surface composition. The 284.8 eV peak in Fig. 1 (d) corresponds to unoxidised C–C bonding and hydrocarbons, while the peaks between 286 eV and 289 eV correspond to oxidised C species so that the oxidation state increases with the binding energy (Table 1). The four components in C 1s of flax fibre (Fig. 1 d) were explained by Fuentes et al. [29] as (1) C–(C, H) linkages of lignin and extractives (at 284.8 eV peak); (2) CC–OH groups of cellulose, hemicelluloses, lignin and extractives, as well as CC–OC–C linkages of lignin and extractives (at 286.4 eV peak); (3) C=O groups in lignin and extractives, as well as OC–CC–O linkages in cellulose and hemicelluloses (at 287.4 eV peak); (4) COOH groups of hemicelluloses, as well as COOC and COOH groups of extractives (at 288.6 eV peak). Considering the XPS analysis, surface modification of flax fibres with oxygen-rich GO crystals might promote further interactions between flax and epoxy resin by enhancing the O/C ratio or the ratio of oxidised C in flax fibres.

Based on the literature, the O/C ratio for natural fibres is expected to decrease by GO-modification due to the presence of oxygen-containing groups in GO [31]. The XPS results show that the overall

O/C ratio of GO and GO-modified flax fibres is similar to the unmodified flax fibres and near 0.4. However, the GO-modified flax contains 50% more oxidised C than flax fibre and GO. The higher oxidised C content can increase the extent of hydrogen bond formation between flax fibres and epoxide groups present in the epoxy resin. Indeed, our previous study showed that GO-modification enhances the apparent interfacial shear strength of flax-epoxy by 40% [15].

The nature of bonding between GO crystals and flax fibre surface was investigated based on the O 1s transitions. The O 1s transition (Fig. 1 g, h) shows one prominent peak below 532 eV on flax and GO, representing O–C and O=C bonds. An interesting change is evident in the O 1s transition of GO-modified flax fibres (Fig. 1 i): A new component/bonding exists at 533.2 eV that is not present in unmodified flax or the graphene oxide film. Overall, the C 1s and O 1s spectra of GO-flax cannot be fitted using a combination of the line shapes of flax and GO, suggesting bond formation between flax and GO. One explanation for the new high binding energy component in O 1s is that hydrogen bonding is formed between GO and flax, as the detected binding energy corresponds, e.g., to water or C–OH [32]. The observed changes in the O 1s component ratios show that when the flax fibres are dip-coated in the aqueous dispersion of graphene oxide, about half of the oxygen in O–C/=C is reacting to C/H–O–H (see Table 1: concentration of O 1s: O–C/=C). At the same time, the relative amount of (H–)O–C=O increased in C 1s.

Table 1. Binding energies of photoelectron transitions and their relative surface atomic concentrations. Traces of Na and S detected in GO are excluded.

Transition: bonding	Binding energy (eV)			Concentration (at. %)		
	Flax	GO	GO-flax	Flax	GO	GO-flax
C 1s: C–C/H	284.8	284.8	284.8	29.93	30.47	15.37
C 1s: C–O(–C/H)	286.4	–	286.1	30.56	–	24.09
C 1s: C=O, (HO/O–)C–O	287.4	287.0	287.2	9.18	36.65	21.69
C 1s: (H–)O–C=O	288.6	288.7	288.6	2.86	4.27	11.58
O 1s: O^{2-}	529.7	–	529.2	1.57	–	1.65
O 1s: O–C/=C	531.8	531.6	531.9	25.90	28.61	12.73
O 1s: C/H–O–H	–	–	533.2	–	–	12.89

The contribution of GO-modification on the polarity of flax fibres is presented in Fig. 2. The fibre diameter and water-contact angle along flax fibres are presented in Fig. 2 (A). The variation in fibre diameter along the wetting length highlights the typical morphological heterogeneity of natural fibres (Fig. 2 A). The diameter values for unmodified and GO-modified fibres are within the 10–30 μm range,

typical for elementary flax fibres. The average advancing water-contact angle of unmodified and GO-modified are respectively 75 ± 10 ° and 66 ± 10 °. It should be noted that the average wetting angles represent the wetting length between 1–4 mm which is the stable measurement range. The hydrophilicity of modified fibres can be ascribed to the oxygen-containing functional groups of GO and the fact that GO-modified flax fibres had more oxidised C components than unmodified flax fibre and GO film based on XPS analysis.

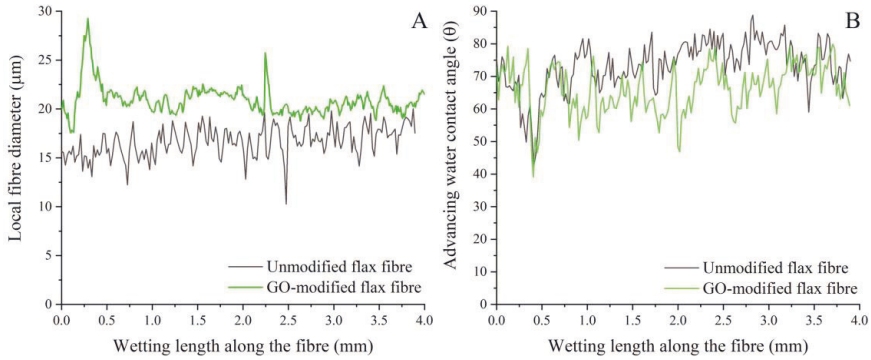

Fig. 2. Variation of local fibre diameter (A) and water contact angle (B) along the fibre length.

The effect of GO-modification on the morphology of flax-epoxy composites is demonstrated in Fig. 3. The volumetric void content of flax-epoxy composites is 2.41% which is reduced to 0.04% with graphene oxide surface modification of fibres. The lower extent of porosities in modified composites shows that graphene oxide having various oxygen-containing functional groups such as epoxide (C–O–C) enhances the compatibility between flax and epoxy. The less porous structure of GO-modified flax-epoxy composites can benefit their fatigue performance and in-service durability.

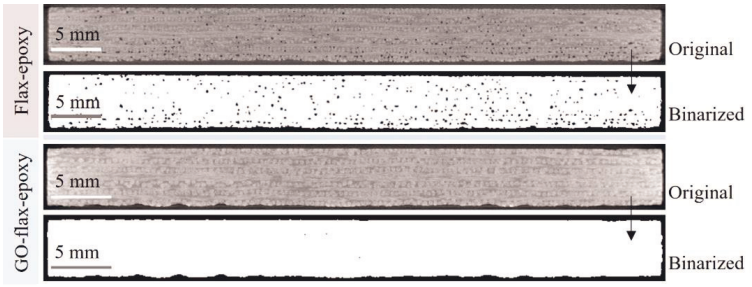

Fig. 3. Internal porosities of flax-epoxy and GO-flax-epoxy composites based on X-CT tomography.

3. 2. Fatigue performance of composites

The collected *S-N* data and normalised fatigue data from flax-epoxy specimens with $[(0,90)]_4$ lay-ups are presented in Fig. 4 (A) and Fig. 4 (B), respectively. In Fig. 4 (A), the average tensile strength of GO-modified composites at the first cycle (S_0 = 110 ± 3 MPa), is 8% lower than the unmodified flax-epoxy composites (S_0 =120 ± 5 MPa), which is also reflected in the fatigue results. The relatively lower strength of GO-modified specimens in Fig. 4 (A) can be related to the effect of water immersion on the tensile performance of flax fibres. Indeed, the pectin and hemicellulose within flax fibres can be partially dissolved in water during the GO fibre modification and alter the tensile performance of fibres [33]. At the 90% loading ratio (in Fig. 4 B), the number of cycles to failure of GO-modified specimens (102 cycles) is one order of magnitude lower than unmodified flax-epoxy (103 cycles). However, at a loading range of 50%–80%, both series are comparable regarding the number of cycles to failure. Therefore, the *S-N* slope of GO-modified composite (−14.45) is less steep than unmodified flax-epoxy (−17.59), indicating a 17% slower fatigue strength degradation rate within the loading range of 50%–90% for GO-flax-epoxy. The more stable fatigue performance of GO-modified specimens can be ascribed to their low void content (less than 0.04% compared to 2.41% for unmodified flax-epoxy) and 40% higher interfacial adhesion with epoxy resin which was studied through microbond tests [15]. The more ductile behaviour of GO-modified specimens within the 50%–80% loading range (compared to the quasi-static and 90% loading cases) can be related to the sliding within multilayer GO crystals which is promoted by cyclic loading and friction between fibre and matrix [14]. Also, under cyclic fatigue loading, the epoxy functional groups of graphene oxide can potentially transform into ether groups [34]. The bond angle within ether groups (R–C–R) can alter and contribute to energy dissipation under cyclic loading conditions [34].

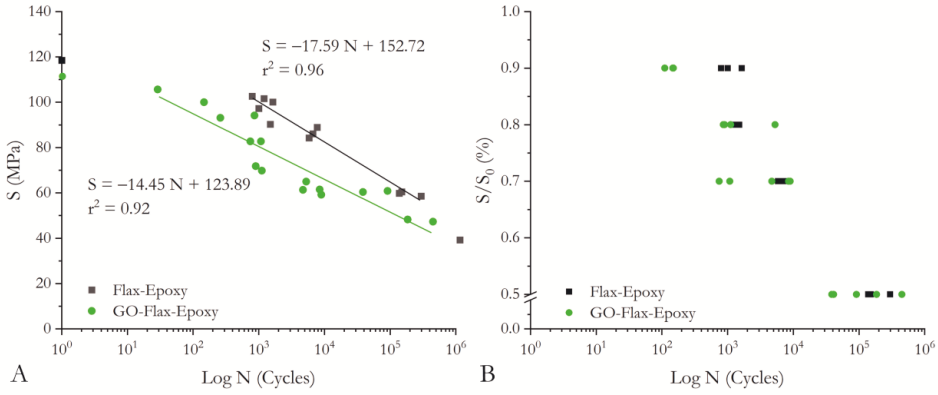

Fig. 4. Collected S-N data (A) and normalised fatigue data (B) of flax-epoxy composites with $[(0,90)]_4$ lay-up.

Fig. 5 and Fig. 6 provide further insight into the contribution of graphene oxide surface modification to the energy dissipation and failure modes of flax-epoxy composites. A general view of the final fatigue failure surface of flax-epoxy composites is presented in Fig. 5 (A), where all plies are visible. In Fig. 5 (A), interfacial debonding and cracks are visible at the crossover of warp and weft yarns. Although fibre pull-out traces are notable in Fig. 5 (B–D), the fracture surface is dominated by clear-cut fibre failure, which indicates the brittle failure of flax-epoxy composites and overall good adhesion between fibre and matrix.

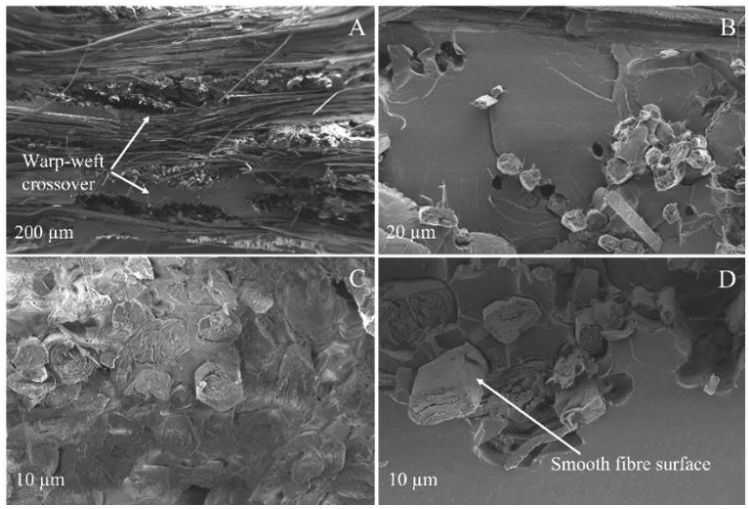

Fig. 5. The final (fatigue) failure surface of flax-epoxy composites (A, B, C, D).

In Fig. 6 (A–D), the fracture surface of GO-flax-epoxy composites after the final fatigue is dominated by extensive fibre pull-out traces. Fibre pull-outs act as a fatigue energy dissipation mechanism through interfacial sliding inside GO layers and at the fibre-matrix interface [14]. The polymer residues on the GO-modified fibre surfaces indicate good compatibility between fibres and matrix (Fig. 6 D).

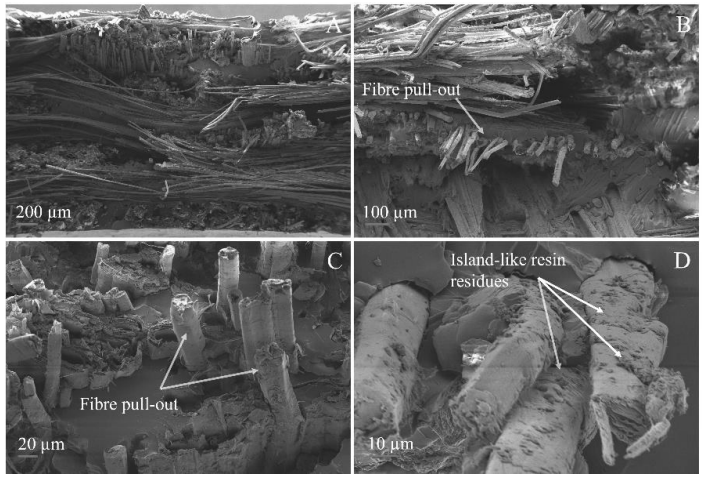

Fig. 6. The final (fatigue) failure surface of GO-flax-epoxy composites.

3. 3. Impact performance of composites

The impact kinetic energy-time histories of cross-ply flax-epoxy composites with $[0/90]_{3S}$ lay-up are outlined in Fig. 7. Generally, when composites are subject to impact loading, part of the kinetic energy is absorbed through plastic deformation and part of the kinetic energy is recovered back to the impactor (Fig. 7 A). At 21 J kinetic energy, the impactor perforates the specimens, and almost all the impact energy is absorbed by plastic deformations. The internal damage patterns of GO-flax-epoxy and flax-epoxy at the perforation energy (4.2 ± 0.1 J/mm) are similar and comprise ply failure, delamination, and fibre pull-out (Fig. 7 B). Regardless of the matrix type, the perforation energy of flax-epoxy (4.2 J/mm, this study), flax-PMMA (4.2 J/mm, [10]), and polylactic acid (PLA) based flax fibre (3.5 J/mm, [35]) composites with the similar specimen and testing configurations are comparable. As fibre failure is an important limiting factor for perforation energy, composites processed with tough polymers can often enhance energy absorption [36–38]. However, the perforation energy of flax fibre reinforced polypropylene (PP) composites (4.9 J/mm) reported by Ramakrishnan et al. [38] is 14% higher than the flax-epoxy and flax-PMMA. The 14% higher perforation energy of flax-PP composites can be ascribed to the weak interfacial strength between flax and PP, which promotes energy dissipation through interfacial sliding [6,21]. Indeed, interfacial strength and toughness are critical for the impact resistance of flax fibre composites [9,10]. For instance, the impact resistance and perforation energy of interfacially toughened flax-epoxy composites (5.9 J/mm, [9]) and flax-PMMA composites processed with ductile non-dry fibres (6.4–8.1 J/mm) are comparable to glass-PP composites (5.1 J/mm, [39]) tested with the similar specimen and testing configurations.

The GO-modification can potentially enhance the impact tolerance (i.e., compressive strength after impact) of flax-epoxy composites by modifying their interfacial shear strength. Therefore, it is beneficial to investigate the effect of GO-modification on the impact resistance of flax-epoxy composites at kinetic energies below the perforation limit. The following paragraphs elaborate on the contribution of GO-modification to the internal damage patterns, contact force-displacement/time behaviour, and in-situ damage initiation and progression of flax-epoxy specimens.

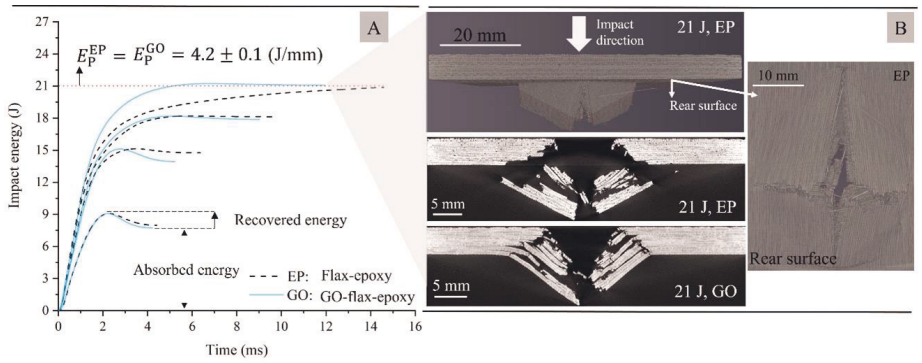

Fig. 7. Energy-time history of composites (A) and internal damage patterns at perforation based on X-CT (B).

The impact energy is partly recovered at kinetic energies below the perforation energy, as shown in Fig. 8 (A). For cross-ply flax-epoxy and GO-flax-epoxy composites in this study, the 9 J kinetic energy can be defined as the perforation threshold (E_{Th}) beyond which through-thickness ply failures prevail, and the elastically recovered portion of the impact energy decreases. The GO-modified composites present higher elastically recovery kinetic energy values at 9 J (by + 24%) and 15 J–18 J (by + 200%) impact kinetic energies. For all non-perforation impact energies, the GO-modification reduces the extent of fibre and ply failure by promoting energy dissipation through interlaminar delamination (Fig. 8 B). For instance, in Fig. 8 (B), the cumulative lengths of delamination lines for GO-flax-epoxy at 9 J (43 mm) and 15 J (77 mm) are respectively 50% and 26% higher than the similar values for flax-epoxy at 9 J (21 mm) and 15 J (57 mm).

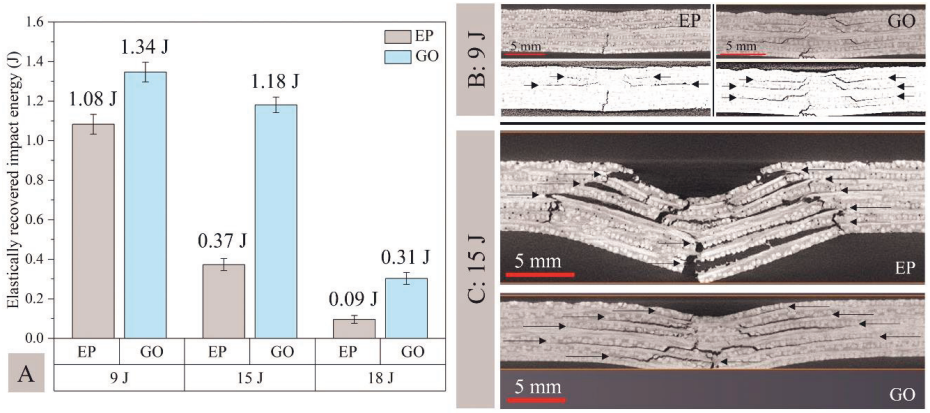

Fig. 8. Elastically recovered impact kinetic energies of composites (A) and the internal damage patterns of specimens based on X-CT tested at 9 J (B) and 15 J (C) kinetic energies.

The contact force-time histories for non-perforation impact energies are presented in Fig. 9. In terms of maximum contact force, modified and unmodified composites have similar performance. At the lowest kinetic energy (9 J), previously defined as the perforation threshold (E_{Th}), GO-modified and unmodified composites have similar impact behaviour. The main contribution of the GO modification is between the perforation threshold energy and the perforation energy.

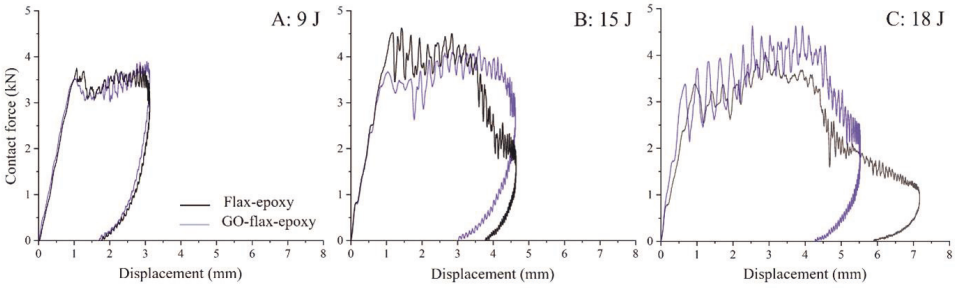

Fig. 9. Contact force-displacement histories of composites at 9 J (A), 15 J (B), and 18 J (C) kinetic energies.

In addition to the impact resistance, it is beneficial to understand the contribution of GO-modification on impact damage initiation and propagation of flax-epoxy composites. The full-field deformations of the specimen's rear surface at 15 J kinetic energy are presented in Fig. 10 and Fig. 11. The in-situ high-speed optical images are synchronised with contact force-time profiles to provide point-specific and comparative data between flax-epoxy and GO-flax-epoxy composites. The von Mises strain maps are superimposed on the optical images to visualise the 2D surface deformations. The deformations after the surface crack opening are provided without strain maps, as the full-field strain data calibration can

be distorted due to the surface discontinuity. The contact force-displacement traces are divided into three regions, namely the initial linear-elastic region (phase I), plateau-like region (phase II), and the last part, where the cross-like surface damage starts with a continuous drop in the force value until complete failure of the specimens (phase III).

The contact force-time trace of unmodified flax-epoxy at 15 J kinetic energy is presented in Fig. 10 (H). Towards the end of the linear-elastic region (phase I), matrix cracking is evident at the centre of the specimen, followed by fibre crack initiation at maximum contact force. (Fig.10 A-C). In the plateau region (phase II), the crack that started at the maximum contact force steadily propagates parallel to the fibre directions on the rear surface of the specimen (Fig. 10 D). At the end of phase II, the crack reaches its maximum length (22 mm) (Fig. 10 E). By phase III, transverse cracks initiate and propagate while the impactor penetrates the specimen (Fig. 10 E-G). The impact damage initiation and progression of cross-ply flax-epoxy are comparable to the case of flax-PMMA composites with similar specimen and testing configurations [10], emphasising the often dominant contribution of fibre failure in the impact performance of natural fibre composites. However, impact-induced ply splitting, reported for tough flax-PMMA composites [10], is not detected for the flax-epoxy composites in this study.

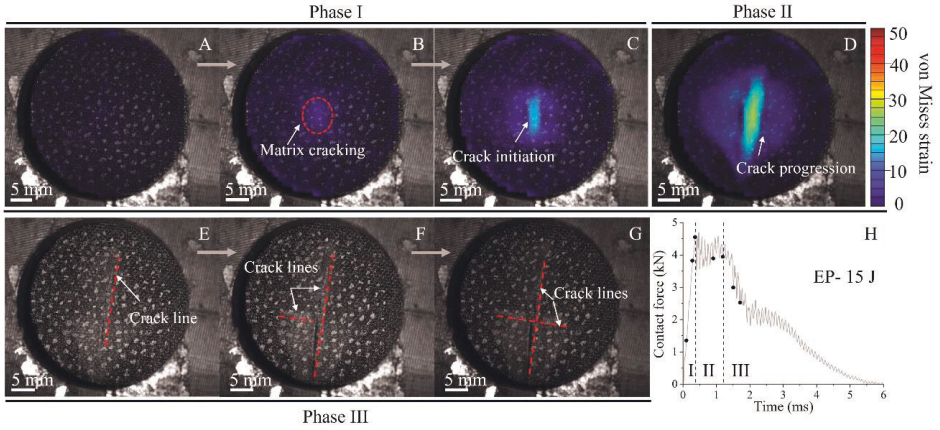

Fig. 10. The impact damage initiation and progression (A–G) on the rear surface of unmodified flax-epoxy composites with $[0/90]_{3S}$ lay-up at 15 J kinetic energy synchronised with the force-time profile (H).

The contact force-time history of GO-modified flax-epoxy composites at 15 J kinetic energy is provided in Fig. 11 (A). The maximum contact force at the end of the linear-elastic region for GO-flax-epoxy (3.32 kN) is lower than for flax-epoxy (4.6 kN), and the damage modes are slightly different. For instance, the (fibre) crack opening at the end of the linear-elastic region for flax-epoxy is replaced by matrix cracking for GO-flax-epoxy and delayed to phase II. The area of the localised von Mises

strain map at the centre of the GO-modified specimen upon matrix cracking (Fig. 11 C) is relatively larger than for unmodified flax-epoxy (Fig. 10 B). This observation could mean that GO-modification facilitates the better distribution of contact force over a larger area on the rear surface of flax-epoxy composites. Also, the length of the plateau-like region (phase II) for GO-flax-epoxy (1.45 ms) is 42% larger than for unmodified flax-epoxy (1.02 ms). The contact force value for GO-flax-epoxy in phase II gradually increases, contrary to the case of unmodified flax-epoxy. The longer contact time and gradual increment of contact force value in phase II indicate that GO-modification improves the impact damage resistance and delays crack growth on the rear surface of flax-epoxy specimens by promoting redistribution of contact force over a larger area. Interestingly, the transverse crack initiation and progression (phase III, Fig. 11 G, H) on the rear surface of GO-flax-epoxy is realised within the plateau region at constant contact force, unlike for the unmodified flax-epoxy.

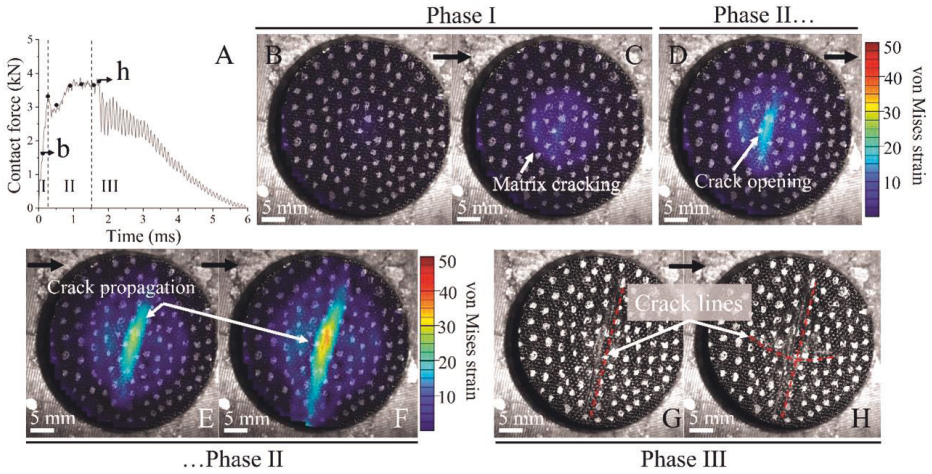

Fig. 11. The contact force-time history of GO-flax-epoxy composite with $[0/90]_{3S}$ lay-up at 15 J kinetic energy (A) and in-situ damage patterns on the rear surface of specimens (B–H).

In summary, this article provides new experimental insights on the nature of bonding between graphene oxide and flax fibres, the effect of GO on the porosity of composites, fatigue performance, and the impact resistance of composites. The surface modification of fibres with graphene oxide prolongs the fatigue life of flax-epoxy composites without compromising the impact perforation energy. Also, GO-surface modification alters the fibre-dominant failure mode of flax-epoxy composites at kinetic energies below perforation by promoting energy dissipation through interfacial sliding and delamination. This study provides new insights into the in-situ impact damage progression and internal damage patterns of composites, which can be valuable for further numerical and experimental investigations.

4. Conclusions

The effects of graphene oxide fibre surface modification on the morphology, fatigue performance, and impact resistance of flax-epoxy composites were investigated. The XPS results proved the existence of hydrogen bonding between flax fibre and deposited GO crystals. Also, the XPS surface analysis showed that the percentage of unoxidised carbon (C-C/H) on flax fibres (30 at. %) was decreased by 50% with GO-coating of the fibres. As a result, the GO-modified fibres were more reactive towards the epoxy resin, and their composites were less porous compared to unmodified flax-epoxy, showing good wetting. The modification of fibres with multilayer GO crystals promoted energy dissipation through interfacial sliding and fibre pull-outs under dynamic cyclic loading. The GO modification reduced the fatigue life degradation rate of flax-epoxy composites by 17% without a negative effect on the low-velocity impact perforation energy of the composites. The GO-modification altered the fibre-dominant impact failure mode of the composites by enhancing the extent of energy dissipation through interlaminar delamination. The contact force-time synchronised in-situ high-speed optical images showed that the GO-modification delays the fibre damage initiation on the rear surface of composites and prolongs the damage progression phase compared to unmodified flax-epoxy composites.

Acknowledgements

This project was funded by the European Union's Horizon 2020 research and innovation programme under the Marie Skłodowska-Curie grant agreement No 764713-FibreNet. This work made use of Tampere Microscopy Center facilities at Tampere University. The authors thank Bcomp (Fribourg, Switzerland) for supplying the flax fabrics. Farzin Javanshour appreciates the contributions made by Apolline Féré for fatigue testing.

References

[1] Prapavesis A, Tojaga V, Östlund S, Willem van Vuure A. Back calculated compressive properties of flax fibers utilising the Impregnated Fiber Bundle Test (IFBT). Composites Part A: Applied Science and Manufacturing 2020;135:105930. https://doi.org/10.1016/J.COMPOSITESA.2020.105930.

[2] Farzin J. Tensile Properties of Flax Fibre Bundles with Graphene Oxide Coating 2019. https://doi.org/10.5281/ZENODO.3382823.

[3] Pil L, Bensadoun F, Pariset J, Verpoest I. Why are designers fascinated by flax and hemp fibre composites? Composites Part A: Applied Science and Manufacturing 2016;83:193–205. https://doi.org/10.1016/J.COMPOSITESA.2015.11.004.

[4] Bourmaud A, Beaugrand J, Shah DU, Placet V, Baley C. Towards the design of high-performance plant fibre composites. Prog Mater Sci, 97 (2018), pp. 347-408. 10.1016/j.pmatsci.2018.05.005.
[5] Díaz-Álvarez A, Jiao-Wang L, Feng C, Santiuste C. Energy absorption and residual bending behavior of biocomposites bumper beams. Composite Structures 2020;245:112343. https://doi.org/10.1016/J.COMPSTRUCT.2020.112343.
[6] Liu T, Butaud P, Placet V, Ouisse M. Damping behavior of plant fiber composites: A review. Composite Structures 2021;275:114392. https://doi.org/10.1016/J.COMPSTRUCT.2021.114392.
[7] Rueppel M, Rion J, Dransfeld C, Fischer C, Masania K. Damping of carbon fibre and flax fibre angle-ply composite laminates. Composites Science and Technology 2017;146:1–9. https://doi.org/10.1016/J.COMPSCITECH.2017.04.011.
[8] Mahboob Z, Fawaz Z, Bougherara H. Fatigue behaviour and damage mechanisms under strain controlled cycling: Comparison of Flax–epoxy and Glass–epoxy composites. Composites Part A: Applied Science and Manufacturing 2022;159:107008. https://doi.org/10.1016/J.COMPOSITESA.2022.107008.
[9] Javanshour F, Prapavesis A, Pärnänen T, Orell O, Lessa Belone MC, Layek RK, et al. Modulating impact resistance of flax epoxy composites with thermoplastic interfacial toughening. Composites Part A: Applied Science and Manufacturing 2021;150:106628. https://doi.org/10.1016/J.COMPOSITESA.2021.106628.
[10] Javanshour F, Prapavesis A, Pournoori N, Soares GC, Orell O, Pärnänen T, et al. Impact and fatigue tolerant natural fibre reinforced thermoplastic composites by using non-dry fibres. Composites Part A: Applied Science and Manufacturing 2022;161:107110. https://doi.org/10.1016/J.COMPOSITESA.2022.107110.
[11] Randall JD, Stojcevski F, Djordjevic N, Hendlmeier A, Dharmasiri B, Stanfield MK, et al. Carbon fiber polypropylene interphase modification as a route to improved toughness. Composites Part A: Applied Science and Manufacturing 2022;159:107001. https://doi.org/10.1016/J.COMPOSITESA.2022.107001.
[12] Eyckens DJ, Demir B, Randall JD, Gengenbach TR, Servinis L, Walsh TR, et al. Using molecular entanglement as a strategy to enhance carbon fiber-epoxy composite interfaces. Composites Science and Technology 2020;196:108225. https://doi.org/10.1016/J.COMPSCITECH.2020.108225.
[13] Koolen G, Soete J, van Vuure AW. Interface modification and the influence on damage development of flax fibre - Epoxy composites when subjected to hygroscopic cycling. Materials Today: Proceedings, vol. 31, Elsevier Ltd; 2019, p. S273–9. https://doi.org/10.1016/j.matpr.2020.01.183.
[14] Gong L, Zhang F, Peng X, Scarpa F, Huang Z, Tao G, et al. Improving the damping properties of carbon fiber reinforced polymer composites by interfacial sliding of oriented multilayer graphene oxide. Composites Science and Technology 2022;224:109309. https://doi.org/10.1016/J.COMPSCITECH.2022.109309.
[15] Javanshour F, Ramakrishnan KR, Layek RK, Laurikainen P, Prapavesis A, Kanerva M, et al. Effect of Graphene Oxide Surface Treatment on the Interfacial Adhesion and the Tensile Performance of Flax Epoxy Composites. Composites Part A: Applied Science and Manufacturing 2021:106270. https://doi.org/10.1016/j.compositesa.2020.106270.
[16] Sarker F, Potluri P, Afroj S, Koncherry V, Novoselov KS, Karim N. Ultrahigh Performance of Nanoengineered Graphene-Based Natural Jute Fiber Composites. ACS Applied Materials and Interfaces 2019;11:21166–76. https://doi.org/10.1021/acsami.9b04696.

[17] Canavy N, Rouilly A, Drouet C, Thouron C, Aufray M. Influence of flax fibers on epoxide-amine composites: Energetics of interphase formation.
Polymer 2022;254:125047. https://doi.org/10.1016/J.POLYMER.2022.125047.
[18] Le Duigou A, Kervoelen A, Le Grand A, Nardin M, Baley C. Interfacial properties of flax fibre–epoxy resin systems: Existence of a complex interphase. Composites Science and Technology 2014;100:152–7. https://doi.org/10.1016/J.COMPSCITECH.2014.06.009.
[19] Alipour A, Lin R, Jayaraman K. Effects of graphene network formation on microstructure and mechanical properties of flax/epoxy nanocomposites. Journal of Materials Research and Technology 2021;15:4610–22. https://doi.org/10.1016/J.JMRT.2021.10.082.
[20] Pereira AC, Monteiro SN, Simonassi NT, Vieira CMF, Lima AM, Costa UO, et al. Enhancement of impact toughness using graphene oxide in epoxy composite reinforced with ramie fabric. Composite Structures 2022;282:115023.
https://doi.org/10.1016/J.COMPSTRUCT.2021.115023.
[21] Woigk W, Fuentes CA, Rion J, Hegemann D, van Vuure AW, Dransfeld C, et al. Interface properties and their effect on the mechanical performance of flax fibre thermoplastic composites. Composites Part A: Applied Science and Manufacturing 2019;122:8–17.
https://doi.org/10.1016/j.compositesa.2019.04.015.
[22] Bensadoun F, Vallons KAM, Lessard LB, Verpoest I, Van Vuure AW. Fatigue behaviour assessment of flax–epoxy composites. Composites Part A: Applied Science and Manufacturing 2016;82:253–66. https://doi.org/10.1016/J.COMPOSITESA.2015.11.003.
[23] Beelen L. Effect of moisture absorption on the performance of flax fibre reinforced composites. Department of Materials Engineering, KU Leuven, Leuven (2022).
https://doi.org/10.31219/OSF.IO/9UFB6.
[24] Timmermans J. Hygroscopic cycling of flax fibre composites: Simultaneous swelling and shrinking of fibre and matrix. Department of Materials Engineering, KU Leuven, Leuven (2022). https://doi.org/10.31219/OSF.IO/AVPZ3.
[25] Ivkov S. A Study on Accelerated Ageing of Flax Fiber Reinforced Composites with Hygrothermal Cycling. Department of Materials Engineering, KU Leuven, Leuven (2022). https://doi.org/10.31219/OSF.IO/6SBW3.
[26] Lu W, Qin F, Wang Y, Luo Y, Wang H, Scarpa F, et al. Engineering Graphene Wrinkles for Large Enhancement of Interlaminar Friction Enabled Damping Capability.
ACS Appl Mater Interfaces 2019;11:30278–89. https://doi.org/10.1021/acsami.9b09393.
https://doi.org/10.1021/ACSAMI.9B09393/SUPPL_FILE/AM9B09393_SI_001.PDF.
[27] Tran L, Fuentes CA, Verpoest I, Van Vuure AW. Interfacial compatibility and adhesion in natural fiber composites. Nat. Fibre Compos., CRC Press; 2015, p. 127-56.
https://doi.org/10.1201/b19062-6.
[28] Qiu S, Fuentes CA, Zhang D, Van Vuure AW, Seveno D. Wettability of a single carbon fiber. Langmuir 2016;32:9697–705. https://doi.org/10.1021/acs.langmuir.6b02072.
[29] Fuentes CA, Ting KW, Dupont-Gillain C, Steensma M, Talma AG, Zuijderduin R, et al. Effect of humidity during manufacturing on the interfacial strength of non-pre-dried flax fibre/unsaturated polyester composites. Composites Part A: Applied Science and Manufacturing 2016;84:209–15. https://doi.org/10.1016/J.COMPOSITESA.2016.01.023.
[30] Johansson LS, Campbell JM, Koljonen K, Stenius P. Evaluation of surface lignin on cellulose fibers with XPS. Applied Surface Science 1999;144–145:92–5. https://doi.org/10.1016/S0169-4332(98)00920-9.

[31] Sarker F, Karim N, Afroj S, Koncherry V, Novoselov KS, Potluri P. High-Performance Graphene-Based Natural Fiber Composites. ACS Applied Materials and Interfaces 2018;10:34502–12. https://doi.org/10.1021/acsami.8b13018.

[32] Kam CS, Leung TL, Liu F, Djurišić AB, Xie MH, Chan WK, et al. Lead removal from water – dependence on the form of carbon and surface functionalisation. RSC Advances 2018;8:18355–62. https://doi.org/10.1039/C8RA02264J.

[33] Acera Fernández J, Le Moigne N, Caro-Bretelle AS, El Hage R, Le Duc A, Lozachmeur M, et al. Role of flax cell wall components on the microstructure and transverse mechanical behaviour of flax fabrics reinforced epoxy biocomposites. Industrial Crops and Products 2016;85:93–108. https://doi.org/10.1016/j.indcrop.2016.02.047.

[34] Najafi F, Wang G, Cui T, Anand A, Mukherjee S, Filleter T, et al. Fatigue resistance of atomically thin graphene oxide. Carbon 2021;183:780–8. https://doi.org/10.1016/J.CARBON.2021.07.062.

[35] Fischer B, Sarasini F, Tirillò J, Touchard F, Chocinski-Arnault L, Mellier D, et al. Impact damage assessment in biocomposites by micro-CT and innovative air-coupled detection of laser-generated ultrasound. Composite Structures 2019;210:922–31. https://doi.org/10.1016/j.compstruct.2018.12.013.

[36] Bensadoun F, Depuydt D, Baets J, Verpoest I, van Vuure AW. Low velocity impact properties of flax composites. Composite Structures 2017;176:933–44. https://doi.org/10.1016/j.compstruct.2017.05.005.

[37] Yudhanto A, Wafai H, Lubineau G, Goutham S, Mulle M, Yaldiz R, et al. Revealing the effects of matrix behavior on low-velocity impact response of continuous fiber-reinforced thermoplastic laminates. Composite Structures 2019;210:239–49. https://doi.org/10.1016/J.COMPSTRUCT.2018.11.040.

[38] Ramakrishnan KR, Corn S, Le Moigne N, Ienny P, Slangen P. Experimental assessment of low velocity impact damage in flax fabrics reinforced biocomposites by coupled high-speed imaging and DIC analysis. Composites Part A: Applied Science and Manufacturing 2021;140:106137. https://doi.org/10.1016/j.compositesa.2020.106137.

[39] Fan J, Guan ZW, Cantwell WJ. Modeling Perforation in Glass Fiber Reinforced Composites Subjected to Low Velocity Impact Loading.
Polym Compos, 32 (2011), pp. 1380-1388. https://doi.org/10.1002/pc.21161.

PAPER III

Supplementary data is available through the online version provided by Elsevier.

Composites: Part A 150 (2021) 106628

Contents lists available at ScienceDirect

Composites Part A

journal homepage: www.elsevier.com/locate/compositesa

Modulating impact resistance of flax epoxy composites with thermoplastic interfacial toughening

F. Javanshour [a,*], A. Prapavesis [b], T. Pärnänen [a], O. Orell [a], M.C. Lessa Belone [a], R.K. Layek [c], M. Kanerva [a], P. Kallio [d], A.W. Van Vuure [b], E. Sarlin [a]

[a] Department of Materials Science and Environmental Engineering, Tampere University, Tampere, Finland
[b] Department of Materials Engineering, KU Leuven, B-3001 Heverlee, Belgium
[c] Department of Separation Science, LUT University, Mukkulankatu 19, 15210 Lahti, Finland
[d] Faculty of Medicine and Health Technology, Tampere University, Tampere, Finland

ARTICLE INFO

Keywords:
A. Natural fibres
B. Interface/interphase
B. Impact behaviour
E. Surface treatments

ABSTRACT

The application of natural flax fibre/epoxy composites is growing in the automotive sector due to their good stiffness and damping properties. However, the impact damage resistance of flax/epoxy composites is limited due to the brittle nature of both epoxy and flax fibres and strong fibre/matrix adhesion. Here, biobased thermoplastic cellulose acetate (CA) is deployed as a fibre treatment to alter the damage development of flax/epoxy composites subjected to low-velocity impact. The perforation threshold energy and the perforation energy of unmodified cross-ply composites increased respectively by 66% and 42% with CA-treated flax fibres. The CA-modification modestly decreased the transverse tensile strength and in-plane tensile shear strength of the composites. However, it altered the brittle nature of flax/epoxy laminates in quasi-static tests into ductile failure with clearly increased fibre–matrix debonding.

1. Introduction

Natural fibres, such as flax, are a class of green fibre reinforcements widely used in the semi-structural composite parts of the automotive and construction sectors [1–3]. Natural fibre composites offer low density as well as excellent damping properties and ecological merits [1,4]. Currently, flax is the only engineering plant fibre in Europe mass-produced in unidirectional and continuous fibre mats [1,5]. Epoxy resins are appealing for the industry based on their high mechanical properties and low viscosities, which are ideal for composites processing. Due to the reactive nature of epoxies, epoxy resins and natural fibres show good fibre/matrix adhesion with hydrogen and covalent bond formation [6]. The lower strength of natural fibres compared to synthetic fibres [7–9], combined with their relatively low strain to failure and the brittle nature of epoxy resins, limit the application of these flax biocomposites in environments where dynamic loads, such as impacts, are expected [10].

Low-velocity impacts (induced, for instance by collision, and dropped tools) can severely affect the further application, i.e. in terms of long term durability, of flax/epoxy composites by generating through-thickness damage in the form of matrix cracking, fibre failure and delamination [11,12]. For example, a 10 J low-velocity impact on flax/epoxy composite with $[0/90/+45/-45]_{2s}$ lay-up, a laminate thickness of 2.85 mm, and fibre volume fraction (V_f) of 44% can reduce its residual compressive strength by 30% [13]. Matrix toughness, stacking sequence, and flax fibres architecture are critical factors for proper impact damage tolerance of flax/epoxy composites [10,14]. Due to the relatively low strength of flax fibres and high interfacial shear strength of flax/epoxy [7], the impact damage pattern of flax/epoxy composites is usually dominated by fibre failure, shear-induced matrix cracks and limited delamination [12,13,15].

It is known that cross-ply composites based on UD plies absorb higher impact energies than ones based on woven plies due to the higher in-plane strength of cross-ply composites based on UD plies and because of much higher energy absorption due to delamination between the plies [16]. Nevertheless, cross-ply composites based on woven reinforcements exhibit limited damage compared to cross-ply laminates based on UD plies and thus tend to have better properties after impact (damage tolerance). This is due to the coarse fibre bundles within the woven fabrics that act as crack-stoppers and because of reduced delamination

* Corresponding author.
E-mail address: farzin.javanshour@tuni.fi (F. Javanshour).

https://doi.org/10.1016/j.compositesa.2021.106628
Received 13 April 2021; Received in revised form 31 May 2021; Accepted 22 August 2021
Available online 25 August 2021

due to nesting of the woven fabrics [16,17]. For dissimilar ply angles, specifically cross-ply configurations (with either UD or woven reinforcements), the composites' tendency to delaminate at the interface between non-aligned fibre plies can be affected by the mismatch of bending stiffness between adjacent plies [18].

By presuming that flax/epoxy composites can be designed so that the impact damage can be restrained, it might be possible to limit the loss in residual strength and finally replace the 'no damage growth' design by limited damage growth designs, which can save substantial amounts of material and energy. For this, the composites' interfacial toughness should be engineered to suppress damage growth, especially near the laminate mid-plane as the most critical failure location [19].

The literature on interfacial and interlaminar toughening of flax/epoxy composites focusing on impact resistance is minimal [20–22]. Ravandi et al. [23] reported a detrimental effect of stitching on interlaminar toughness and low-velocity impact resistance of flax/epoxy composites due to fibre distortion and resin-rich pockets. Prasad et al. [21] reported that the addition of TiO_2 to epoxy resin improves the mode I and mode II fracture toughness of flax/epoxy composites by 52% and 73%, respectively, due to crack deflection/blunting near fibre/matrix interfaces. However, they did not study the contribution of TiO_2 to the impact resistance of composites. Gassan et al. [22] and Koolen et al. [20] evaluated the effect of a silicone-rich interface on the properties of flax fibre composites. Gassan et al. [22] reported an increase of Charpy impact strength of composites by 100% with an expense of 50% reduction in the flexural modulus and strength of the composites. Koolen et al. [20] hypothesised that interfacial toughening by the insertion of a thin silicone elastomer might improve the resistance to hygroscopic ageing. However, the fibre coating did not have the desired effect since an accelerated reduction of the transverse strength of UD flax-epoxy composites and increased fibre–matrix debonding after ageing indicated a weaker interface. This observation was explained by premature adhesive or cohesive failure in the silicone interlayer, which stresses the importance of material selection. An alternative route to mitigate the low impact resistance of fibre reinforced epoxy composites is to coat a thin layer of tough thermoplastic into the fibre/matrix interface [24–29]. For instance, Lin et al. [24] showed that 1.39% fibre sizing content of thermoplastic polyurethane improved the apparent fibre/matrix interfacial shear strength of aramid/epoxy by 67.7% as the ductile interface had higher deformation and delayed the debonding by crack deflection. Narducci et al. [25] suppressed and controlled the delamination growth of carbon/epoxy composites by polylactic acid based surface modification of carbon fibres.

In this study, the flax fibre surface was modified with fully biobased cellulose acetate (CA) thermoplastic coating to enhance flax/epoxy composites' interfacial toughness. The aim was to limit fibre failure and suppress primary delamination during the low-velocity impact of flax/epoxy laminates while preserving optimised quasi-static performance. CA is selected based on its excellent compatibility with flax fibre and epoxy resin, being green and cost-effective, and having high ductility (failure strain 13.5 ± 3%) and good mechanical properties [30].

The surface chemistry and morphology of CA treated flax yarns were characterised with Fourier transform infrared spectroscopy (FTIR) and scanning electron microscopy (SEM). The mechanical properties (tensile and bending resistance) of flax yarns were compared with those of CA modified flax yarns. Composites' mechanical performance under various loading conditions was evaluated by applying quasi-static tensile testing, short beam bending tests, and drop-weight impact analysis.

2. Methodology

Bcomp (Fribourg, Switzerland) provided non-crimp flax yarn fabric of unidirectional (UD) type 5009 with an areal density of 300 g/m^2. Pure cellulose acetate (CA) powder (average MW 100,000) was supplied by Acros Organics (New Jersey, United States). The degree of substitution of CA was 1.3. Technical acetone by Kiilto Oy (Lempäälä, Finland) was used as a solvent for CA powder. Standard epoxy resin Epopox A28 by Amroy Europe Oy (Lahti, Finland) and a Jeffamine D-23 polyether diamine hardener by Huntsman (Texas, USA) with 35 wt% hardener to resin ratio were used as the matrix polymer system.

Flax fabrics were modified with CA by dip-coating into a CA-acetone solution of 5% CA concentration (5 g CA in 100 mL acetone) as described in Supplementary data (S.1.1). CA, based on its acetyl content and degree of substitution, can dissolve in various solvents such as acetone, chloroform, 2-methoxyethanol, and dichloromethane. In this study, acetone was selected as a solvent, based on an extensive review on the green solvent guides by Byrne et al. [31], which categorised solvents into six subgroups from green (e.g. ethanol, water), between green and problematic (e.g. acetone), problematic (e.g. DMSO), between problematic and hazardous (e.g. dichloromethane), hazardous (e.g., 2-methoxyethanol), and highly hazardous (e.g. chloroform). Compared to other CA-solvents, acetone has the best environmental, health, safety, and energy demand and can be sourced renewably [31]. Also, dip-coating of flax fabrics in acetone solution is an energy-efficient and cost-effective method as it does not require specialised devices and an oven to evaporate the solvent.

The untreated and CA-modified flax fabrics and pure CA film were analysed by Fourier transform infrared (FTIR) spectroscopy (Perkin-Elmer Spectrum One, Perkin-Elmer, Beaconsfield, UK). The morphology of the fabrics was examined with an ULTRAplus (Zeiss, Oberkochen, Germany) scanning electron microscope (SEM). A thin gold coating was used to ensure enough conductivity for the SEM samples. The bending resistance of untreated and modified (as a flax-CA 'preform fabric') strips of UD flax fabrics was studied with a L&WTM bending resistance tester (Lorentzen & Wettre, Sweden). The test was performed according to the SCAN-P 29:95 standard (samples were 38 mm in width and 70 mm in length). Further descriptions of the bending resistance test are described in Supplementary data (Fig. S1). Transverse strength of UD CA-flax fabrics ('preforms') was tested with a universal tester (Instron 5967, MA, USA) with 500 N load cell, gauge length of 50 mm and a crosshead speed of 1 mm/min. The samples were 15 mm in width and 150 mm in length. The thickness of the fabrics was determined by the average thickness at three points along the gauge length. Masking tape was used as tabs at the gripping area. The polyester weft threads of the fabrics were removed before testing. The average results of ten samples were reported for bending resistance and transverse fabric tests.

Composite panels of flax/epoxy and CA-flax/epoxy with a fibre volume fraction (V_f) of 40% were manufactured based on the manual lay-up method (Supplementary data, S.1.3). The bulk density of composites was measured based on the Archimedes principle [32] (as described in Supplementary data S.1.4). The V_f and composites' morphology were characterised by X-ray computed tomography (Phoenix Nanotom, General Electric, Germany) as described in Supplementary data (S.1.5). The quasi-static tensile performance of composites with $[0]_4$ and $[\pm 45]_s$ lay-ups was studied according to ASTM D3039 and ASTM D3518 standards, respectively. The effect of CA surface modification on fibre/matrix adhesion was studied based on transverse tensile strength tests of $[90]_4$ composites (ASTM D3039 standard) and short-beam testing of $[0/90]_{3s}$ composites (ASTM D2344 standard). The testing specifications are reported in Supplementary data (Table S1). The impact strength of UD ($[0]_4$ lay-up) CA-flax/epoxy and flax/epoxy were comparatively studied by a Ceast Resil 5.5 Charpy impact tester (Ceast, Torino, Italy) according to EN ISO 179–1 standard. The impact performance of structural flax/epoxy and CA-flax/epoxy composites, with a $[0/90]_{3s}$ lay-up, was studied with a drop-weight test (per ASTM D7136 and ASTM D5628 standards), without rebound impacts. To present a range of damage (e.g. local ply splitting/delamination for low impact energies to complete perforation of the specimen at the upper bound energy), the drop height was adjusted to 0.11, 0.22, 0.32, 0.44, 0.55, 0.66, 0.77, 0.88, 0.99, and 1.11 m to target the kinetic energies of 3, 6, 9, 12, 15, 18, 21, 24, 27, and 30 J, respectively; the mass of the impactor was 2772 g. Further specifications of the impact testing and the

relevant terminology are presented in Supplementary data (S.1.6). The post-impact assessment of failure mechanisms in the impacted specimens was evaluated with a DM 2500 M (Leica, Wetzlar, Germany) optical microscope using a dark field mode. The samples were embedded in an epoxy resin before polishing. The surface deformations on the back-face of composites (opposite to the impacted surface after the drop-weight test) were inspected with three-dimensional optical profilometry with an InfiniteFocus G5 (Alicona, Graz, Austria).

3. Results and discussions

3.1. Fibre surface characterisation

Fig. 1 shows the FTIR transmittance spectra of untreated flax and CA-modified flax fibres. The FTIR spectrum of the flax fibre shows the typical vibration bands of cellulose, hemicellulose, and lignin, as reported previously [33]. The–OH stretching vibration (mainly related to cellulose) band of hydroxyl groups [34] in CA, flax fibre and CA-flax fibre appeared as broadband with the highest intense band positions 3490 cm^{-1}, 3344 cm^{-1} and 3357 cm^{-1}, respectively. It is clear from the figure that the –OH stretching vibration band of CA-flax fibre is shifted to the higher wavenumber with respect to neat flax fibre. It indicates strong intermolecular hydrogen bonding between the hydroxyl group of flax fibre and CA. The pure CA spectrum reveals characteristic peaks at 1735 cm^{-1} and 1221 cm^{-1} related to the stretching vibration of the C═O bond of ester groups and C—O bond of the ether group, respectively [34]. These distinct CA (C═O and C—O) peaks are shifted to 1740 cm^{-1} and 1232 cm^{-1} in CA-modified flax fibres, indicating hydrogen bonding between the C═O and C—O groups of CA and the hydroxyl group of flax.

SEM images, in Fig. 2, compare the morphology of flax and CA-flax yarns. A distinctive coating is evident on the CA-modified flax yarns, which bonds flax fibres together into a kind of flax-CA preform. SEM images of modified flax yarns show the thickness of CA coating to be ≈3μm. In Supplementary data (Table S3), CA-flax preforms show significantly higher bending resistance (442 ± 22 mN) than unmodified flax preforms (4 ± 1 mN). The CA-flax preforms possessed a transverse tensile strength of 268 ± 24 kPa, whereas flax preforms had no measurable transverse tensile strength. The tensile rupture force was similar for flax and CA-flax yarns (Supplementary data, Table S3 and Fig. S2). These results show that flax fibres have good compatibility with CA, and a uniform CA film can be achieved by dip-coating flax fabrics in CA-acetone solution. Furthermore, the CA bonds the flax fibres/yarns together so that it has enough structural integrity to be regarded as a flax-CA preform fabric.

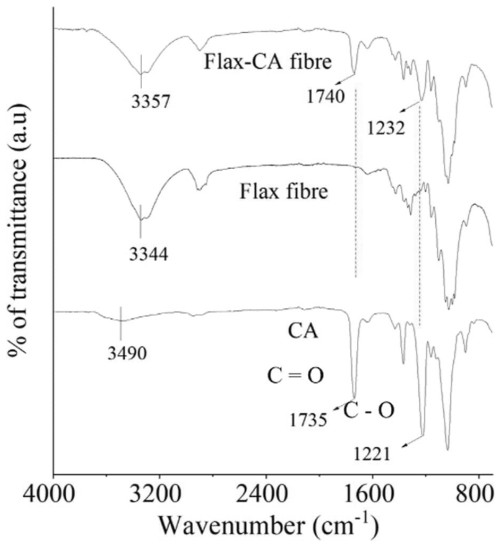

Fig. 1. FTIR transmittance spectra of untreated flax and CA-modified flax fibres. (For interpretation of the references to colour in this figure legend, the reader is referred to the web version of this article.)

3.2. Composites

3.2.1. Morphological properties

In Fig. 3, the morphology of UD flax/epoxy and CA-flax/epoxy composites is compared. The CA-flax/epoxy presents a well-organised ply architecture, and the spacing between yarns and plies is consistent. The distribution of flax yarns within flax/epoxy is relatively random, and resin-rich areas (without fibre) are more extensive than in CA-flax/epoxy. The more organised ply architecture of the modified composites can be due to the higher stiffness of the CA-flax fabrics than of the unmodified UD flax fabrics. Better flax fibre distribution within the CA-flax/epoxy composites with a lower amount of resin-rich areas can improve the ultimate behaviour of composites, such as fatigue and impact resistance where resin-rich areas can negatively affect the damage onset [23,35]. Both composites had a similar fibre volume fraction (40%) and densities (1.21 ± 0.30 g/cm^3).

3.2.2. Quasi-static tensile properties

Table 1 compares the quasi-static tensile performance of the prepared composites. The flax/epoxy and the CA-flax/epoxy composites with a $[0]_4$ lay-up have almost the same longitudinal chord modulus of elasticity (below 0.1% strain) in the range of 25 GPa and ultimate tensile strength in the range of 260 MPa, respectively. The ultimate tensile strain of the CA-modified laminates in the longitudinal and transverse directions to the fibre direction are respectively 13% and 39% higher than the corresponding values for the flax/epoxy; in the 45° orientation, the failure strain is even 52% higher.

Fig. 4 A, B show the longitudinal tensile stress–strain plots for flax/epoxy and CA-flax/epoxy laminates exhibiting very similar behaviour of the composites. As shown in Fig. 4 B, the brittle failure mode of UD flax/epoxy composites (transverse to fibre direction) changes into a more ductile shear-type of failure along the fibre direction in CA-modified composites, which is a favourable failure type in many structural applications. The failure along the fibre direction in longitudinal tensile tests shows better interfacial toughness [19].

Fig. 4 C shows the representative stress–strain behaviour of the composites under transverse ($[90]_4$ lay-up) loading condition. The CA-modified composite had ≈13% lower transverse tensile strength than the flax/epoxy version. The fibre/matrix adhesion between flax and epoxy is partly based on covalent/hydrogen bonding [33]. In CA-flax/epoxy, the adhesion is based on hydrogen bonding between flax and CA-coating and covalent/hydrogen bonding between CA-coating and epoxy resin, in addition to some microscale mechanical interlocking. The presence of only hydrogen bonding between CA-flax can be the reason for the lower transverse strength of CA-flax/epoxy. Similarly, Koolen et al. [20] assigned the reduction in transverse strength of UD flax composites having a silicone rich interface to the poor adhesion between the silicone coating and epoxy matrix, which relies solely on Van der Waals forces and few chemical bonds. The transverse tensile modulus for flax/epoxy and CA-flax/epoxy composites are similar in their value (a bit more than 4 GPa). However, CA-modified composites exhibit a 39% higher transverse failure strain (compared to unmodified flax/epoxy), which can increase the damage tolerance of composites [36]. The comparison between transverse tensile fracture surfaces of flax/epoxy (in Fig. 5) and CA-flax/epoxy (in Fig. 6) provides further insight. In Fig. 5, the fracture surface of unmodified flax/epoxy is matrix dominated (cohesive) without fibre failure as expected. The residual epoxy on flax yarns in Fig. 5 A shows good fibre/matrix adhesion. In

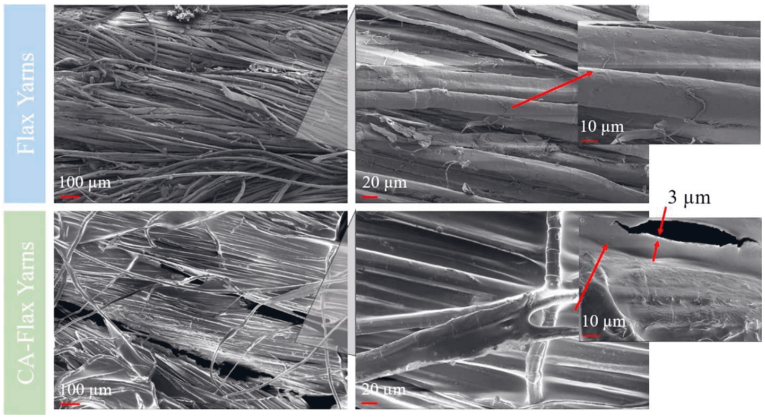

Fig. 2. SEM images of untreated and CA-treated flax yarns. (For interpretation of the references to colour in this figure legend, the reader is referred to the web version of this article.)

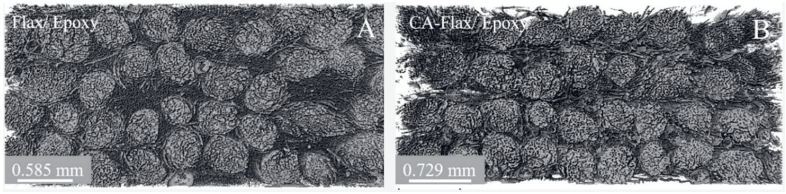

Fig. 3. Morphology of (A) UD flax/epoxy and (B) CA-flax/epoxy composites based on the μCT scans.

Table 1
Quasi-static tensile properties of the flax/epoxy and the CA-flax/epoxy composites.

Lay-up	Fibre	$E_{(0.1\%)}$ (GPa)	$\sigma_{Ultimate}$ (MPa)	$\varepsilon_{Ultimate}$ (%)	Tensile toughness (MJ/m^3)
$[0]_4$	Flax	24.98 ± 0.85	260 ± 7	1.66 ± 0.04	23.8 ± 1.1
	CA-Flax	24.55 ± 0.56	260 ± 11	1.88 ± 0.07	26.6 ± 1.6
$[90]_4$	Flax	4.51 ± 0.52	18.58 ± 1.54	0.49 ± 0.14	0.6 ± 0.1
	CA-Flax	4.22 ± 0.74	16.41 ± 1.31	0.68 ± 0.13	0.7 ± 0.1
$[\pm45]_s$	Flax	5.21 ± 0.25	67 ± 2	3.72 ± 0.49	19.2 ± 4.5
	CA-Flax	4.82 ± 0.43	52 ± 5	5.64 ± 0.37	23.6 ± 4.3

Fig. 5 B-D, the mirror-like (without texture) surface of epoxy in the interlayer regions shows the brittle nature of failure [19].

In Fig. 6 A, the transverse tensile fracture surface of CA-flax/epoxy demonstrates a preferential fracture at the fibre/matrix interface, unlike flax/epoxy. The presence of fibre imprints and flax yarns without bulk epoxy residuals indicates weaker fibre/matrix adhesion than for unmodified flax/epoxy. In Fig. 6 B-D, scarps (cleavage steps) are evident at the fracture surface of epoxy in the interlayer regions, which shows the progressive nature of failure contrary to unmodified flax/epoxy. The progression and coalescence of microcracks starting from the fibre debonding sites dissipates energy by creating new surfaces and delays the failure of composites [19] which explains higher elongation at failure and plasticity of CA-flax/epoxy compared to unmodified flax/epoxy. In Fig. 4 D, there is a comparison of the in-plane shear behaviour of unmodified and CA-modified flax/epoxy composites with a $[\pm45]_s$ lay-up. Both composites indicate similar initial stiffness of around 5 GPa. The ±45° tensile strength of CA-flax/epoxy (52 ± 5 MPa) is manifested by extensive interlaminar and intra-ply shear failure. For flax/epoxy (indicated ±45° tensile strength 67 ± 2 MPa), the failure mode is not dominated by shear modes but by brittle fibre failure (as visible in the micrographs of Fig. 4 D). The achieved increase in the overall shear toughness is evident from the dissipated fracture energy (comparison from integrated areas under stress–strain curves) that is 23.9 ± 6.8% higher compared to the non-modified composite. The ultimate failure strain is 52% higher for CA-flax/epoxy (5.64 ± 0.37%) compared to flax/epoxy (3.72 ± 0.49%).

Fig. 7 A, B show the brittle failure mode of flax/epoxy composites dominated by fibre failures with minor shear deformation and the mirror-like surface of epoxy within the interlayer regions. Fig. 7 C, D show the fracture surfaces of CA-flax/epoxy after $[\pm45]_s$ tensile test. In Fig. 7 C, the characteristic shear induced deformation of epoxy along the fibre direction (known as cusp features) and fibre imprints are evident, which indicate failure mainly based on shear loading [19]. Contrary to the mirror-like texture of epoxy in flax/epoxy, the cleavage marks of epoxy (known as scarps) are visible in Fig. 7 D, indicating the progressive failure of CA-flax/epoxy and further dissipation of energy. So, the CA modification allows extensive plastic deformation in shear for both interlaminar and intra-ply modes. In summary, tensile toughness (area under stress–strain curve) of CA-flax/epoxy composites with longitudinal ($[0]_4$) configuration is 11.6 ± 1.4 % higher than for unmodified flax/epoxy composites while both composites show similar transverse tensile ($[90]_4$) toughness (Table 1). Specifically, CA-surface modification significantly improves the tensile toughness of composite laminates subjected to in-plane shear loading. These improvements are further anticipated to lead to better impact damage resistance.

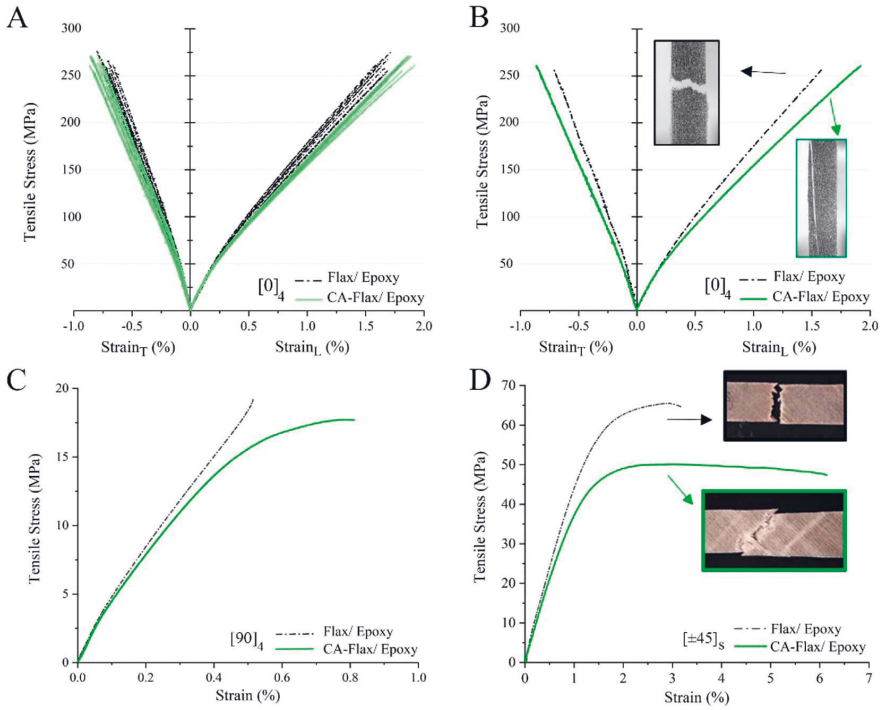

Fig. 4. Quasi-static stress–strain results. Plot A shows all longitudinal test results, and plots B, C, D are examples of the typical, representative curves for longitudinal, transverse and ±45° tensile tests. (For interpretation of the references to colour in this figure legend, the reader is referred to the web version of this article.)

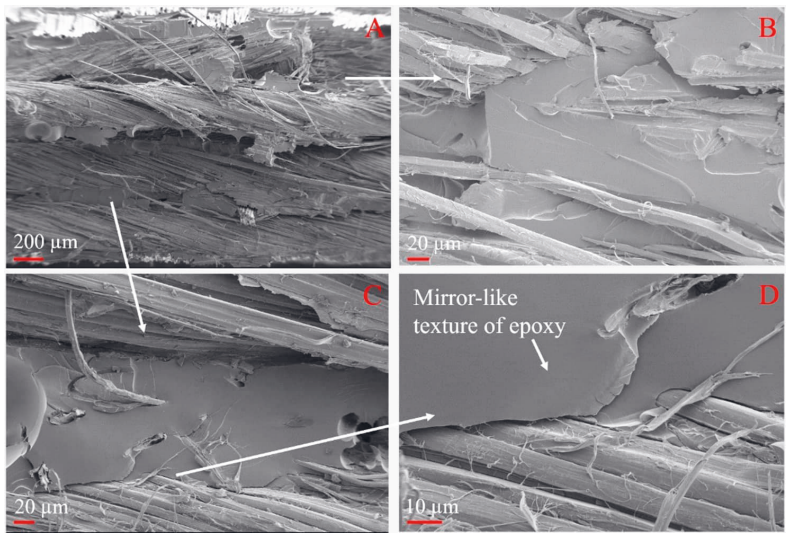

Fig. 5. The transverse tensile fracture surface of flax/epoxy (A, B, C, D). (For interpretation of the references to colour in this figure legend, the reader is referred to the web version of this article.)

3.2.3. *Flexural performance*

Fig. 8 presents short-beam shear stress-displacement curves for flax-epoxy and CA-flax/epoxy composites with a $[0/90]_{3s}$ lay-up. The apparent interlaminar shear strength (ILSS) of flax/epoxy (27.41 ± 0.44 MPa) was 17% higher than for CA-flax/epoxy (23.27 ± 0.53 MPa). Thermoplastic surface modification of flax fibres with CA changed the

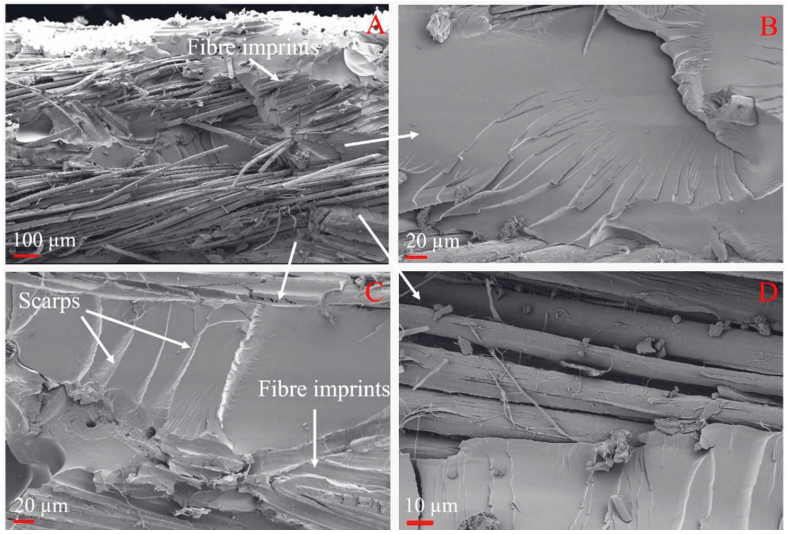

Fig. 6. The transverse tensile fracture surface of CA-flax/epoxy (A, B, C, D). (For interpretation of the references to colour in this figure legend, the reader is referred to the web version of this article.)

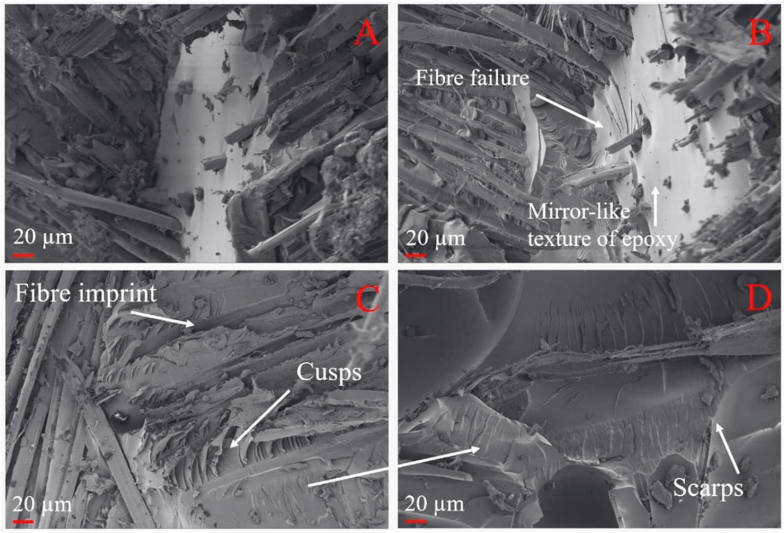

Fig. 7. The $[\pm 45]_s$ tensile fracture surface of flax/epoxy (A, B) and CA-flax/epoxy (C, D). (For interpretation of the references to colour in this figure legend, the reader is referred to the web version of this article.)

failure mode from fibre failure (at the tension/bottom side of the sample, as shown in Fig. 8 I) into fibre/matrix debonding and delamination (Fig. 8 II). CA-flax/epoxy follows a moderately progressive failure after reaching the ultimate load peak – resembled by a significant increase in ductility compared to the performance of flax/epoxy with a brittle failure mode. The step-like force (stress) drops in Fig. 8 are believed to occur due to local fibre–matrix debonding and delamination and local fibre failure. The dissipated energy upon short-beam flexure of CA-flax/epoxy (defined as the area under the short-beam force–displacement curve) was equal to 2.77 ± 0.29 J which was 95% higher than for flax/epoxy (1.42 ± 0.17 J). The improvement in the short-beam test energy dissipation of flax/epoxy composites with CA-coating can be beneficial for the damage tolerance of thin composite laminates subjected to local impact incidents. These results indicate that the CA-surface modification can impart a better toughness based on crack deflection due to increased debonding and spread of damage compared to flax/epoxy composites under flexural load.

3.2.4. *Impact performance*

Fig. 9 illustrates examples of the typical contact force-central displacement traces of the drop-weight impacted specimens (3 J, 18 J and 21 J energies) for the $[0/90]_{3s}$ lay-ups. In the initial loading phase,

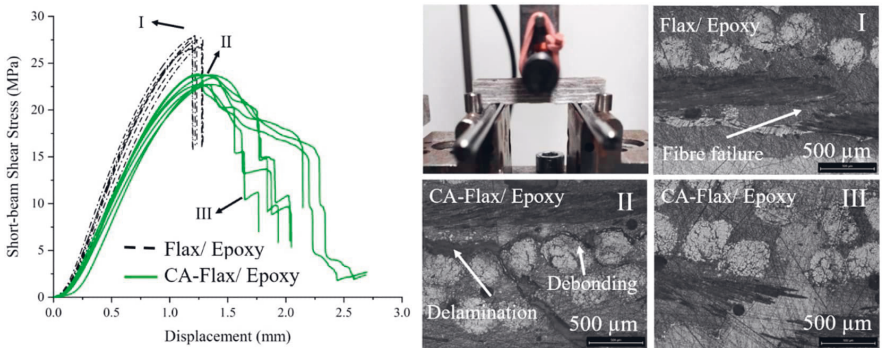

Fig. 8. Short-beam shear stress-displacement curves and failure mode analysis together with cross-sectional micrographs. (For interpretation of the references to colour in this figure legend, the reader is referred to the web version of this article.)

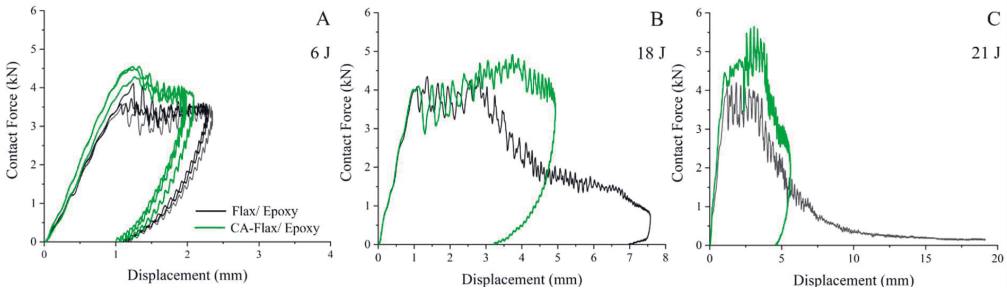

Fig. 9. Typical contact force-central displacement traces of the flax/epoxy and the CA-flax/epoxy composites at 6 J (A), 18 J (B), and 21 J (C) drop-weight impact energies. (For interpretation of the references to colour in this figure legend, the reader is referred to the web version of this article.)

contact force–displacement curves extend linearly from the origin towards the maximum force. The maximum contact force in drop-weight impact incident of composites indicates the resistance of specimens against impact event and mainly depends on fibre strength [8,10,16] and fibre dominated ultimate fractures [16]. Right after reaching the maximum force, shown in Fig. 9, the damages develop and propagate within the composite while the impactor still moves against the specimen until the movement stops at the turning/rebound point. The extension of the force fluctuations in the zone (between loading and rebound phases) is typically associated with various damages (e.g., delamination, shear-induced and bending induced matrix cracks, and fibre failure) [8,37]. The energy absorbed during the impact incident is equal to the enclosed area under the force–displacement curve (hysteresis loop), and the recovered (elastic) impact energy is equal to the difference between total impact energy (area before a rebound) and absorbed energy [38]. In the perforation impact incident, the specimen absorbs all the impact energy, and there is no recovered elastic impact energy like the contact force–displacement curve of unmodified flax/epoxy in Fig. 9 C.

In Fig. 9, the extent of damage (displacement within the fluctuation

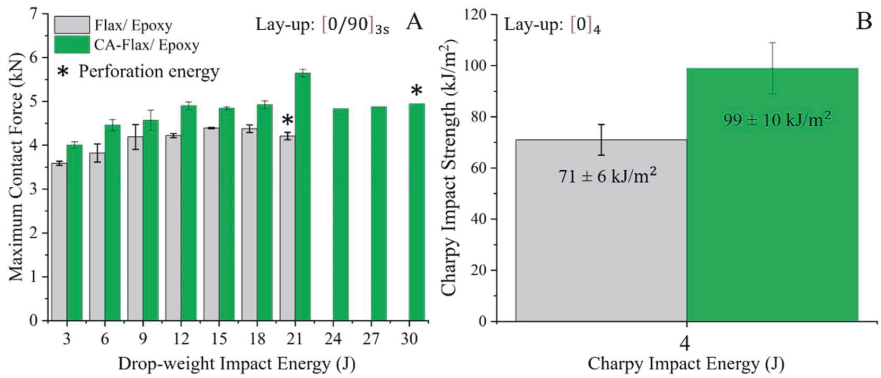

Fig. 10. Maximum drop-weight impact force (A) and Charpy impact strength (B) of composites. (For interpretation of the references to colour in this figure legend, the reader is referred to the web version of this article.)

phase) increases for tests with impact energies from 6 J to 21 J. The extent of damage progression within CA-flax/epoxy is lower than in the case of flax/epoxy. The lower damage progression indicates that the impactor encounters continuous, ductile resistance when penetrating the composite system due to the CA-flax/epoxy's higher toughness. Naturally, the suppressed impact damage of flax/epoxy with CA-surface modification is anticipated to enhance the post-impact-tested residual flexural/compression strength [10,13].

Fig. 10 A shows the maximum drop-weight contact force of composites subjected to impact energies from 3 J to perforation energy which is 21 J for unmodified flax/epoxy and 30 J for CA-flax/epoxy. The contact force of flax/epoxy got enhanced by 12% for all impact energy levels with CA-modification, which was expected according to the higher toughness of the CA-flax/epoxy composite (see Table 1). Likewise, in Fig. 10 B the Charpy impact strength of UD flax/epoxy composites with a $[0]_4$ lay-up was 71 ± 6 kJ/m^2, which got improved by 38% (to 99 ± 10 kJ/m^2) due to the CA-surface modification The brittle fracture mode of UD flax/epoxy composites related to the Charpy impact tests transformed into a combination of fibre debonding and delamination with the CA surface modification (as reported in Supplementary data, Fig. S4).

Fig. 11 A, B clearly show the contribution of CA-surface modification to the perforation resistance of flax/epoxy composites. The impactor's overall contact time with CA-flax/epoxy specimens is lower than for flax/epoxy specimens, which indicates that CA-modified composites have a better resistance against impacts – better overall elasticity under impact loading. After 15 J, flax/epoxy composite absorbed almost all the (initial) impact energy and transferred it into ply failure and, finally, complete perforation and almost no recovered elastic energy occurred at 21 J. Fig. 11 B shows that the CA-surface modification enhances the perforation energy of flax/epoxy by 42% to 30 J which is a significant contribution to the impact resistance and safety of flax/epoxy composites. Based on the results from tensile tests, tensile shear tests, and short beam flexural tests, the higher perforation energy of CA-flax/epoxy is due to the higher interfacial toughness and ductility of the CA-modified composite laminates.

Fig. 11 C, D compare the absorbed and recovered (elastic) impact energies, respectively. The absorbed energies of flax/epoxy and CA-flax/epoxy increase linearly with impact energies. Both composites have very similar absorption capability for energies of 3 J and 6 J. At 9, 12, 15, 18 and 21 J impact energies, the flax/epoxy, respectively, absorbed 1.7%, 4.6%, 7.7%, 8.5%, and 5% more impact energy than the CA-modified composite. The reason for the higher energy absorption of unmodified flax/epoxy is the greater extent of damage compared to CA-flax/epoxy [10,16]. The recovered (elastic) energy, shown in Fig. 11 D, increases linearly from 3 J to 9 J for modified and unmodified composite specimens. The recovered energy of flax/epoxy starts to decrease after the 9 J energy level to zero at 21 J, indicated by the final perforation of these reference composites. Based on Fig. 11 D, the perforation threshold energy (defined here as the point where recovered energy starts to degrade) shifts from 9 J (for flax/epoxy) to 15 J (66% improvement) with the CA thermoplastic fibre surface modification.

Fig. 12 presents typical damage patterns of flax/epoxy composites subjected to low-velocity impact. The majority of matrix cracks and local fibre failures are towards the rear-face, and shear induced matrix cracks are seen near the mid-plane of composites [10,37], similar to Fig. S7 and Fig. S8 micrographs in the supplementary data.

Fig. 13 A compares the damage in flax/epoxy and CA-flax/epoxy specimens subjected to drop-weight impact incidents. Both flax/epoxy and CA-flax/epoxy specimens do not significantly damage after a 3 J

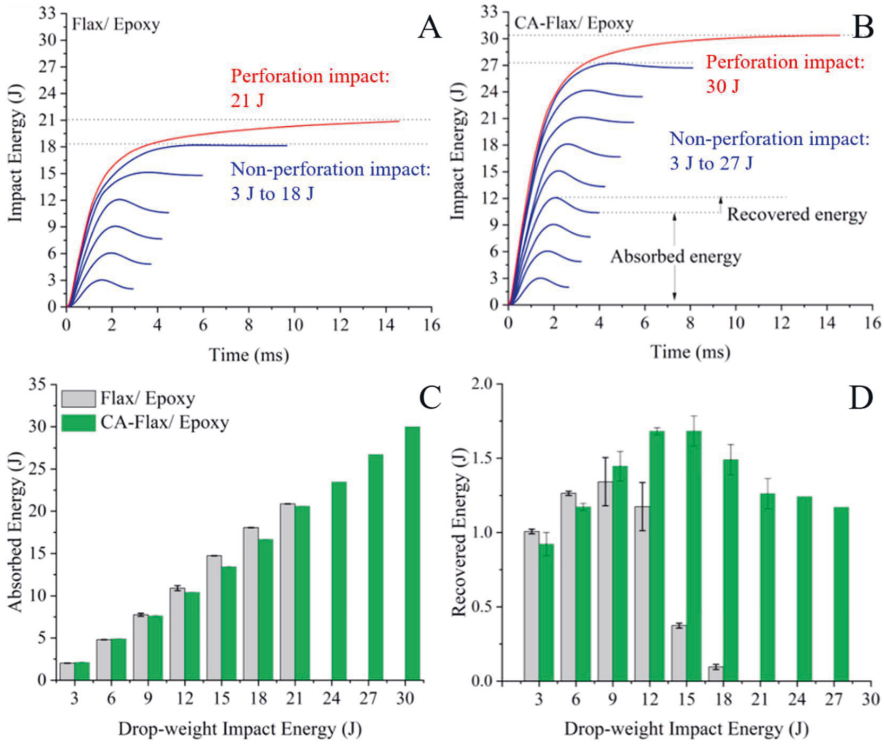

Fig. 11. Energy-time history of 3 J to complete perforation impact energies for flax/epoxy (A) and CA-flax/epoxy (B) composites and their corresponding absorbed energy (C) and recovered energy (D). (For interpretation of the references to colour in this figure legend, the reader is referred to the web version of this article.)

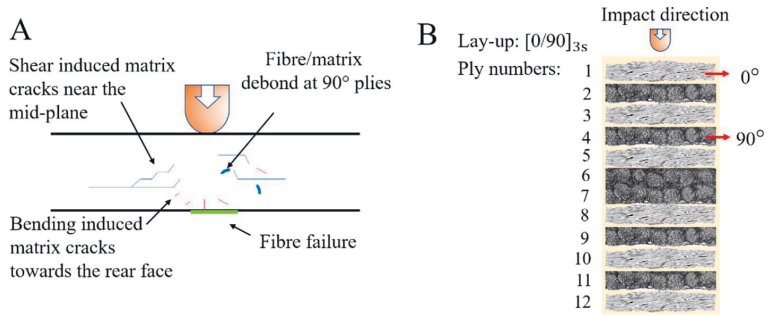

Fig. 12. Illustration of typical damage patterns of the flax/epoxy composites subjected to low-velocity drop-weight impact (A), and the composite cross-section before an impact test (B). (For interpretation of the references to colour in this figure legend, the reader is referred to the web version of this article.)

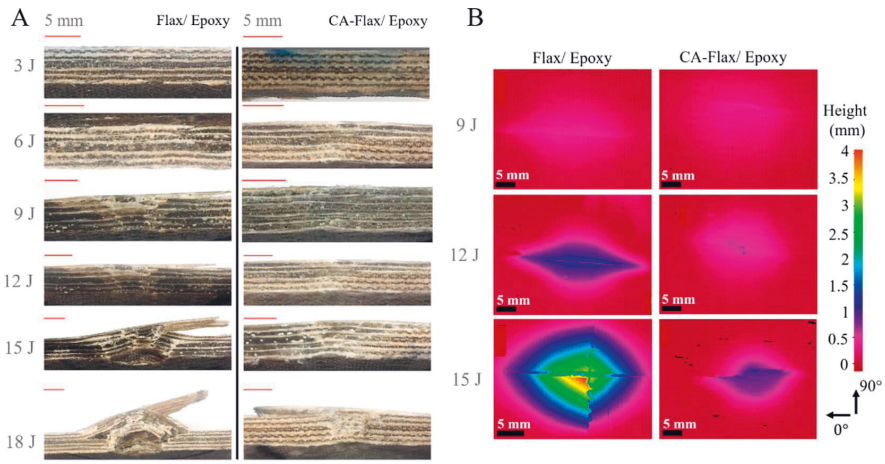

Fig. 13. A: Through thickness inspection of the flax/epoxy and CA-flax/epoxy specimens after 3 J to 18 J impact events. B: Profilometer images from rear-face surface permanent deformation after 9 J, 12 J, and 15 J impact events. The 3 J and 6 J impacts did not cause any deformation at the rear-face. (For interpretation of the references to colour in this figure legend, the reader is referred to the web version of this article.)

impact except for minor matrix cracks on the composites' rear-face (12th ply defined in Fig. 12 B). After the 6 J impact, a fibre failure is evident at the rear-face of the flax/epoxy specimen, but no damage is visible for CA-flax/epoxy (detailed microscopy images are available in the Supplementary data, Fig. S7). After 9 J and 12 J impacts, shear-induced matrix cracks near mid-plane were noted for flax/epoxy (being more severe for higher energy impact), but only local fibre/matrix debonds at 6th and 7th plies were visible for CA-flax/epoxy. These

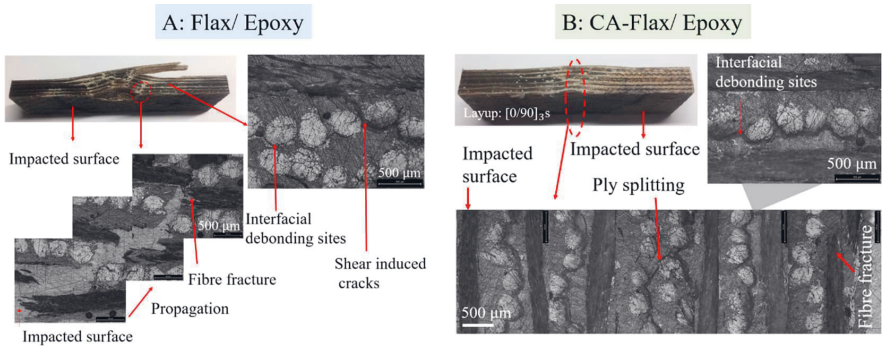

Fig. 14. Through thickness damage patterns of flax/epoxy (A) and CA-flax/epoxy (B) specimens after 15 J drop-weight impact incident. (For interpretation of the references to colour in this figure legend, the reader is referred to the web version of this article.)

damages are visible in microscopy images in Supplementary data (Fig. S8). In Fig. 13 B, the permanent surface deformation at the rear-face of flax/epoxy (based on the profilometer surface measurement on 12th ply) is increased from 0.5 mm after the 9 J impact incident to 2 mm after the 12 J impact, which is considerably higher than for CA-flax/epoxy specimens.

Fig. 14 compares in more detail the damage of flax/epoxy and CA-flax/epoxy specimens after 15 J impacts. Flax/ epoxy specimen experiences a six ply breakage, interfacial debonding, and ply splitting. However, CA-flax/epoxy specimens exhibited only fibre failure at the rear-face and fibre/matrix debonding at 90° plies (namely 2nd, 4th, 6th, 7th, 9th, and 11th plies). The limited fibre breakage in CA-modified composites compared to unmodified ones corroborates with the higher recovered elastic energy of CA-flax/epoxy compared to flax/epoxy, especially at 12 J (by +43%), 15 (by +354%), and 18 J (by +1452%) impact energies in Fig. 11 D. The profilometer-measured rear-face surface deformations of unmodified and CA-modified flax/epoxy specimens after the 15 J impact test (in Fig. 13 B) correlate with the cross-sectional optical microscope images. Similar improvement with the CA surface modification was evident after the 18 J impact energy test. In toughened multi-axial cross-ply composites (with thermosetting resin), fibre splitting only appears within the outer ply (rear-surface) without extensive delamination and splitting on internal plies [16] as in the case of CA-flax/epoxy.

Our results showed that it is possible to control how the impact damage manifests itself in flax/epoxy composites from ply splitting and extensive fibre failure to fibre/matrix debonding (at 90° plies) and fibre failure at rear-face ply (Fig. 14). The findings showed that interfacial and interlaminar toughness plays a critical role in the damage resistance of flax/epoxy composites and agrees with previous reports for different composites [10]. This investigation revealed a potential to control natural fibre composites' impact damage progression with cellulose-based thermoplastic surface modification. Especially the 42% improvement in the perforation energy of cross-ply flax/epoxy composites with CA-surface modification can promote the further application of natural fibre composites in structural applications such as automotive, where impact resistance is critical. In future work, the fatigue performance of flax/epoxy composites will have to be analysed to understand further the quantitative toughening effects on dynamic load range and practical load spectra.

4. Conclusions

This paper presents a novel surface modification method to improve the interfacial toughness and low-velocity impact resistance of flax/epoxy composites by deploying thin (≈3 μm) and distinct biobased cellulose-acetate (CA) thermoplastic coating at the fibre surface. The CA-modification allowed extensive plastic deformation in shear for all quasi-static loading modes. Short-beam flexural testing showed a 17% decrease in apparent interlaminar shear strength of flax/epoxy composites with CA-modification. However, the CA-surface modification altered the brittle catastrophic failure of flax/epoxy composites into progressive failure with considerably larger energy dissipation based on crack deflection due to increased debonding and spread of damage. The maximum drop-weight impact contact forces of cross-ply CA-flax/epoxy laminates were 12% higher than for flax/epoxy for all the tested impact energies. Similarly, the Charpy impact strength of UD CA-flax/epoxy was 38% higher than for flax/epoxy. The CA-treatment enhanced perforation threshold energy and perforation energy of flax/epoxy by 66% and 42%, respectively. The CA-surface modification significantly improved the recovered (elastic) energy of flax/epoxy composites. The improvement in the recovered energy manifested itself with a lower extent of fibre failure. The surface modification presented in this investigation provides the potential to manipulate the damage progression due to dynamic loads, such as impact.

CRediT authorship contribution statement

F. Javanshour: Conceptualization, Methodology, Formal analysis, Investigation, Writing – original draft, Visualization. **A. Prapavesis:** Investigation, Formal analysis. **T. Pärnänen:** Investigation, Formal analysis. **O. Orell:** Investigation. **M.C. Lessa Belone:** Investigation. **R.K. Layek:** Writing – review & editing. **M. Kanerva:** Supervision, Methodology. **P. Kallio:** Funding acquisition. **A.W. Van Vuure:** Supervision, Funding acquisition. **E. Sarlin:** Investigation, Supervision, Funding acquisition.

Declaration of Competing Interest

The authors declare that they have no known competing financial interests or personal relationships that could have appeared to influence the work reported in this paper.

Acknowledgements

This project is funded by the European Union's Horizon 2020 research and innovation programme under the Marie Skłodowska-Curie grant agreement No 764713-FibreNet. This work made use of Tampere Microscopy Center facilities at Tampere University. The authors are grateful to Bcomp (Fribourg, Switzerland) for supplying the flax fabrics and providing valuable insights.

Appendix A. Supplementary material

Supplementary data to this article can be found online at https://doi.org/10.1016/j.compositesa.2021.106628.

References

[1] Bourmaud A, Beaugrand J, Shah DU, Placet V, Baley C. Towards the design of high-performance plant fibre composites. Prog Mater Sci 2018;97:347–408. https://doi.org/10.1016/j.pmatsci.2018.05.005.

[2] Zhang Z, Cai S, Li Y, Wang Z, Long Yu, Yu T, et al. High performances of plant fiber reinforced composites—A new insight from hierarchical microstructures. Compos Sci Technol 2020;194:108151. https://doi.org/10.1016/j.compscitech.2020.108151.

[3] Li Mi, Pu Y, Thomas VM, Yoo CG, Ozcan S, Deng Y, et al. Recent advancements of plant-based natural fiber–reinforced composites and their applications. Compos Part B Eng 2020;200:108254. https://doi.org/10.1016/j.compositesb:2020.108254.

[4] Duc F, Bourban PE, Plummer CJG, Månson J-A-E. Damping of thermoset and thermoplastic flax fibre composites. Compos Part A Appl Sci Manuf 2014;64:115–23. https://doi.org/10.1016/j.compositesa.2014.04.016.

[5] Corbin A-C, Sala B, Soulat D, Ferreira M, Labanieh A-R, Placet V. Development of quasi-unidirectional fabrics with hemp fiber: a competitive reinforcement for composite materials. J Compos Mater 2021;55(4):551–64. https://doi.org/10.1177/0021998320954230.

[6] Islam MS, Pickering KL, Foreman NJ. Influence of alkali fiber treatment and fiber processing on the mechanical properties of hemp/epoxy composites. J Appl Polym Sci 2011;119(6):3696–707. https://doi.org/10.1002/app.v119.610.1002/app.31335.

[7] Haggui M, El Mahi A, Jendli Z, Akrout A, Haddar M. Static and fatigue characterization of flax fiber reinforced thermoplastic composites by acoustic emission. Appl Acoust 2019;147:100–10. https://doi.org/10.1016/j.apacoust.2018.03.011.

[8] Barouni AK, Dhakal HN. Damage investigation and assessment due to low-velocity impact on flax/glass hybrid composite plates. Compos Struct 2019;226:111224. https://doi.org/10.1016/j.compstruct.2019.111224.

[9] Dhakal HN, Sarasini F, Santulli C, Tirillò J, Zhang Z, Arumugam V. Effect of basalt fibre hybridisation on post-impact mechanical behaviour of hemp fibre reinforced composites. Compos Part A Appl Sci Manuf 2015;75:54–67. https://doi.org/10.1016/j.compositesa.2015.04.020.

[10] Bensadoun F, Depuydt D, Baets J, Verpoest I, van Vuure AW. Low velocity impact properties of flax composites. Compos Struct 2017;176:933–44. https://doi.org/10.1016/j.compstruct.2017.05.005.

[11] Hull D, Yi BS. Damage mechanism characterisation in composite damage tolerance investigations. Compos Struct 1993;23(2):99–120.

[12] Ramakrishnan KR, Corn S, Le Moigne N, Ienny P, Slangen P. Experimental assessment of low velocity impact damage in flax fabrics reinforced biocomposites by coupled high-speed imaging and DIC analysis. Compos Part A Appl Sci Manuf 2021;140:106137. https://doi.org/10.1016/j.compositesa:2020.106137.

[13] Liang S, Guillaumat L, Gning PB. Impact behaviour of flax/epoxy composite plates. Int J Impact Eng 2015;80:56–64. https://doi.org/10.1016/j.ijimpeng.2015.01.006.
[14] Chew E, Liu JL, Tay TE, Tran LQN, Tan VBC. Improving the mechanical properties of natural fibre reinforced laminates composites through Biomimicry. Compos Struct 2021;258:113208. https://doi.org/10.1016/j.compstruct.2020.113208.
[15] Bensadoun F, Vanderfeesten B, Verpoest I, Van Vuure AW, Van Acker K. Environmental impact assessment of end of life options for flax-MAPP composites. Ind Crops Prod 2016;94:327–41. https://doi.org/10.1016/j.indcrop.2016.09.006.
[16] Schrauwen B, Peijs T. Influence of matrix ductility and fibre architecture on the repeated impact response of glass-fibre-reinforced laminated composites. Appl Compos Mater 2002;9:331–52. https://doi.org/10.1023/A:1020267013414.
[17] Awais H, Nawab Y, Anjang A, Md Akil H, Zainol Abidin MS. Effect of fabric architecture on the shear and impact properties of natural fibre reinforced composites. Compos Part B Eng 2020;195:108069. https://doi.org/10.1016/j.compositesb.2020.108069.
[18] Cantwell W. Geometrical effects in the low velocity impact response of GFRP. Compos Sci Technol 2007;67(9):1900–8. https://doi.org/10.1016/j.compscitech.2006.10.015.
[19] Greenhalgh ES. Failure analysis and fractography of polymer composites. Cambridge, UK: Woodhead Publishing Ltd.; 2009.
[20] Koolen G, Soete J, van Vuure AW. Interface modification and the influence on damage development of flax fibre - Epoxy composites when subjected to hygroscopic cycling. Mater. Today Proc., vol. 31, Elsevier Ltd; 2019, p. S273–9. https://doi.org/10.1016/j.matpr.2020.01.183.
[21] Prasad V, Sekar K, Varghese S, Joseph MA. Enhancing Mode I and Mode II interlaminar fracture toughness of flax fibre reinforced epoxy composites with nano TiO2. Compos Part A Appl Sci Manuf 2019;124:105505. https://doi.org/10.1016/j.compositesa.2019.105505.
[22] Gassan J, Dietz T, Bledzki AK. Effect of silicone interphase on the mechanical properties of flax-polyurethane composites. Compos Interfaces 2000;7(2):103–15. https://doi.org/10.1163/156855400300184262.
[23] Ravandi M, Teo WS, Tran LQN, Yong MS, Tay TE. Low velocity impact performance of stitched flax/epoxy composite laminates. Compos Part B Eng 2017;117:89–100. https://doi.org/10.1016/j.compositesb.2017.02.003.
[24] Lin J, Wang L, Liu L, Lu K, Li G, Yang X. Two-stage interface enhancement of aramid fiber composites: establishment of hierarchical interphase with waterborne polyurethane sizing and oxazolidone-containing epoxy matrix. Compos Sci Technol 2020;193:108114. https://doi.org/10.1016/j.compscitech.2020.108114.
[25] Narducci F, Lee KY, Pinho ST. Interface micro-texturing for interlaminar toughness tailoring: a film-casting technique. Compos Sci Technol 2018;156:203–14. https://doi.org/10.1016/j.compscitech.2017.10.016.
[26] Wu Z, Yi XS, Wilkinson A. Interlaminar fracture toughness of carbon fibre/RTM6-2 composites toughened with thermoplastic-coated fabric reinforcement. Compos Part B Eng 2017;130:192–9. https://doi.org/10.1016/j.compositesb.2017.08.003.
[27] Liu WenBo, Zhang S, Li B, Yang F, Jiao WeiCheng, Hao LiFeng, et al. Improvement in interfacial shear strength and fracture toughness for carbon fiber reinforced epoxy composite by fiber sizing. Polym Compos 2014;35(3):482–8. https://doi.org/10.1002/pc.v35.310.1002/pc.22685.
[28] Eyckens DJ, Randall JD, Stojcevski F, Sarlin E, Palola S, Kakkonen M, et al. Examining interfacial interactions in a range of polymers using poly(ethylene oxide) functionalized carbon fibers. Compos Part A Appl Sci Manuf 2020;138:106053. https://doi.org/10.1016/j.compositesa:2020.106053.
[29] Zhang Bo, Jia L, Tian M, Ning N, Zhang L, Wang W. Surface and interface modification of aramid fiber and its reinforcement for polymer composites: a review. Eur Polym J 2021;147:110352. https://doi.org/10.1016/j.eurpolymj.2021.110352.
[30] Uddin ME, Layek RK, Kim HY, Kim NH, Hui D, Lee JH. Preparation and enhanced mechanical properties of non-covalently-functionalized graphene oxide/cellulose acetate nanocomposites. Compos Part B Eng 2016;90:223–31. https://doi.org/10.1016/j.compositesb.2015.12.008.
[31] Byrne FP, Jin S, Paggiola G, Petchey THM, Clark JH, Farmer TJ, et al. Tools and techniques for solvent selection: green solvent selection guides. Sustain. Chem Process 2016;4(1). https://doi.org/10.1186/s40508-016-0051-z.
[32] Hallak Panzera T, Jeannin T, Gabrion X, Placet V, Remillat C, Farrow I, et al. Static, fatigue and impact behaviour of an autoclaved flax fibre reinforced composite for aerospace engineering. Compos Part B Eng 2020;197:108049. https://doi.org/10.1016/j.compositesb:2020.108049.
[33] Javanshour F, Ramakrishnan K, Layek RK, Laurikainen P, Prapavesis A, Kanerva M, et al. Effect of graphene oxide surface treatment on the interfacial adhesion and the tensile performance of flax epoxy composites. Compos Part A Appl Sci Manuf 2021:106270. https://doi.org/10.1016/j.compositesa.2020.106270.
[34] Fei P, Liao L, Cheng B, Song J. Quantitative analysis of cellulose acetate with a high degree of substitution by FTIR and its application. Anal Methods 2017;9:6194–201. https://doi.org/10.1039/c7ay02165h.
[35] Korkiakoski S, Sarlin E, Suihkonen R, Saarela O. Influence of reinforcement positioning on tension-tension fatigue performance of quasi-unidirectional GFRP laminates made of stitched fabrics. Compos Part B Eng 2017;112:38–48. https://doi.org/10.1016/j.compositesb.2016.12.017.
[36] Gamstedt EK, Sjögren BA. Micromechanisms in tension-compression fatigue of composite laminates containing transverse plies. Compos Sci Technol 1999;59(2):167–78. https://doi.org/10.1016/S0266-3538(98)00061-X.
[37] Yasaee M, Bond IP, Trask RS, Greenhalgh ES. Damage control using discrete thermoplastic film inserts. Compos Part A Appl Sci Manuf 2012;43(6):978–89. https://doi.org/10.1016/j.compositesa:2012.01.011.
[38] Xu Z, Yang F, Guan ZW, Cantwell WJ. An experimental and numerical study on scaling effects in the low velocity impact response of CFRP laminates. Compos Struct 2016;154:69–78. https://doi.org/10.1016/j.compstruct.2016.07.029.

PAPER IV

Supplementary is data available through the online version provided by Elsevier.

Composites: Part A 161 (2022) 107110

Contents lists available at ScienceDirect

Composites Part A

journal homepage: www.elsevier.com/locate/compositesa

Impact and fatigue tolerant natural fibre reinforced thermoplastic composites by using non-dry fibres

F. Javanshour [a,*], A. Prapavesis [b], N. Pournoori [a], G.C. Soares [a], O. Orell [a], T. Pärnänen [a], M. Kanerva [a], A.W. Van Vuure [b], E. Sarlin [a]

[a] Unit of Materials Science and Environmental Engineering, Tampere University, Tampere, Finland
[b] Department of Materials Engineering, Composite Materials Group, KU Leuven, 3001 Leuven, Belgium

ARTICLE INFO

Keywords:
B. Adhesion
B. Debonding
B. Delamination
A. Thermoplastic matrix

ABSTRACT

This article introduces stiff and tough biocomposites with in-situ polymerisation of poly (methyl methacrylate) and ductile non-dry flax fibres. According to the results, composites processed with non-dry fibres (preconditioned at 50% RH) had comparable quasi-static in-plane shear strength but 42% higher elongation at failure and toughness than composites processed with oven-dried fibres. Interestingly, the perforation energy of flax–PMMA cross-ply composites subjected to low-velocity impact increased up to 100% with non-dry flax fibres. The in-situ impact damage progression on the rear surface of composites was evaluated based on strain and thermal field maps acquired by synchronised high-speed optical and thermal cameras. Impact-induced delamination lengths were investigated with tomography. Non-dry fibres also decreased the tension–tension fatigue life degradation rate of composites up to 21% and altered the brittle failure mode of flax–PMMA to ductile failure dominated by fibre pull-out.

1. Introduction

Natural flax fibre reinforced thermoplastic composites offer low density structural composites with good damping properties and recyclability [1–3]. Currently, the major application areas of continuous flax fibre reinforced composites are in the construction and sporting sectors [4]. The long-term durability of structural biocomposites is essential to promote the inherent ecological merit of natural fibres. The impact and fatigue tolerance of flax fibre composites are critical for their long-term durability [5–8]. The toughness of the reinforcing fibres and the polymer matrix [3,6,9], lay-up and architecture of the reinforcing fabrics [6], and interfacial toughness [10–12] are the critical parameters for composites' impact and fatigue tolerance. The primary failure mode of flax fibre composites is fibre failure with minor delamination, specifically in low-velocity impact incidents, limiting the energy dissipation potential [6,10]. Strong and tough interfacial adhesion can enhance stress transfer between fibre and matrix, deflect the interfacial cracks towards the matrix, and improve fatigue and impact tolerance [13]. The interfacial toughness of flax fibre composites should be designed to allow limited damage growth and further energy dissipation through interfacial debonding and delamination under low-velocity impact [10]. A tough interface can enhance the fatigue tolerance of composites [14,15]. Common methods to enhance interfacial toughness are chemical grafting of polymer chains on reinforcing fibres to induce polymer chain entanglement between fibre and matrix [16,17], depositing functionalised nanomaterials on the fibres [18–20], and deploying a thin ductile phase between fibre and matrix [10,13]. For instance, Hsieh et al. [15] showed that adding 0.5 wt% carbon nanotubes increases epoxy resin's fatigue crack growth threshold by 204% from 24 J/m^2 to 73 J/m^2. They reported a significant effect of nanotube debonding and pull-out on fracture toughness of epoxy, based on fractography observations and micromechanical modelling [15].

An alternative approach to enhance the toughness of natural fibre composites is to use non-dry (swollen) fibres and take advantage of the moisture present in the fibres [21–23]. The radial swelling coefficient of technical flax fibres ($\beta_{f,r}$: 1.9 [24]) is many orders of magnitude higher than their thermal expansion coefficient ($\alpha_{f,r}$:78 $\times$ 10^{-6}/°C [25]). In climates where the relative humidity is around 50% RH, processing biocomposites with fibres stored in the ambient condition (e.g., 23 °C, 50% RH) can be beneficial as the in-service swelling and shrinkage of fibres within composites will be limited compared to composites processed with oven-dried fibres [26,27]. Also, preserving the moisture of

* Corresponding author.
E-mail address: farzin.javanshour@tuni.fi (F. Javanshour).

https://doi.org/10.1016/j.compositesa.2022.107110
Received 24 May 2022; Received in revised form 15 July 2022; Accepted 20 July 2022
Available online 22 July 2022

flax fibres during the processing of composites can improve the ductility and tensile strength of reinforcing fibres and raise the impact and fatigue tolerance of composites [21,22,28].

In this study, non-dry flax fibre reinforced thermoplastic composites were manufactured through resin infusion by in-situ polymerisation of poly (methyl methacrylate) (PMMA). It was hypothesised that in-situ polymerisation of PMMA could be insensitive to water molecules as the MMA monomers are often emulsion polymerised in an aqueous medium [29]. Due to the reactive nature of in-situ polymerisation, good bonding between fibre and matrix was expected. The motivation to use non-dry fibres was to benefit from the enhancement in the ductility of flax fibres and to potentially raise interfacial toughness. Additionally, it was envisioned that the proposed processing method would save cost and energy by eliminating the need for oven-drying fibres, often required in manufacturing natural fibre composites [23,30].

The interfacial adhesion between fibre and matrix was evaluated based on quasi-static transverse tensile and in-plane shear testing of flax–PMMA composites. The fatigue and impact tolerance of cross-ply composites were assessed by applying low-cycle tension–tension fatigue and low-velocity drop-weight impact tests. After fatigue tests, the fracture surfaces of composites were investigated by scanning electron microscopy (SEM). The damage mechanism, deformation, and heat release on the rear surface of composites during impact testing were monitored with synchronised high-speed optical and infrared (IR) imaging. The internal through-thickness damage of impacted composite specimens was studied by X-ray computed tomography.

2. Methodology

Non-crimp flax yarn fabrics of unidirectional (UD) and twill 2/2 types with an areal density of 300 g/m^2 were provided by Bcomp (Fribourg, Switzerland). A thin polyester weft thread connected the yarns of the UD flax fabrics. The manufacturer treated the flax fibres with boiling water to remove waxes from the surface. The mechanical properties of these fibres are reported in Supplementary data (S.1.1). A liquid thermoplastic resin based on methyl methacrylate (Elium 188, Arkema, Colombes, France) and dibenzoyl peroxide initiator (BP-50-FT1, United Initiators GmbH, Pullach, Germany) with 3 wt% initiator to resin was used as the polymer matrix system. Elium 188 resin system was selected based on its excellent mechanical properties (see S.1.1) and the possibility of free radical polymerisation at ambient conditions [31,32]. Room temperature (23 °C) in-situ polymerisation of Elium 188 was selected to avoid evaporation of the moisture present in non-dry flax fibres. For simplicity, the resin system in this article (Elium 188) was named PMMA throughout the text.

In-situ polymerised flax–PMMA composite panels with a fibre volume fraction (V_f) of 40% were manufactured based on the vacuum-assisted resin infusion method (see Supplementary data, S.1.2). The V_f and composites' morphology were characterised by X-ray computed (X-CT) tomography (UniTom HR, TESCAN, Ghent, Belgium) with a voxel size of 800 nm as described in Supplementary data (S.1.3). Three types of composites (labelled as Dry, RT, and RH) were processed with flax fabrics stored in three different conditions for 24 h before resin infusion. Dry fabrics were oven-dried at 115 °C (for 24 h), RT fabrics were conditioned at 50% RH (23 °C, for 24 h), and RH fabrics were conditioned at 90% RH (23 °C, 24 h). The moisture content of fibres was measured by an analytical balance (model GR-202, A&D Ltd, Tokyo, Japan). The average weight for three pieces of fabrics (10 mm × 10 mm; width × length) was measured consecutively after oven-drying and humidity conditioning. The weight gains of RT and RH fabrics after conditioning were respectively 8.1 ± 0.2 wt% and 16.8 ± 0.2 wt% compared to oven-dried (Dry) fabrics. Laminates were then stored in a controlled environment (50% RH, 23 °C) for three months to reach equilibrium before testing. The weight gain values of Dry and RT composites at equilibrium were respectively 2.3 ± 0.1 wt% and 0.2 ± 0.1 wt %. The weight of RH-type composites was reduced by 4.1 ± 0.2 wt% upon reaching an equilibrium due to moisture desorption of swollen fibres. In this study, all relative humidity (RH) conditionings for both fabrics and composites were done in a humidity chamber (model VC 0018, Vötschtechnik, Balingen, Germany).

Quasi-static tensile testing was carried out with a universal testing machine (model 5967, Instron, MA, USA). The effect of non-dry fibres on interfacial adhesion was studied based on quasi-static transverse tensile strength of UD composites and in-plane shear testing of composites with $[+45/-45]_{SE}$ lay-ups according to ASTM D3039 and ASTM D3518 standards, respectively (for details see the Supplementary data S.1.4). The in-plane quasi-static properties were studied based on tensile testing of composites with $[(0,90)]_4$ lay-ups composed of four twill 2/2 woven fabric plies (ASTM D3039). Full-field deformation was measured with a stereo optical extensometer (StrainMaster Compact, LaVision, Göttingen, Germany). The specimen and test specifications are reported in Supplementary data (S.1.4). The average results of seven specimens per series (excluding grip failure) were reported.

The contribution of non-dry fibres to the fatigue resistance of flax–PMMA composites was evaluated by performing tension–tension cyclic tests of composites with $[(0,90)]_4$ lay-ups following the ASTM D3479 standard. Rectangular-shaped specimens were used with dimensions of 250 mm × 25 mm × 2 mm (length × width × thickness). Tapered glass-epoxy tabs were used to reduce the stress concentration at the gripped section of the specimens (as described in Supplementary data S.1.4). The tests were performed with a servo-hydraulic tester (MTS 180, Minnesota, USA) equipped with a 100 kN load cell and a gauge length of 150 mm. A constant-load amplitude and a sinusoidal wave shape were applied at a frequency of 5 Hz. The loading frequency of 5 Hz was chosen to avoid a temperature rise of more than 10 °C according to the ASTM D3479. The stress ratio (R) of the nominal minimum to maximum applied stress was 0.1. S-N graphs were acquired by registering the number of cycles to failure and the nominal maximum stress for each specimen. The load levels (90%, 80%, 70%, and 50%) for the low-cycle fatigue tests were selected as the ultimate tensile strength fractions. Three specimens per load level (excluding any grip failure) were tested. The temperature of the specimens during testing was monitored by a longwave IR camera (model Ti400, Fluke, Washington, USA) with thermal sensitivity of 0.05 °C at 30 °C. The ambient conditions during tests were 23 °C and 50% RH. The fracture surface analysis of composites was carried out with a ULTRAplus (Zeiss, Oberkochen, Germany) scanning electron microscope (SEM). A thin platinum-palladium (Pt-Pd) coating was used to ensure enough conductivity for the SEM samples.

The impact performance of structural flax–PMMA composites with a $[0/90]_{3SE}$ lay-up was studied with an instrumented drop-weight tester (Type 5, Rosand, Ohio, USA) without rebound impacts per ASTM D7136 and ASTM D5628 standards. Rectangular-shaped specimens with dimensions of 60 mm × 60 mm × 5 mm (length × width × thickness) were clamped between two steel fixtures with a circular test area (diameter 40 mm) representing a fixed support. The drop height was adjusted to 0.11, 0.22, 0.32, 0.44, 0.55, 0.66, 0.77, 0.88, 0.99, 1.11, 1.21, 1.32, 1.43, and 1.57 m to reach kinetic energies of 3, 6, 9, 12, 15, 18, 21, 24, 27, 30, 33, 36, 39, and 42 J, respectively; the mass of the impactor was 2772 g. A hemispherical steel-made head (diameter 12.7 mm) was fixed to the impactor. The contact force was measured using a load sensor (60 kN) between the head and the impactor structure. The force data were recorded at a 180 kHz frequency. The displacement of the impactor was numerically integrated from the measured contact force–time curve. For each impact energy level, three composite specimens were tested.

The rear surfaces of composites (opposite to the impacted surface) during the impact testing were in-situ monitored via mirrors placed under the specimens with a synchronised high-speed optical camera (Fastcam SA-X2, Photron, Tokyo, Japan) and high-speed IR camera (Fast IR-1500 M2K, Telops, Quebec City, Canada). A 50.8 by 50.8 mm unprotected gold mirror (PFSQ20-03-M03, THORLABS, Newton, United States) at 80 cm lens distance and a conventional mirror at 35 cm lens

distance were placed at an angle below the impact specimen to reflect the IR electromagnetic radiation and full-field deformations respectively. The emissivity of the composites in the infrared range (ability to emit infrared energy) was measured to convert radiometric temperature to surface temperature. Further information on the optical and infrared imaging methods and the DIC analysis is available in Supplementary data S.1.5. The impact-induced internal damage of composites was studied with X-ray computed (X-CT) tomography (UniTOM XL, TESCAN, Ghent, Belgium) with a voxel size of 35 μm (see Supplementary data S.1.3).

3. Results and discussions

3.1. Morphology analysis of composites based on X-CT tomography

The internal microstructures of flax–PMMA composites after three months of stabilisation at 50% RH (23 °C) are presented in Fig. 1. The Dry, RT and RH composites, which are respectively processed with oven-dried (at 115 °C) fibres and humidity-conditioned fibres at 50% RH (23 °C) and 90% RH (23 °C), all are nearly void-free within the matrix phase. The void-free structure of composites and moisture insensitivity of the PMMA resin is relevant to the synthesis type of methyl methacrylate, which is emulsion polymerisation in an aqueous medium [29]. However, the porosities in composites were mainly detected within flax yarns between the fibre and matrix region. The volume fraction of porosities was 0.2 ± 0.05% for Dry and RT composites, while the 4.33 ± 0.29% volume fraction of the RH-type composites was comprised of interfacial porosities. The fibre volume fractions of composites were 41.91 ± 1.92% (for Dry), 39.27 ± 1.72% (for RT), and 45.02 ± 3.05% (for RH). In Fig. 1, minimal traces of interfacial debonding between fibre and matrix are evident within fibre yarns in Dry composites (Fig. 1). The limited debonding lines (cracks) in Dry-type composite can be related to the swelling of oven-dried flax fibres during the stabilisation period at 50% RH. Debonding traces are visible in RT to a lesser extent, as fibres were stored in the 50% RH before and after manufacturing. On the contrary, highly swollen RH fibres have shrunk during the drying (stabilisation) period at 50% RH (Fig. 1). The extensive interfacial debonding lines (cracks) within fibre yarns are evident for RH-type composite. The average width of the cracks within fibre bundles (bundle splits) in RH is 9.7 ± 3.1 μm, which is 177% higher than the average width of bundle splits in Dry-type composite (3.5 ± 0.3 μm). The large debondings can dramatically reduce the interfacial shear strength of RH composites but enhance the damping potential of composites through interfacial sliding between fibre and matrix.

3.2. Quasi-static tensile properties of composites

Fig. 2 shows examples of the typical representative shear stress–strain curves of flax–PMMA composites with $[+45/-45]_{SE}$ lay-up. Also, a complete set of in-plane shear stress–strain curves are presented in the Supplementary data (Fig. S5). In this study, the τ_{12}^{offset} and τ_{12}^{max} respectively correspond to the stress values at 0.2% and 5% engineering shear strain according to the testing standard (ASTM D3518).

The in-plane shear performances of the Dry, RT and RH composites are summarised in Table 1. The shear chord modulus of elasticity (G_{12}^{chord}) for both Dry and RT composites is 1.6 ± 0.1 GPa showing that processing flax–PMMA composites with non-dry fibres does not have any adverse effect on the G_{12}^{chord}. A slightly lower mean value of G_{12}^{chord} for RH composites (−18.75%) compared to the reference Dry composites can be ascribed to the local interfacial porosities [33] due to the shrinkage of swollen RH fibres during the stabilisation period at 50% RH (23 °C). The mean τ_{12}^{offset} and τ_{12}^{max} values of RT composites are respectively 5.6% and 3.9% lower than Dry composites, which indicates comparable interfacial adhesion of flax–PMMA composites with both

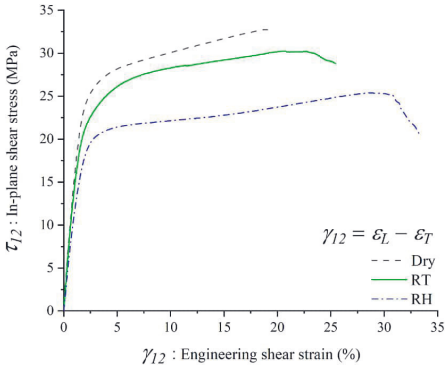

Fig. 2. The representative (average) in-plane shear stress–strain plots of flax–PMMA composites with $[+45/-45]_{SE}$ lay-up. (For interpretation of the references to colour in this figure legend, the reader is referred to the web version of this article.)

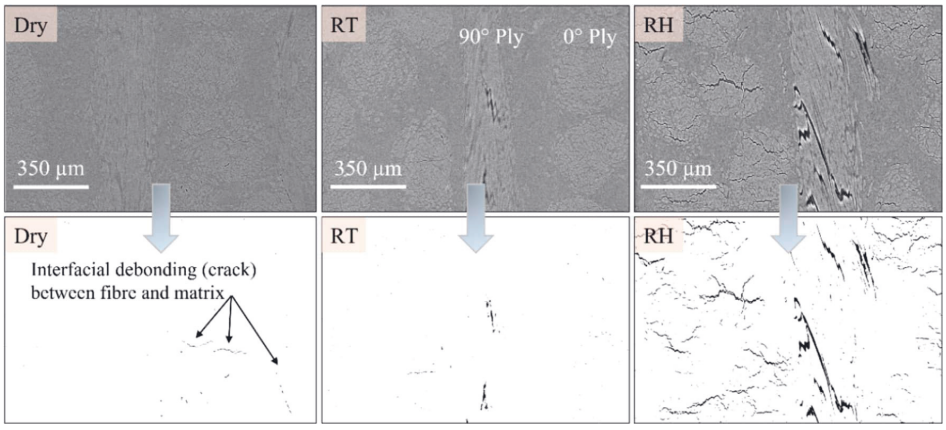

Fig. 1. X-CT tomography of flax–PMMA composites stabilised for three months at 50% RH (23 °C). (For interpretation of the references to colour in this figure legend, the reader is referred to the web version of this article.)

Table 1
In-plane shear properties of flax–PMMA composites with $[+45/-45]_{SE}$ lay-up.

Property	Dry Composites	RT Composites	RH Composites
G_{12}^{chord}, (GPa)	1.6 ± 0.1	1.6 ± 0.1	1.3 ± 0.1
τ_{12}^{offset}, (MPa)	17.6 ± 1.7	16.6 ± 1.4	13.1 ± 1.8
τ_{12}^{max}, (MPa)	27.7 ± 1.9	26.6 ± 1.3	21.3 ± 1.5
$\gamma_{12}{}^{failure}$, (%)	19.4 ± 1.2	27.6 ± 1.7	34.4 ± 1.9
Toughness, (MJ/m^3)	540.8 ± 8.1	768.2 ± 7.9	791.2 ± 9.9

oven-dried and non-dried (RT) fibres. However, the mean τ_{12}^{offset} and τ_{12}^{max} values of RH composites are 25.5% and 23.1% lower than of the Dry composites, which can be attributed to the lower adhesion between RH-flax fibre and PMMA and lower adhesion between elementary RH-flax fibres. Lower adhesion between fibre and matrix in RH composites is related to the extensive interfacial debonding sites due to fibre shrinkage, as discussed in the previous section through X-CT tomography analysis. The effect of humidity on technical flax fibres has been reported in the literature [22]. At humidity levels above 70% RH, the cementitious pectin layer on the elementary flax fibres binding fibres together within the technical fibres may soften by the water molecules [22]. The high humidity-induced softening can cause defibrillation of the technical flax fibres and reduce the strength of composites [23]. The mean elongation at failure values ($\gamma_{12}{}^{failure}$) of RT and RH composites are respectively 42.2% and 77.3% higher than for Dry composites. The tensile toughness values based on the area under stress–strain curves have a similar trend as the $\gamma_{12}{}^{failure}$. The significantly higher elongation at failure and tensile toughness of non-dry composites than the Dry specimens can be explained by the plasticising effect of moisture on the flax fibres [22] and modestly lower interfacial adhesion of RT and RH composites [10].

The quasi-static transverse tensile and in-plane tensile performance of the Dry, RT, and RH composites are provided in Table 2. Dry and RT composites have almost the same transverse tensile properties. The elastic modulus of PMMA (3.17 ± 0.2 GPa) dominates composites' transverse elastic (E_T) modulus. Similar E_T modulus values (3.1 GPa) of Dry and RT composites show that the in-situ polymerisation of flax–PMMA composites is not sensitive to the presence of moisture. The transverse elastic modulus and transverse tensile strength of RH composites are 48.4% and 38.6% lower than for the reference Dry composites. The extensive interfacial debonding sites caused by the shrinkage of swollen fibres (at 90% RH) are the reason for the degradation in the transverse tensile strength and E_T of RH composites. The quasi-static tensile performance of composites (in Table 2) with $[(0,90)]_4$ lay-up follows the same trend as in transverse tensile and in-plane shear. The quasi-static results showed that the in-situ polymerisation of flax–PMMA composites is not sensitive to ambient moisture. In summary, non-dry composites offered a unique combination of ductility and good in-plane shear strength, beneficial characteristics for fatigue and impact tolerant structural biocomposites.

3.3. Fatigue performance of composites

Fig. 3(A) demonstrates the tension–tension fatigue performance of flax–PMMA composites. The fatigue behaviour of Dry, RT and RH composites follows a similar trend in the various loading ranges. The S-N slope of RH (−12.45) is less steep compared to Dry (−15.87), which indicates a 21% longer fatigue life for RH composites that have a more significant elongation at failure (see Table 2). For instance, at the 80% load level, the number of cycles to failure of RH composites is 80% higher than Dry-type composites. The S-N slope of Dry and RT composites are similar. As shown in Fig. 3(B), processing composites with non-dry fibres alters the brittle fatigue failure mode of Dry flax–PMMA composites into a more ductile failure dominated by the fibre pull-out which enhances the energy dissipation and fatigue tolerance of composites due to interfacial sliding [34]. Figs. 4 and 5 provide further insights into the fatigue failure mode of composites.

Table 2
Quasi-static tensile properties of the flax–PMMA composites. The $[90]_4$ and $[(0,90)]_4$ lay-ups are respectively composed of four UD and twill-woven fabric layers.

Composite, Lay-up	E^{chord}, (GPa)	σ^{max}, (MPa)	$\varepsilon^{failure}$, (%)
Dry, $[90]_4$	3.1 ± 0.3	14.5 ± 0.3	0.41 ± 0.05
RT, $[90]_4$	3.1 ± 0.2	13.7 ± 0.7	0.42 ± 0.02
RH, $[90]_4$	1.6 ± 0.1	8.9 ± 0.6	0.72 ± 0.01
Dry, $[(0,90)]_4$	11.7 ± 0.2	110.2 ± 1.8	1.62 ± 0.06
RT, $[(0,90)]_4$	11.4 ± 0.1	105.2 ± 1.2	1.83 ± 0.05
RH, $[(0,90)]_4$	8.4 ± 0.1	94.5 ± 1.4	2.44 ± 0.08

Fig. 4(A) presents a general view of the tension–tension fatigue fracture surface of the Dry composites with ply divisions. Fig. 4(B and C) suggest overall good adhesion between fibre and matrix and brittle fibre failure in Dry-type flax–PMMA composites with some extent of fibre pull-out and fibre imprints. Fig. 4(D) demonstrates regular wave-like features commonly known as striations. The striations form due to the molecular chain fracture at the crack tip following limited stretching [35]. The striations on the fracture surface show the incremental nature of damage growth following the loading cycles [35].

In Fig. 5(A, B), the fatigue fracture surfaces of RT composite resemble those of Dry specimens (Fig. 4A, B) except for a more considerable extent of fibre pull-out. The polymer residues on the fibre surfaces of RT composites indicate good compatibility between fibre and matrix (Fig. 5B). The fracture surface of the RH composite in Fig. 5(C, D) is dominated by extensive and lengthy fibre pull-outs with smooth fibre surfaces. The fractographic results in this section confirm the ductile nature and higher fatigue energy dissipation capability of non-dry composites by interfacial fibre-sliding compared to Dry composites.

3.4. Drop-weight impact performance

Composites can absorb part of the impact energy by plastic deformation and transfer the remaining elastic part of the energy back to the impactor, depending on their impact resistance and elasticity. The perforation energy (E^P) is a characteristic where the specimen fails without recovered elastic energy. Fig. 6 (A) provides an overview of the drop-weight impact energy-time history of cross-ply flax–PMMA composites with a $[0/90]_{3SE}$ lay-up. The energy-time curves show that processing flax–PMMA composites with non-dry fibres enhances the E^P of the reference Dry composites (21 J) by 57% (RT: 33 J) and 100% (RH: 42 J). Fig. 6 (B) summarises the E^P values of composites normalised to the thickness of the specimens. It is worth noting that the 21 J (4.06 ± 0.13 J/mm) perforation energy (E^P) of the Dry flax–PMMA composites in this study is equal to the E^P of flax/epoxy composites with a similar reinforcement type and lay-up ($[0/90]_{3SE}$ lay-up, 5 mm in thickness, 40% V_f) [10]. Compared to the flax fibre reinforced poly (lactic acid) (PLA) composites, the E^P of the Dry flax–PMMA composites (21 J, 4.06 ± 0.13 J/mm) is 16% higher than flax/PLA composites (E^P = 3.49 ± 0.41 J/mm) made of 2 × 2 twill flax/PLA commingled textile with $[(0/90)]_{12}$ lay-up, 4 mm in thickness and 32% V_f [36]. Also, processing flax fibre reinforced composites with thermoplastic matrix systems, which are more ductile compared to PMMA, can result in better E^P values for biocomposites. For instance, flax fibre reinforced polypropylene (PP) composites with $[(0,90)]_{10}$ lay-up made of 2 × 2 twill flax/PP commingled textile, 40% V_f, and 3 mm in thickness have the perforation energy of 15 J (or 5 J/mm) [37] which is 23% higher than the E^P value for Dry-type flax–PMMA (4.06 ± 0.13 J/mm). However, the non-dry RT and RH composites reported in this study offer the highest perforation energy for natural fibre composites in the literature with a unique combination of stiffness, toughness, and fatigue tolerance.

Fig. 7 shows the internal damage patterns of cross-ply specimens after 21 J impact testing. Contrary to the fully perforated Dry specimen, the damage patterns of the RT specimen are shear-induced ply splitting

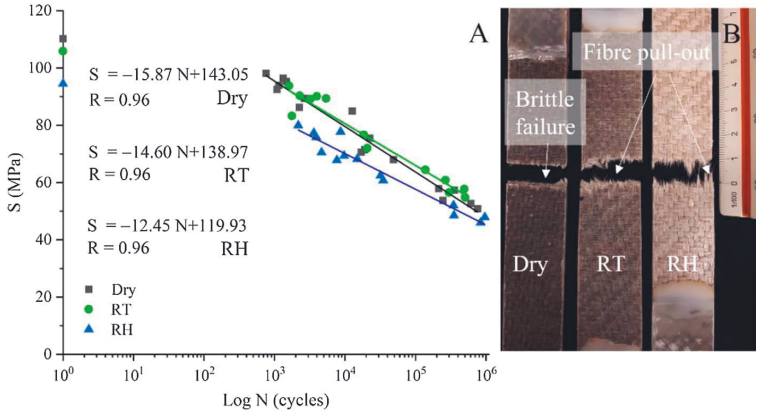

Fig. 3. Determined S-N curves of composites (A) and examples of the typical specimen failure modes (B). (For interpretation of the references to colour in this figure legend, the reader is referred to the web version of this article.)

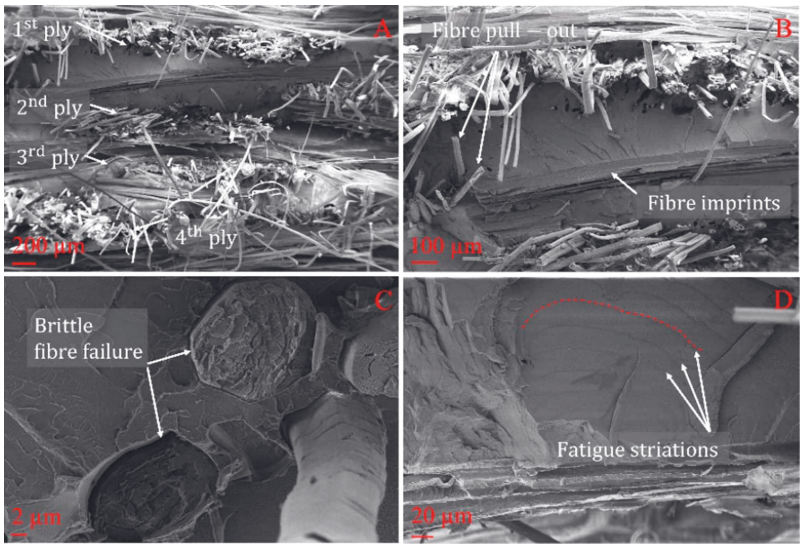

Fig. 4. The tension–tension fatigue fracture surface of Dry composites (A, B, C, D). (For interpretation of the references to colour in this figure legend, the reader is referred to the web version of this article.)

and five clear delamination lines with a cumulative length of 112.56 mm. The internal damage patterns of the RH specimen are local interfacial debonding and four clear delamination lines with a cumulative length of 82.05 mm, which is 27% lower than the corresponding value for RT (112.56 mm). The RH's lower extent of delamination and fibre failure agrees with RH's higher recovered impact energy than for RT at 21 J impact energy (see Fig. 6A). The X-CT results reflect the tough nature of non-dry composites, which allows dissipation of impact energy through interfacial sliding/debonding and delamination.

Fig. 8 shows the contact force–time history of composites at 21 J impact energy. Overall, the contact force–time profiles of the RT and RH composites are smoother and more symmetric compared to the profile for the Dry specimens, which indicates a higher degree of elastic deformation for non-dry specimens during the impact testing. Further data on full-field deformation of the specimen's rear surface is provided (in Figs. 9 and 10) for a better understanding of the impact damage mechanisms of flax– PMMA composites at perforation energy and the contribution of non-dry fibres. The full-field strain maps in Figs. 9 and 10 are synchronised with the contact force–time profiles (Fig. 8) to provide insights into specific force values.

The impact damage initiation and progression on the rear surface of the Dry specimen at 21 J impact energy is presented in Fig. 9 based on the in-situ high-speed optical and thermal-field imaging. The A–H images in Fig. 9 correspond to the specified force–time values (I–VII) in Fig. 8(A). For better visualisation of the 2D damage initiation and progression on the rear surface of the specimen, the von Mises strain maps are superimposed on the high-speed optical images in Fig. 9(A–D). However, the strain maps are removed after the crack opening on the rear surface of the specimen (Fig. 9E–G) due to the strain field discontinuity, especially in the vicinity of the crack.

In Fig. 9(A and B), the impact damage on the rear surface of Dry composite initiates as matrix cracking and develops further with ply

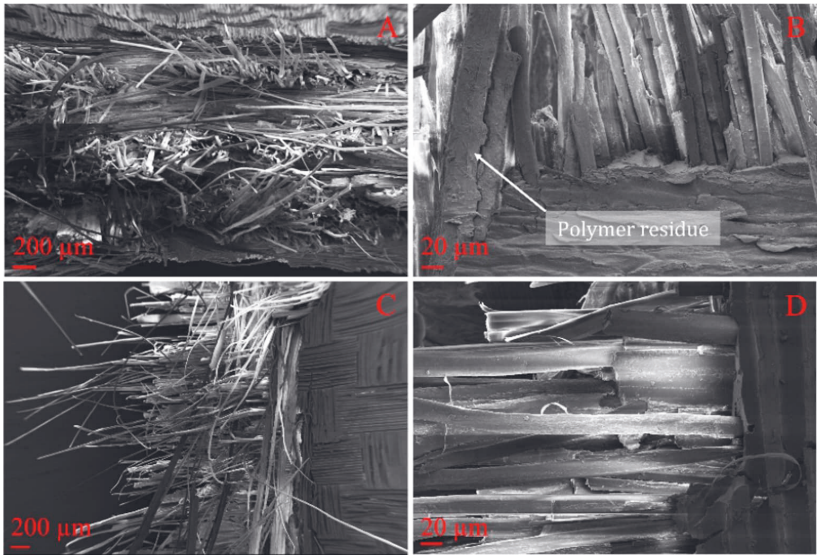

Fig. 5. The tension–tension fatigue fracture surface of RT (A, B) and RH (C, D) composites. (For interpretation of the references to colour in this figure legend, the reader is referred to the web version of this article.)

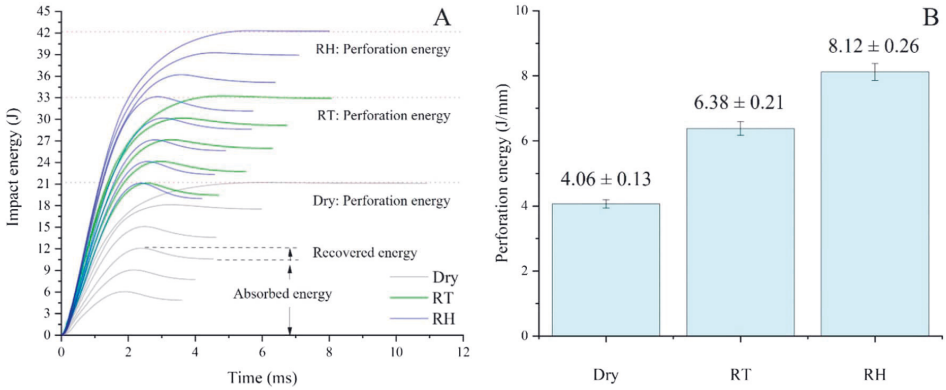

Fig. 6. Energy-time history of composites (A) and perforation energies normalised to thickness (B). (For interpretation of the references to colour in this figure legend, the reader is referred to the web version of this article.)

splitting (i.e., cracks between fibres) traces. The first crack opening (Fig. 9C) occurs at the maximum contact force (F^{max}). The crack propagates parallel to the fibre direction on the rear surface of the composite (Fig. 9D), which corresponds to the plateau region between the force values of III and IV in the contact force–time profile in Fig. 8(A). Fig. 8 (A) shows that the contact force continuously decreases after the plateau region (III-IV) until complete perforation. After the plateau region, the first drop in the contact force follows the development of extensive ply splitting and fibre pull-outs on the rear surface of the specimen (Fig. 9E and F). Transverse cracks develop just before the complete perforation (point VII in Fig. 8A), as shown in Fig. 9(G). The shape of surface cracks is visible in the thermal field image (Fig. 9H), which shows how the specimen dissipates the mechanical energy by heat generation.

To compare the Dry, RT, and RH composites, the von Mises strain maps at the maximum contact force (F^{max}) are presented in Fig. 10. In all cases, the crack opening happens at the F^{max}. The extent of the surface deformations is notably higher in RT and RH composites than in the Dry specimen. The strain maps at F^{max} show that the RT and RH composites have better ductility under impact loading than the Dry specimen.

The contact force-central displacement traces of composites at 21 J kinetic energy are presented in Fig. 11(A). Compared to Dry, the force–displacement curves of RT and RH composites are smoother and more symmetric, showing that the non-dry composites have a higher degree of elastic behaviour. In Fig. 11 (B), the maximum contact force (F^{max}) of the RT and RH composites at 21 J kinetic energy are respectively 13% and 19% above the similar value for the Dry specimens. The higher F^{max} values for RT and RH compared to the Dry specimens can be explained by the limited degree of the fibre and ply failure within non-dry composites at 21 J kinetic energy (as shown previously in Fig. 7), which enhances the load-bearing capacity of RT and RH. It is worth noting that the F^{max} of the Dry flax–PMMA composites in this study is in the same range as the F^{max} of flax/epoxy composites (4.209 ± 0.08 kN)

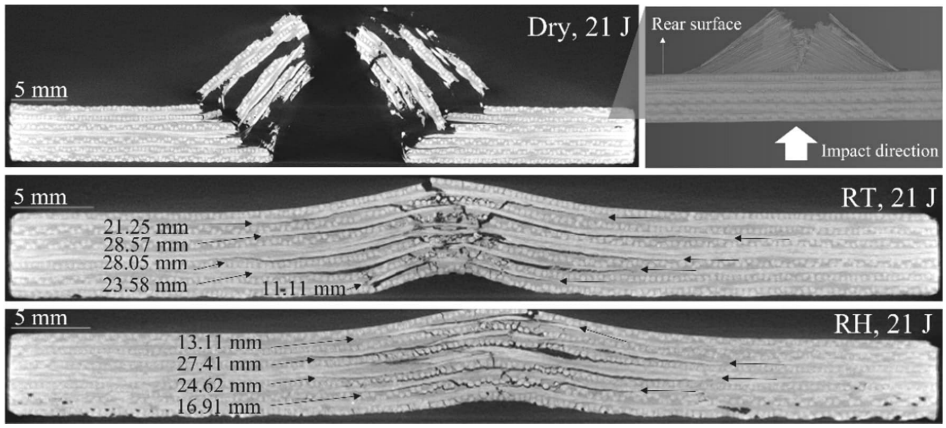

Fig. 7. Non-destructively captured internal damage patterns, including delamination lengths based on X-CT. (For interpretation of the references to colour in this figure legend, the reader is referred to the web version of this article.)

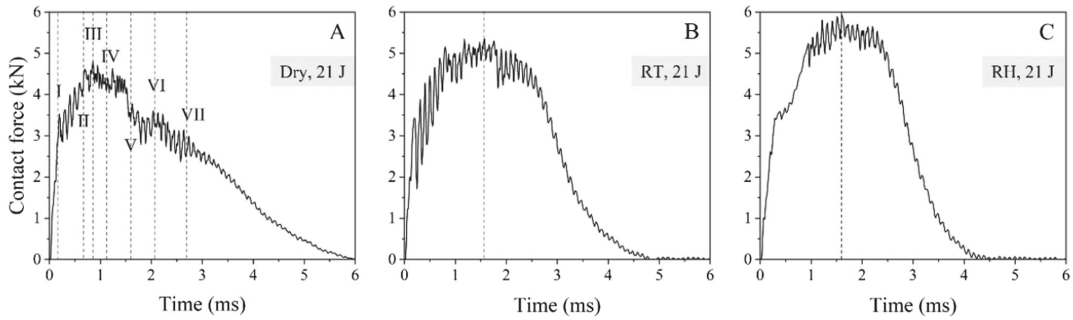

Fig. 8. Typical contact force–time history of composites at 21 J drop-weight impact energy. (For interpretation of the references to colour in this figure legend, the reader is referred to the web version of this article.)

with $[0/90]_{3SE}$ lay-up, 40% V_f, and 5 mm in thickness [10].

In Fig. 11(C), the average displacement values at F^{max} for RT and RH are respectively 45% and 61% higher than those values for Dry. The higher displacement values in Fig. 11 (C) for RT and RH compared to the Dry agree with the strain values reported in Fig. 10 and prove that the non-dry specimens present more ductile resistance against the impactor. Further data on contact force-central displacement traces of composites at various kinetic energies are available in the Supplementary data (Figs. S6–S8).

Fig. 12 shows the synchronised profiles of the contact force–time and temperature on the rear surface of composites at 21 J impact energy. In all composites, the average surface temperature rises only after the first peak in the contact force–time history, which corresponds to the initiation of matrix cracks and ply splitting on the rear surface of the composites. So, the increase in the surface temperature of specimens is directly related to and proportional to the plastic deformations during the impact incident. Therefore, it can be concluded that the extent of plastic deformations is the highest for the Dry specimen, while RT and RH specimens present more elastic resistance against the impactor. It is worth noting that the increase in the average surface temperature of natural fibre composites (for both perforated and non-perforated specimens) is less than 5 °C (Fig. 12). However, low-velocity impact is not an adiabatic process, and specimens have sufficient time to dissipate the mechanical energy as heat [38]. The specimens have sufficient time to dissipate low-velocity impact energy as heat to a large volume before reaching the rear surface, where an IR camera collects temperature maps. So, the initial temperature rise inside the specimens might be higher than at the rear surface as the damage propagates through the thickness. Additional studies are necessary to understand further the effect of impact-induced heat release on the material behaviour of composites.

4. Summary and outlook

In summary, non-dry fibres modified the brittle nature of flax–PMMA composites through toughening due to the plasticising effect of moisture bound to fibres [22] and interfacial toughening by allowing interfacial sliding. Especially, RT composites with preconditioned fibres (stored in 50% RH, 23 °C for 24 h) can positively impact further use of environmentally friendly natural fibres in structural applications. RT offered good adhesion between fibre and matrix, same as oven-dried fibres, higher in-plane shear strain (42%), lower fatigue life degradation, and 57% higher perforation energy than commonly used oven-dried flax fibre composites. These results are valuable as designing stiff and tough composites with simultaneous fatigue and impact tolerance enhancement can be challenging. The polymerisation kinetic studies in the literature [32,39] suggest the possibility of processing thick composite laminates in the range of 10–20 mm without reaching 100 °C (at ambient pressure) to avoid boiling MMA monomers and the moisture present in the fibres. However, further research is required to

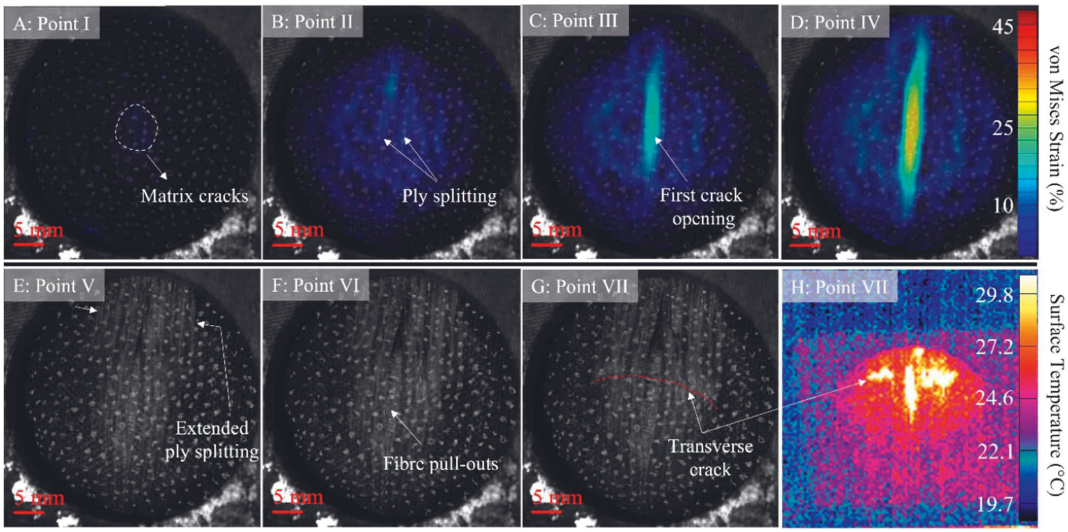

Fig. 9. Damage progression on the rear surface of Dry composite at 21 J impact energy. Figures A-H correspond to the specified force values (I-VII points in Fig. 8) in the force–time history of Dry composites. (For interpretation of the references to colour in this figure legend, the reader is referred to the web version of this article.)

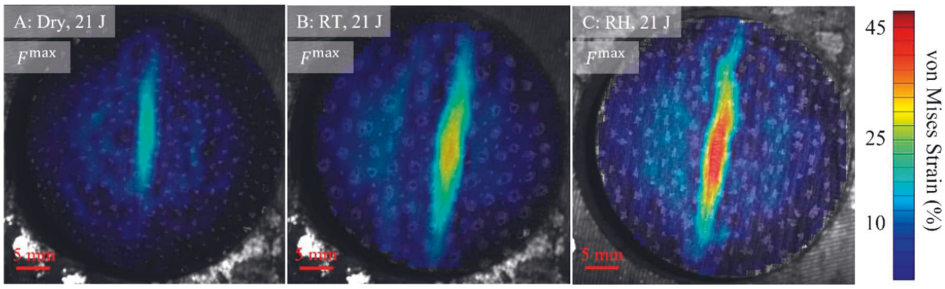

Fig. 10. Damage patterns on the rear surface of Dry (A), RT (B), and RH (C) composites at 21 J impact energy. (For interpretation of the references to colour in this figure legend, the reader is referred to the web version of this article.)

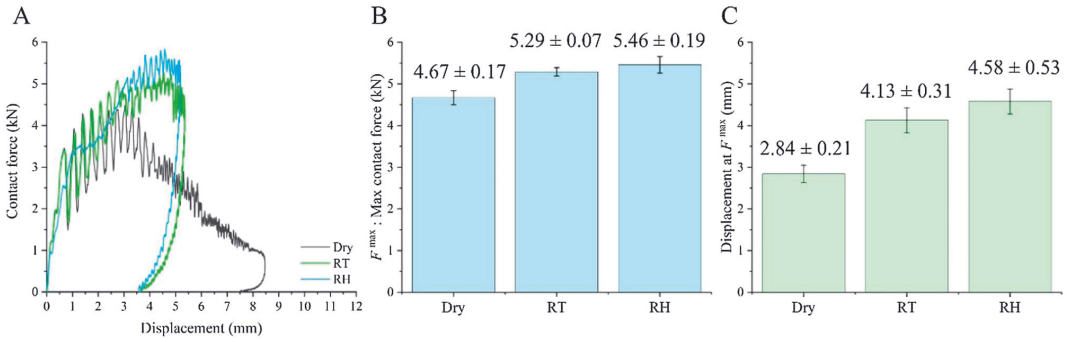

Fig. 11. Typical contact force-central displacement traces of the flax–PMMA composites after drop-weight impact testing at 21 J kinetic energy (A). The maximum contact force (F^{max}) and the corresponding displacement at F^{max} at 21 J kinetic energy are respectively presented in (B) and (C). (For interpretation of the references to colour in this figure legend, the reader is referred to the web version of this article.)

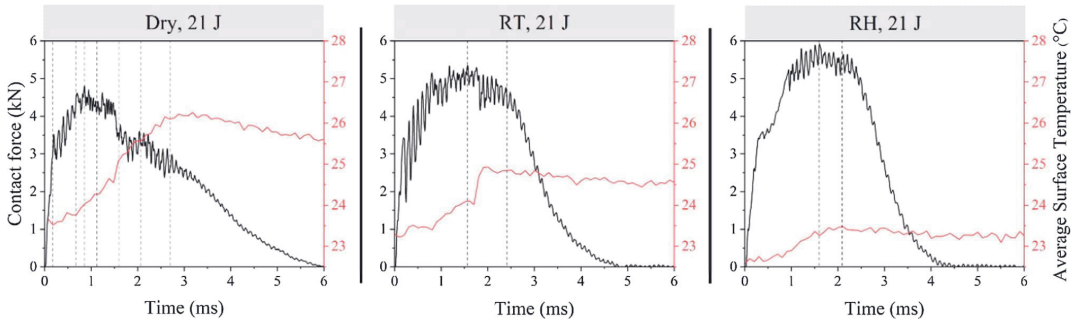

Fig. 12. Contact force–time and corresponding surface temperature–time history of composites at 21 J drop-weight impact energy. (For interpretation of the references to colour in this figure legend, the reader is referred to the web version of this article.)

understand the viability of processing in-situ polymerised non-dry natural fibre–PMMA composites with complex geometries of variable thicknesses [32]. It should be noted that the results in this article are valid only for composites equilibrated at the 50% RH (23 °C). In future work, the hygrothermal fatigue performance of flax–PMMA will have to be analysed to understand the effect of non-dry fibres on the long-term durability and dimensional stability of composites.

5. Conclusions

This paper proved the feasibility of processing stiff and tough structural flax–PMMA composites with non-dry fibres, which are relatively ductile compared to commonly used oven-dried fibres. The results presented in this article are valid mainly for indoor applications and composites equilibrated at 50% RH (23 °C). Composites with oven-dried and preconditioned (50% RH, 23 °C for 24 h) fibres had similar tensile moduli, transverse tensile strength, and in-plane shear strength. Preconditioning fibres in 90% RH decreased the transverse tensile strength (−38%) and in-plane shear strength (−23%) of composites because of the interfacial debonding sites due to the fibre shrinkage and plasticising effect of moisture on the fibres. Non-dry fibres preconditioned at 50% RH (RT), and 90% RH (RH) respectively enhanced the in-plane shear strain to failure of flax–PMMA (Dry) by 42% and 77%. Non-dry composites had a lower fatigue life degradation rate than oven-dried flax–PMMA composites. The fracture surface analysis manifested the better fatigue life and damage tolerance of non-dry composites as the result of ductile failure with extensive fibre pull-outs. In low-velocity drop-weight impact testing of cross-ply specimens, modified composites (RT and RH) had overall better elasticity against the impact loading, limited fibre failure and higher energy dissipation through extensive fibre pull-out and delamination compared to unmodified (Dry) material. RT and RH composites, respectively, raised the perforation energy of Dry by 57% and 100%. The synchronised strain and contact force data effectively could be linked to in-situ impact damage progression on the rear surface of composites. The DIC and IR data were coherent and complementary to the internal impact damage patterns acquired by X-CT.

CRediT authorship contribution statement

F. Javanshour: Conceptualization, Methodology, Formal analysis, Investigation, Writing – original draft, Visualization. **A. Prapavesis:** Investigation, Formal analysis, Writing – review & editing. **N. Pournoori:** Investigation, Formal analysis, Writing – review & editing. **G.C. Soares:** Investigation, Formal analysis, Writing – review & editing. **O. Orell:** Investigation, Formal analysis, Writing – review & editing. **T. Pärnänen:** Formal analysis. **M. Kanerva:** Funding acquisition, Writing – review & editing. **A.W. Van Vuure:** Funding acquisition, Writing – review & editing. **E. Sarlin:** Supervision, Investigation, Funding acquisition, Writing – review & editing.

Declaration of Competing Interest

The authors declare that they have no known competing financial interests or personal relationships that could have appeared to influence the work reported in this paper.

Data availability

Data will be made available on request.

Acknowledgements

This project is funded by the European Union's Horizon 2020 research and innovation programme under the Marie Skłodowska-Curie grant agreement No 764713-FibreNet. This work made use of Tampere Microscopy Center facilities at Tampere University. The authors thank Bcomp (Fribourg, Switzerland) for supplying the flax fabrics. Farzin Javanshour appreciates the contributions made by Apolline Féré (for fatigue testing) and Quynh Nguyen (for processing of composites).

Appendix A. Supplementary material

Supplementary data to this article can be found online at https://doi.org/10.1016/j.compositesa.2022.107110.

References

[1] Awais H, Nawab Y, Amjad A, Anjang A, Md Akil H, Zainol Abidin MS. Environmental benign natural fibre reinforced thermoplastic composites: a review. Compos Part C Open Access 2021;4:100082. https://doi.org/10.1016/J.JCOMC.2020.100082.

[2] Rueppel M, Rion J, Dransfeld C, Fischer C, Masania K. Damping of carbon fibre and flax fibre angle-ply composite laminates. Compos Sci Technol 2017;146:1–9. https://doi.org/10.1016/J.COMPSCITECH.2017.04.011.

[3] Woigk W, Fuentes CA, Rion J, Hegemann D, van Vuure AW, Kramer E, et al. Fabrication of flax fibre-reinforced cellulose propionate thermoplastic composites. Compos Sci Technol 2019;183:107791.

[4] Pil L, Bensadoun F, Pariset J, Verpoest I. Why are designers fascinated by flax and hemp fibre composites? Compos Part A Appl Sci Manuf 2016;83:193–205. https://doi.org/10.1016/J.COMPOSITESA.2015.11.004.

[5] Panciroli R, Giannini O. Comparing the impact resistance of flax/epoxy and glass/epoxy composites through experiments and numerical simulations. Compos Struct 2021;264:113750. https://doi.org/10.1016/J.COMPSTRUCT.2021.113750.

[6] Bensadoun F, Depuydt D, Baets J, Verpoest I, van Vuure AW. Low velocity impact properties of flax composites. Compos Struct 2017;176:933–44. https://doi.org/10.1016/j.compstruct.2017.05.005.

[7] Mahboob Z, Bougherara H. Fatigue of flax-epoxy and other plant fibre composites: Critical review and analysis. Compos Part A Appl Sci Manuf 2018;109:440–62. https://doi.org/10.1016/J.COMPOSITESA.2018.03.034.

[8] Mahboob Z, Fawaz Z, Bougherara H. Fatigue behaviour and damage mechanisms under strain controlled cycling: comparison of Flax–epoxy and Glass–epoxy composites. Compos Part A Appl Sci Manuf 2022;159:107008. https://doi.org/10.1016/J.COMPOSITESA.2022.107008.
[9] Van Vuure AW, Vanderbeke J, Mosleh Y, Verpoest I, El-Asmar N. Ductile woven silk fibre thermoplastic composites with quasi-isotropic strength. Compos Part A Appl Sci Manuf 2021;147:106442. https://doi.org/10.1016/J.COMPOSITESA.2021.106442.
[10] Javanshour F, Prapavesis A, Pärnänen T, Orell O, Lessa Belone MC, Layek RK, et al. Modulating impact resistance of flax epoxy composites with thermoplastic interfacial toughening. Compos Part A Appl Sci Manuf 2021;150:106628.
[11] Woigk W, Fuentes CA, Rion J, Hegemann D, van Vuure AW, Dransfeld C, et al. Interface properties and their effect on the mechanical performance of flax fibre thermoplastic composites. Compos Part A Appl Sci Manuf 2019;122:8–17.
[12] Randall JD, Stojcevski F, Djordjevic N, Hendlmeier A, Dharmasiri B, Stanfield MK, et al. Carbon fiber polypropylene interphase modification as a route to improved toughness. Compos Part A Appl Sci Manuf 2022;159:107001.
[13] Lin J, Wang L, Liu L, Lu K, Li G, Yang X. Two-stage interface enhancement of aramid fiber composites: establishment of hierarchical interphase with waterborne polyurethane sizing and oxazolidone-containing epoxy matrix. Compos Sci Technol 2020;193:108114. https://doi.org/10.1016/j.compscitech.2020.108114.
[14] AhmadvashAghbash S, Breite C, Mehdikhani M, Swolfs Y. Longitudinal debonding in unidirectional fibre-reinforced composites: Numerical analysis of the effect of interfacial properties. Compos Sci Technol 2022;218:109117. https://doi.org/10.1016/J.COMPSCITECH.2021.109117.
[15] Hsieh TH, Kinloch AJ, Taylor AC, Kinloch IA. The effect of carbon nanotubes on the fracture toughness and fatigue performance of a thermosetting epoxy polym. J Mater Sci 2011;46:7525–35. https://doi.org/10.1007/S10853-011-5724-0/FIGURES/9.
[16] Eyckens DJ, Demir B, Randall JD, Gengenbach TR, Servinis L, Walsh TR, et al. Using molecular entanglement as a strategy to enhance carbon fiber-epoxy composite interfaces. Compos Sci Technol 2020;196:108225.
[17] Randall JD, Eyckens DJ, Sarlin E, Palola S, Andersson GG, Yin Y, et al. Mixed surface chemistry on carbon fibers to promote adhesion in epoxy and PMMA polymers. Ind Eng Chem Res 2022;61:1615–23. https://doi.org/10.1021/ACS.IECR.1C04409/ASSET/IMAGES/LARGE/IE1C04409_0008.JPEG.
[18] Javanshour F, Ramakrishnan KR, Layek RK, Laurikainen P, Prapavesis A, Kanerva M, et al. Effect of graphene oxide surface treatment on the interfacial adhesion and the tensile performance of flax epoxy composites. Compos A Appl Sci Manuf 2021;142:106270.
[19] Kanerva M, Korkiakoski S, Lahtonen K, Jokinen J, Sarlin E, Palola S, et al. DLC-treated aramid-fibre composites: tailoring nanoscale-coating for macroscale performance. Compos Sci Technol 2019;171:62–9.
[20] Palola S, Javanshour F, Azari SK, Koutsos V, Sarlin E. One Surface Treatment, Multiple possibilities: broadening the use-potential of para-aramid fibers with mechanical adhesion. Polym 2021;13:3114. https://doi.org/10.3390/POLYM13183114.
[21] Berges M, Léger R, Placet V, Person V, Corn S, Gabrion X, et al. Influence of moisture uptake on the static, cyclic and dynamic behaviour of unidirectional flax fibre-reinforced epoxy laminates. Compos Part A Appl Sci Manuf 2016;88:165–77.
[22] Thuault A, Eve S, Blond D, Bréard J, Gomina M. Effects of the hygrothermal environment on the mechanical properties of flax fibres: Http://DxDoiOrg/101177/0021998313490217 2013;48:1699–707. https://doi.org/10.1177/0021998313490217.
[23] Fuentes CA, Ting KW, Dupont-Gillain C, Steensma M, Talma AG, Zuijderduin R, et al. Effect of humidity during manufacturing on the interfacial strength of non-pre-dried flax fibre/unsaturated polyester composites. Compos Part A Appl Sci Manuf 2016;84:209–15.
[24] Lu MM, Fuentes CA, Van Vuure AW. Moisture sorption and swelling of flax fibre and flax fibre composites. Compos Part B Eng 2022;231:109538. https://doi.org/10.1016/J.COMPOSITESB.2021.109538.
[25] le Duigou A, Merotte J, Bourmaud A, Davies P, Belhouli K, Baley C. Hygroscopic expansion: A key point to describe natural fibre/polymer matrix interface bond strength. Compos Sci Technol 2017;151:228–33. https://doi.org/10.1016/J.COMPSCITECH.2017.08.028.
[26] Lu MM, Van Vuure AW. Improving moisture durability of flax fibre composites by using non-dry fibres. Compos Part A Appl Sci Manuf 2019;123:301–9. https://doi.org/10.1016/J.COMPOSITESA.2019.05.029.
[27] Newman RH. Auto-accelerative water damage in an epoxy composite reinforced with plain-weave flax fabric. Compos Part A Appl Sci Manuf 2009;40:1615–20. https://doi.org/10.1016/J.COMPOSITESA.2009.07.010.
[28] Ahmad F, Abbassi F, Ul-Islam M, Jacquemin F, Hong JW. Enhanced impact-resistance of aeronautical quasi-isotropic composite plates through diffused water molecules in epoxy. Sci Rep 2021.1–13.;2021(111):11. https://doi.org/10.1038/s41598-021-81443-w.
[29] Krys P, Matyjaszewski K. Kinetics of Atom Transfer Radical Polymerization. Eur Polym J 2017;89:482–523. https://doi.org/10.1016/J.EURPOLYMJ.2017.02.034.
[30] Liu L, Zhang H, Zhou Y. Quasi-static mechanical response and corresponding analytical model of laminates incorporating with nanoweb interlayers. Compos Struct 2014;111:436–45. https://doi.org/10.1016/J.COMPSTRUCT.2014.01.021.
[31] Obande W, Ó Brádaigh CM, Ray D. Continuous fibre-reinforced thermoplastic acrylic-matrix composites prepared by liquid resin infusion – a review. Compos Part B Eng 2021;215:108771.
[32] Suzuki Y, Cousins D, Wassgren J, Kappes BB, Dorgan J, Stebner AP. Kinetics and temperature evolution during the bulk polymerisation of methyl methacrylate for vacuum-assisted resin transfer molding. Compos Part A Appl Sci Manuf 2018;104:60–7. https://doi.org/10.1016/j.compositesa.2017.10.022.
[33] Madsen B, Thygesen A, Lilholt H. Plant fibre composites–porosity and stiffness. Compos Sci Technol 2007;67:1584–600. https://doi.org/10.1016/j.compscitech.2006.07.009.
[34] Abdullah SIBS, Iannucci L, Greenhalgh ES. On the translaminar fracture toughness of Vectran/epoxy composite material. Compos Struct 2018;202:566–77. https://doi.org/10.1016/J.COMPSTRUCT.2018.03.004.
[35] Greenhalgh ES. Failure analysis and fractography of polymer composites. Cambridge, UK: Woodhead Publishing Ltd.; 2009.
[36] Fischer B, Sarasini F, Tirillò J, Touchard F, Chocinski-Arnault L, Mellier D, et al. Impact damage assessment in biocomposites by micro-CT and innovative air-coupled detection of laser-generated ultrasound. Compos Struct 2019;210:922–31.
[37] Ramakrishnan KR, Corn S, Le Moigne N, Ienny P, Slangen P. Experimental assessment of low velocity impact damage in flax fabrics reinforced biocomposites by coupled high-speed imaging and DIC analysis. Compos Part A Appl Sci Manuf 2021;140:106137. https://doi.org/10.1016/j.compositesa.2020.106137.
[38] Pournoori N, Corrêa Soares G, Orell O, Palola S, Hokka M, Kanerva M. Adiabatic heating and damage onset in a pultruded glass fiber reinforced composite under compressive loading at different strain rates. Int J Impact Eng 2021;147:103728. https://doi.org/10.1016/J.IJIMPENG.2020.103728.
[39] Han N, Baran I, Zanjani JSM, Yuksel O, An LL, Akkerman R. Experimental and computational analysis of the polymerisation overheating in thick glass/Elium® acrylic thermoplastic resin composites. Compos Part B Eng 2020;202:108430. https://doi.org/10.1016/J.COMPOSITESB.2020.108430.